Study of Resonance Hairpin Probe for Electron Density Measurements in Low Temperature Plasmas

Gurusharan Singh Gogna

July 2012

STUDY OF RESONANCE HAIRPIN PROBE FOR ELECTRON DENSITY MEASUREMENTS IN LOW TEMPERATURE PLASMAS

A thesis for the degree of

PHILOSOPHIAE DOCTOR

Presented to

DUBLIN CITY UNIVERSITY

By

GURUSHARAN SINGH GOGNA

School of Physical Sciences

Dublin City University

Research Supervisors:

Dr. Shantanu Kumar Karkari

and

Prof. Miles Turner

External Examiner: Dr. Jean-Paul Booth

Internal Examiner: Dr. Stephen Daniels

July 2012

Declaration

I hereby certify that this material which I now submit for assessment on the programme of study leading to the award of Philosophiae Doctor is entirely my own work, that I have exercised reasonable care to ensure that the work is original, and does not to the best of my knowledge breach any law of copyright, and has not been taken from the work of others save and to the extent that such work has been cited and acknowledged within the text of my work.

Signed: ....

Gurusharan Singh Gogna

Student ID. No.: 58100938

Date: July 2012

This thesis is dedicated to my parents for their love, endless support, and encouragement.

Abstract

The thesis deals with a plasma diagnostic device, the Hairpin Probe, popularly used for measuring electron density in rarefied gaseous plasma. Electron density, n_e, is an important plasma parameter as electrons are mainly responsible for inelastic collision with background neutrals resulting in ionization, excitation, and various chemical processes in plasma. Besides, the basic plasma parameters such as plasma frequency, Debye length, plasma permittivity, and plasma conductivity are all based on n_e. Therefore accurate measurement of n_e is fundamentally desirable for quantifying the state of plasma.

The underlying principle relies on measuring the effective permittivity of medium surrounding the hairpin. If length of hairpin is chosen equal to a quarter-wavelength of an incident microwave signal, a standing wave is set-up along its length. Under this condition, a strong absorbance of incident em signal is observed as hairpin is driven to resonance. When hairpin is immersed in plasma, the cold plasma permittivity is related to n_e. However if adjacent dielectrics are present in the vicinity of probe, it can adversely affects the measurement. As one of the practical applications of hairpin, high refractory material is coated on the probe surface when applied to reactive etch plasmas. However, the contribution of external dielectric on probe resonances in plasma is an outstanding problem.

In this thesis, we have primarily addressed the above issues. A comprehensive study is also devoted towards application of probe in strongly magnetized plasmas. The electrons gyro motion modifies the plasma permittivity and results in the observance of dual resonances as compared with non-magnetized plasmas. The other important issues addressed are different loss mechanisms causing dispersion of resonance signal in plasma. This is particular topic of interest in order to broaden the range of n_e measurement by probe.

Contents

List of Publications/Awards/Memberships

Invention Disclosure

S. K. Karkari and G. S. Gogna: Methods of constructing and calibrating a resonance hairpin probe for measuring electron density in plasma processing tools, IDF - DCU internal reference 2009/02/DCU/PS/NCPST.

Peer Reviewed Publications and Conference Proceedings

- G. S. Gogna, S. K. Karkari, M. M. Turner: Partially shielded hairpin probe for high density measurements, Applied Physics Letter, Submitted in June 2012 (under review).
- G. S. Gogna, C. Gaman, S. K. Karkari, M. M. Turner: Dielectric shielded hairpin probe for its application in reactive plasmas, Applied Physics Letter, July 2012 (accepted).
- G. S. Gogna, S. K. Karkari: Microwave resonances of a hairpin probe in a magnetized plasma, Applied Physics Letter, 96, No. 151503, 2010.
- S. K. Karkari, G. S. Gogna, D. Boilson, M. M. Turner, A. Simonin: Performance of floating hairpin probe in strongly magnetized plasma, Contribution to Plasma Physics Journal, Vol. 50, Issue 9, pp. 903-908, September 2010.
- G. A. Curley, L. Gatilova, S. Guilet, S. Bouchoule, G. S. Gogna, N. Sirse, S.

K. Karkari, J. P. Booth: Surface loss rates of H and Cl atoms in an inductively coupled plasma etcher time-resolved electron density and OES measurement, Journal of Vacuum Sci. and Tech. A, no. 28, 360-372, March 2010.

- G. S. Gogna, S. K. Karkari, M. M. Turner: Dual resonances by hairpin resonator probe in strongly magnetized plasma, 30th International conference on phenomena in ionized gases (ICPIG), Belfast, United Kingdom, 28th August to 2nd September 2011.

- G. S. Gogna, C. Gaman, S. K. Karkari: Effect of the dielectric on the electron density measurement by hairpin probe, 30th International conference on phenomena in ionized gases (ICPIG), Belfast, United Kingdom, 28th August to 2nd September 2011.

- G. S. Gogna, S. K. Karkari: The microwave resonance probe: concept, theory and application in magnetized plasma, 25th symposium on plasma science, Guwahati, India, 8-11 December 2010.

- G. S. Gogna, S. K. Karkari, M. M. Turner: Affect of strong magnetic field on the properties of resonance hairpin probe, International conference on reactive plasma, Paris, France, 4-8 October 2010.

- G. S. Gogna, S. K. Karkari: Factor influencing the quality of the resonance signal of hairpin probe in low temperature plasma, 37th European physical society conference on plasma physics, P4307, Dublin City University, Dublin, Ireland, 21-25 June 2010.

- G. S. Gogna, S. K. Karkari, D. Boilson, M. M. Turner: Theory and application of hairpin probe in magnetized plasma, 37th European physical society conference on plasma physics, P5109, Dublin City University, Dublin, Ireland, 21-25 June 2010.

Academic Awards and Achievements

- Third prize winner of 3rd NCPST postgraduate poster competition at Dublin City University, Ireland, December 2011.

- IEEE Student Travel Grant at 38th International Conference on Plasma Science (ICOPS), Chicago, IL, USA, June 2011.

- Winner of BUTI Young Scientist Award for best oral presentation in plasma conference organized by Plasma Science Society of India, Guwahati, India, 8-11 December 2010.

- Second prize winner of British Oxygen Company (BOC) gas poster competition at DCU, Ireland, 24 September 2010.

- Nominated for best oral presentation at 63rd Annual Gaseous Electronics Conference, Paris, France, 4-8 October 2010.

- Oral presentation at the 15th Steering committee fusion meeting, DCU, September 2010.

Organization Memberships

- Associate member of Institute of Physics (IOP).

- Life time member of Plasma Science Society of India (PSSI).

Symbols and Abbreviations

l	length (mm)
$\omega_{r,o}$	resonance frequency (rad s^{-1})
n_i	ion density (cm^{-3})
n_e	electron density (cm^{-3})
e	absolute electron charge ($\simeq 1.6022 \times 10^{-19}$ C)
E	electric field (Vm^{-1})
B	magnetic field (Tesla)
λ_D	electron Debye length (m)
T	temperature (Kelvin, Volts or Joule)
ϵ_0	vacuum permittivity ($\simeq 8.8542 \times 10^{-12}$ Fm^{-1})
ϵ_p	magnetic field free Plasma Permittivity
κ_p	magnetized plasma permittivity
n_0	plasma density (cm^{-3})
n_g	neutral gas density (m^{-3})
ω	angular frequency (rad s^{-1})
ω_{pi}	ion plasma frequency (rad s^{-1})
ω_{ce}	electron gyro frequency (rad s^{-1})

u_B	Bohm velocity (ms^{-1})
k_B	Boltzmann's constant ($1.3807 \times 10^{-23} JK^{-1}$)
c	speed of light in air ($3.0 \times 10^8 ms^{-1}$)
m_i	ion Mass (kg)
Q	electric Charge (C)
P	power (Watt); Polarization per unit volume
J	current density (Am^{-2})
σ_p	plasma conductivity ($\Omega^{-1} m^{-1}$)
$\omega_{pe,pi}$	electron and ion Plasma Frequency (rad s^{-1})
$\nu_{en,m}$	collision frequency (Hertz)
λ_e	electron mean free path (m)
$m_{e,i}$	electron mass, ion mass, and particle mass (kg)
v	velocity (ms^{-1})
$\bar{v}_e$	mean electron thermal velocity (ms^{-1})
t	time (s)
F	force (Newton)
ρ	charge density (Cm^{-3})
λ_i	ion mean free path (m)
p	pressure (Torr)
Γ	particle flux ($m^{-2}s^{-1}$); reflection coefficient
μ_e	electron mobility ($m^2 s^{-1} V^{-1}$)
μ_i	ion mobility ($m^2 s^{-1} V^{-1}$)
D_e	electron diffusion coefficient ($m^2 s^{-1}$)
D_i	ion diffusion coefficient ($m^2 s^{-1}$)
D_a	ambipolar diffusion coefficient ($m^2 s^{-1}$)
ϕ	angle (rad)
n	particle number density (ms^{-3}); refractive index
k	wavenumber (m^{-1}); spring constant
T_i	ion temperature (eV)

N	number of elementary dipoles
V	potential (Volts)
A_p	area of probe (m^2)
a	wire radius (m)
λ	wavelength (m)
Z	impedance (Ohm)
R	resistance (Ohm)
G	conductance (Siemens)
δ	skin depth (m)
X	reactance (Ohm)
α	attenuation constant (m^{-1})
β	phase constant (m^{-1})

List of Figures

Acknowledgments

It is my pleasure to express my gratitude to all those people who have made this thesis work possible by contributed in numerous ways.

Firstly, I am heartily thankful to my supervisor, Dr. Shantanu Kumar Karkari, whose encouragement and direction from the initial to the final level enabled me to develop an understanding about my research problem. His availability and regular discussion allowed me to develop a scientific approach to tackle fundamental problems of physics. The final year thesis writing work was not possible to complete without his specific guidance and organizing extra time from his busy schedule at Institute for Plasma Research (IPR) in India.

I would like to express my gratitude to my supervisor, Prof. Miles Turner, Director of National Centre for Plasma Science and Technology for fruitful scientific discussions and for giving me opportunity to get involved in the fusion mobility programme and various scientific meetings.

During fusion mobility programme at CEA, France, I had chance to work with Dr. Deirdre Boilson whose team work is evident throughout the work. Also, I sincerely thanks to Dr. Sophie Bouchoule and group for organizing and supporting my research visit at Laboratoire de Photonique et de Nanostructures (LPN)-CNRS in France. I would also like to express my gratitude to Prof. P. K. Kaw for allowing me to stay at IPR for the purpose of thesis writing work and collaborative research work with Dr. Pramod Sharma. I have learned and experienced many things from these visits.

I would like to enlarge my gratitude to Dr. Paul swift for his valuable feedback on my work, Dr. Cezar Gaman for doing mutual research work on hairpin probe, and Prof. Valery Godyak for fruitful discussion about the various probe techniques used for plasma diagnostics.

I would like to thank Prof. Greg Hughes, Head of Physics School at DCU for his kind financial support during the final year of PhD. I am also thankful to him for giving me opportunity to get involved in undergraduate physics experiments as a Laboratory Demonstrator during my PhD programme.

I am also thankful to Mr. James Lalor, Mr. Ray Murphy, Mr. Conor Murphy, Mr. Des Lavelle, and Mr. Pat Wogan for there technical assistance, and the NCPST operational manager, Ms. Samantha Fahy, the secretaries, Ms. Patricia James and administrator, Ms. Sarah Hayes and Ms. Sheila Boughton; and the School of Physics secretary, Ms. Lisa Peyton. I would like to thank all Library staff for helping me to find the quality documents I was looking for.

I am grateful to many of my friends cum colleagues for fruitful scientific discussions and for keeping friendly environment at work place.

Lastly, and most importantly, I wish to thank my father, Mr. Sukhvinder Singh Gogna, and my mother, Ms. Madhujeet Kaur Gogna, for there valuable teachings, love, and blessings which always help me to achieve my goals. I would like to dedicate this thesis to them.

Gurusharan Singh Gogna

CHAPTER 1

Introduction

Modern life-style is immensely dependent on plasma [3–5] technologies for communication. Fast computer processors, memory storage devices, bio-medicine, food packaging, plasma display, solar photo-voltaic, lighting, protective coatings, creation of exotic new materials, rocket thrusters, bio-medical application are to name a few. Plasma is the only means for producing fusion energy that can fulfill the energy requirement for our growing future needs [6, 7].

Plasma diagnostics [8–10] play a key role in the basic understanding of complex discharge properties. Typically plasma consists of electrons, positive and negative ions present in quasi-neutral equilibrium in conjunction with energetic metastable atoms and molecules. Plasmas are generally characterized in terms of its characteristic temperatures of electrons and ions. Low temperature, non-equilibrium plasmas are the ones in which $T_e >> T_i \approx T_g$. These plasmas are generally produced at low pressures in an evacuated chamber by means of radio frequency or D.C. electric field applied to a set of electrodes. Low temperature plasmas are widely used in plasma processing industries for the manufacturing of Pentium chips, surface modification, coatings on glass surfaces, and several others [11, 12]. On the other hand an equilibrium plasma is described having, $T_e \approx T_i$. These plasmas can be either hot (fusion) or cold (atmospheric plasmas). Plasmas can be also classified in terms of fractional ionization. The fusion plasma in a Tokamak and in the sun are examples of fully ionized gas as compared to partially ionized plasmas those used in plasma manufacturing industries, lightning application etc. The state of the plasma is not unique. It depends on the manner in which the discharge is created and the constituent gases that are used for creating the discharge. A typical example is the plasmas used for manufacturing of integrated circuits in which a silicon wafer is processed through a range of reactive gaseous plasma. The properties of these plasmas are highly complex, as it comprise of different charge states of positive ions in conjunction with electrons, metastable neutrals and negative ions. Quantification of the state of plasma at various steps is therefore necessary for achieving unique property of the processed substrate. Plasma diagnostics and monitoring techniques in terms of real-time output of electron temperature, floating potential, and ion saturation current, ability to track changes in plasma parameters are pivotal for ensuring unique processing conditions, the health, and regular maintenance of the plasma tools used in these industries. On the other hand fusion plasmas [13] are characterized by strong magnetic field which confines the hot plasma of several millions of degree Kelvin's in a dough nut shaped vessel. The positive charged α-particles formed as a byproduct during fusion of hydrogen / deuterium atoms are guided by the special magnetic field to a diverter plate, neutralized, and pumped out. The plasmas close to the diverter is an example of strongly magnetized non-equilibrium plasma which comprise of dust generated from erosion of target wall materials. Another example of strongly magnetized plasma is the ion beam source [14] used for the production of neutral beams for plasma heating in fusion devises. Characterization of plasma parameters in these devices is therefore important in determining the efficiency of the source and the extraction of laminar beams.

Plasma diagnostics [8–10] can be classified in terms of invasive or noninvasive nature. Optical diagnostic is a common example of noninvasive method of characterization of the plasma. It provides useful information about the plasma, such as the relative ratios of the optical signal intensities gives the different gas constituents in plasma. The basic principle is based on the excitation and emission of optical light by species formed during the various processes occurring in the discharge [15]. For obtaining the actual plasma parameters such as electron number density, electron temperature etc.; the calculations are based on PIC or hydrodynamic models which rely on experimentally produced cross-sections and accurate knowledge of the boundary conditions. Another non-invasive measurement of plasma properties is possible via gross measurement of voltage and current at the substrate or at the path of the discharge circuit. Microwave interferometry [9, 16–18] is also an example of noninvasive technique. The basic principle is based on probing a beam of wavelength λ along the path z through the plasma and from the relative phase shift of the wave gives the so-called line-integrated density. The density profile can be obtained by taking number of independent measurements along different lines of sight. While being non-intrusive these techniques have certain advantages however one has to rely on intrusive diagnostic such as electric probes [5, 19–21] for comprehensive and local measurement of plasma parameters. An electric probe usually a piece of conducting wire inserted in the plasma is an invasive diagnostic technique. The primary principle is based on measuring the response of plasma species towards a given steady state or time-varying perturbation imposed by the probe in the surrounding plasma. For example, measurement of drifts and fields generated by currents are measured using B-dot probes [22, 23]. Plasma potential, floating potential, electron energy distribution, charge densities require a Langmuir probe [19] which is based on discriminating fluxes of electrons and ions by means of biasing the probe with respect to a reference electrode in contact with the plasma.

One of the important plasma properties is the electron number density. The electrons are mainly responsible for different kinetics, discharge impedance, light emission via excitation of neutrals etc. Measurement of electron density gives an indirect measure of ion density in multi-component plasmas. Besides electron density is one of the fundamental plasma properties on which Debye length, plasma frequency, dielectric property of the plasma is based. For measuring negative ion density [24–28], laser photo detachment and probe is used in conjunction for the measurement of photo-detached electron density etc. Therefore measurement of electron density in a discharge is most crucial for basic understanding of plasma phenomenon.

Though Langmuir probes are simple diagnostic tool for measuring electron density, however it has several disadvantages in terms of introducing strong perturbation to the plasma, it needs a reference electrode for the return current path, complex sheath properties in the case of strongly magnetized plasma [29–31] and highly sensitive to the surface conductivity in the case of depositing plasmas such as PECVD [32–34]. An ideal device must be free from these limitations and that can give direct and accurate measurement of electron density.

1.1 Motivation

This thesis is motivated from a relatively new diagnostic device called Hairpin probe for measuring electron density. The principle is based on measuring cold plasma permittivity, which is directly related to the electron density. Though Stenzel [35, 36] invented the technique around 35 years ago, however it became popular in the last decade after the published work by Peijak et al in 2004 [2]. Since then the technique has been used in wide range of plasma environments. However, the key application of the technique has not been thoroughly investigated. Some of the key issues are sensitivity, accuracy, repeatability of the device as it is susceptible to the influence of additional dielectrics in the form of probes feed-through, insulating deposition on the probes surface etc, which can lead to under-estimation of the measures electron density. The practical range of density measurement is also limited to a range between $10^9 - 10^{12} cm^{-3}$, whereas in ECR, edge plasmas in Tokamaks the plasma density can be 2.0 orders in magnitude higher. So far the hairpin probe was used only in weakly magnetized plasma. However in the presence of very strong magnetic field one must consider the modified plasma permittivity because of the electron cyclotron frequency. The magnetic field also makes the permittivity anisotropic [11]. This implies that application of hairpin is sensitive to the manner in which the probe is oriented with respect to the external field lines. A comprehensive part of the thesis is devoted to the physical understanding of the hairpin in strongly magnetized plasmas.

Before an in depth discussion of the subject a comprehensive discussion of the plasma property is presented in the following section 1.2. In section 1.3 we present a brief review of well-known techniques for measuring electron density in plasmas. In the penultimate section 1.4, we present the historical perspective of hairpin probe followed by an outline of the thesis in Section 1.5.

1.2 Fundamentals Role of Plasma Electrons

1.2.1 Debye Shielding

The plasmas can have the property similar to the conductors where the surface charges arrange themselves so that the electric field becomes zero inside the material. When the electrostatic potential is introduced in to the plasma then the charged particles redistribution takes place in order to shield the potential up to a distance called the Debye length [6, 11, 37] which is given by the expression:

$$\lambda_D^2 = \frac{\epsilon_o k_B T_e}{e^2 n_e} \tag{1.1}$$

where T_e is the electron temperature in eV, n_e is the electron density in cm^{-3}, and λ_D is the Debye length in cm. Clearly, λ_D is independent of the particle mass and hence generally comparable for different species in the plasma. The shielding effect results in the formation of the boundary layer at the interface between plasma and a material wall placed in the plasma. Thus, the plasma has its own scale length which defines over which the electric field penetrates into the plasma. It is the appropriate scale of the transition region for the case when the wall or electrode assumes its potential only via the plasma and no additional potential is applied to it. The most important example of this is the Debye sheath which is defined as the formation of non-neutral boundary layer in front of material surface in contact with plasma and in the presence of electrical fields. It is generally few Debye lengths thick depending upon the temperature and density of charged particles.

1.2.2 Plasma Frequency

Plasma tends to maintain approximate charge neutrality to a very high degree at a distance larger compared to the Debye length. Any small deviation in the neutrality give rise to self-generated electric fields in order to limit the charge builds up. The quasi neutrality condition can be written as:

$$\Sigma Q_i e n_i - e n_e = 0 \tag{1.2}$$

where Q_i is the ion charge state and sum is taken over all the ion species. In the simplest case, but common, when the ions are positive we can write $n_i = n_e$. Small perturbation results in disturbance of charge neutrality. A restoring force (electric field) limits the charge accumulation in a region via restoring force as in the case of a spring forcing the electrons to exhibits plasma oscillations [5, 6, 11, 37, 38]. Plasma has number of natural modes of oscillations. The most fundamental mode is the electron plasma frequency. It is denoted by the symbol ω_{pe} and is given by:

$$\omega_{pe}^2 = \frac{e^2 n_e}{\epsilon_o m_e} \tag{1.3}$$

where, ϵ_o is the permittivity of free space. The ions can also oscillate at their own natural frequency such as in standing acoustic waves. This is called the ion plasma frequency, ω_{pi} and is given by,

$$\omega_{pi}^2 = \frac{Q^2 e^2 n_i}{\epsilon_o m_i} \tag{1.4}$$

where Q is the ion charge state, n_e, n_i are the electron and ion densities in cm^{-3} and m_i is the ion mass in amu. Usually, the electron plasma frequency is in the microwave band, some GHz; the ion plasma frequency is usually in the rf band, low MHz.

1.2.3 Dielectric Permittivity

The dielectric permittivity is the intrinsic property of the medium which describes how the charged particles respond to an externally applied time varying fields. It depends on the applied frequency, temperature, and charge particles number densities. Considering the case of insulator, conductor, and the plasma in to which the external electromagnetic field is applied. The applied electric field polarizes the medium and thus creating an electric dipole moment. The dielectric response of material is studied by Lorentz Dielectric model where the charges in the material are treated as harmonic oscillators. For free or unbound charged particles, it is called Drude model [39–41]. For instance, the equation of motion for the bound electrons in a dielectric for displacement x in presence of electric field $\vec{E}$ is given by:

$$m\ddot{x} = F_{E,local}(= eE) + F_{spring}(= -kx) + F_{Damping}(= -m\gamma\dot{x}) \tag{1.5}$$

where, $\dot{x} = dx/dt$ and the electric field is assumed to be acting in the x-direction and there is a spring like restoring force due to the binding of the electron to the nucleus, and a friction-type force proportional to the velocity of the electron. The parameter γ is the collision frequency. The spring constant k is related to the resonance frequency of the spring via the relationship $\omega_o = \sqrt{k/m}$ or $k = m\omega_o^2$. Therefore, we may rewrite Eq. 1.5 as follows:

$$\ddot{x} + \gamma\dot{x} + \omega_o^2 x = \frac{e}{m}E \tag{1.6}$$

By solving above differential equation one can obtain the displacement and velocity of the elementary dipole. Therefore, the polarization per unit volume for N elementary dipoles per unit volume will be:

$$P = Np = Nex = \frac{\frac{Ne^2}{m}E}{\omega_o^2 - \omega^2 + j\omega\gamma} \equiv \epsilon_o(\epsilon(\omega) - 1)E \tag{1.7}$$

Thus, the effective dielectric permittivity $\epsilon(\omega)$ is given by:

$$\epsilon(\omega) = \epsilon_o + \frac{\frac{Ne^2}{m}}{\omega_o^2 - \omega^2 + j\omega\gamma} \tag{1.8}$$

where, $\omega_p^2 = \frac{Ne^2}{m\epsilon_o}$ is so-called plasma frequency of the material.The real and imaginary parts of $\epsilon(\omega)$ characterizes the refractive and absorptive properties of the material. They are given by:

$$\epsilon^{'}(\omega) = \epsilon_o + \frac{\epsilon_o\omega_p^2(\omega_o^2 - \omega^2)}{(\omega_o^2 - \omega^2)^2 + \omega^2\gamma^2} \tag{1.9}$$

$$\epsilon^{''}(\omega) = \frac{\epsilon_o\omega_p^2\omega\gamma}{(\omega_o^2 - \omega^2)^2 + \omega^2\gamma^2} \tag{1.10}$$

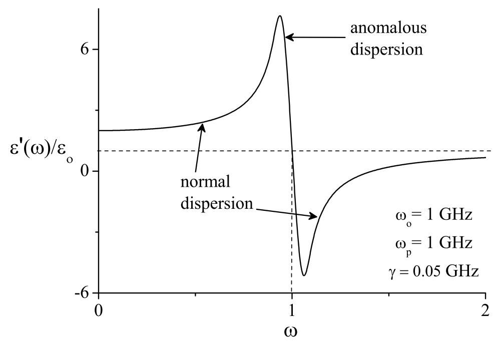

Figure 1.1: Real part of dielectric permittivity versus applied frequency.

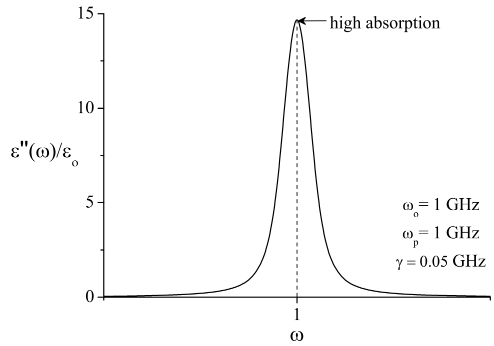

Figure 1.2: Imaginary part of dielectric permittivity versus applied frequency

Figs. 1.1 and 1.2 shows a plot of $\epsilon^{'}(\omega)$ and $\epsilon^{''}(\omega)$. Around the resonant frequency ω_o, the real part behaves in an anomalous manner, that is, it drops rapidly with frequency to values less than ϵ_o and the material exhibits strong absorption. The term 'normal dispersion' refers to an $\epsilon^{'}(\omega)$ that is an increasing function of ω, as is the case to the far left and right of the resonant frequency. It is also clear that the imaginary part of the refractive index is only appreciable in those regions of the electromagnetic spectrum where anomalous dispersion takes place.

To describe a plasma in relation of applied frequency and collisional frequency, the simple model considered for the dielectrics can be specialized by choosing approximation $\omega_o = \gamma = 0$. The corresponding effective permittivity becomes purely real which is given by:

$$\epsilon(\omega) = \epsilon_o \left(1 - \frac{\omega_p^2}{\omega^2}\right) \tag{1.11}$$

In presence of external magnetic field, the plasma permittivity is similar to Eq. 1.9 which is given by:

$$\epsilon_\perp(\omega) = \epsilon_o \left(1 - \frac{\omega_p^2}{\omega^2 - \omega_c^2}\right) \tag{1.12}$$

where $\omega_c = eB/m$ is the electron cyclotron frequency. The subscript $\perp$ indicates that the permittivity given in Eq. 1.12 pertains to wave electric fields perpendicular to the external magnetic field. The permittivity for electric field parallel to the magnetic field is still given by Eq. 2.3. In other words, the permittivity of a magnetized plasma is anisotropic and depends on the direction of the electric field with respect to the magnetic field. The appearance of the cyclotron frequency in the perpendicular permittivity is expected because for perpendicular electric field, electrons undergoing cyclotron motion are equivalent to those undergoing bound harmonic motion in dielectrics.

1.2.4 Plasma Conductivity, Mobility, and Diffusion

Plasma Conductivity

Ohm's Law defines the conductivity of the material. Plasma is conductive in nature due to presence of free particles. The charged particles in it react strongly with the electric and magnetic fields. To derive the relation for the conductivity, we use the formula for current density, $J = Nev$, where v can be evaluated by solving differential equation given in Eq. 1.6. Therefore,

$$J = \frac{j\omega \frac{Ne^2}{m} E}{\omega_o^2 - \omega^2 + j\omega\gamma} \equiv \sigma(\omega)E \tag{1.13}$$

Thus, the conductivity can be written as follows:

$$\sigma(\omega) = \frac{j\omega \frac{Ne^2}{m}}{\omega_o^2 - \omega^2 + j\omega\gamma} = \frac{j\omega\epsilon_o\omega_p^2}{\omega_o^2 - \omega^2 + j\omega\gamma} \tag{1.14}$$

However, in a plasma the charges are unbound, we may take $\omega_o = 0$ in above equation. Therefore obtain:

$$\sigma(\omega) = \frac{\epsilon_o\omega_p^2}{\gamma + j\omega} \tag{1.15}$$

The plasma can be considered as dielectric ϵ_p or a conductor σ_p as per our usefulness [11]. For low frequencies $\omega << \gamma_m, \omega_{pe}$, we find that the σ_p becomes σ_{dc},

$$\sigma_{dc} = \frac{\epsilon_o\omega_{pe}^2}{\gamma_m} \tag{1.16}$$

This is *dc plasma conductivity* under the cold plasma approximation. Similarly, for high frequencies ($\omega >> \gamma_m$), the plasma is represented as a dielectric with permittivity given by Eq. 2.3. However, in the presence of externally applied magnetic field the plasma becomes spatially anisotropic therefore conductivity is represented by a tensor quantity.

Plasma Diffusion and Mobility

For a constant electron temperature, slightly non-uniform electron density, and in the absence of electromagnetic forces in weakly ionized plasma, the diffusion equation for electrons is given by [37]:

$$\Gamma_e = -D_e \nabla n_e \tag{1.17}$$

where the electron free-diffusion coefficient is given by:

$$D_e = -\frac{k_B T_e}{m_e v_e} \tag{1.18}$$

where, v_e is the electron velocity.

Similarly, the diffusion equation for ions can be written as:

$$\Gamma_e = -D_e \nabla n_e \tag{1.19}$$

where the ion free-diffusion coefficient is given by:

$$D_e = -\frac{k_B T_i}{m_i v_i} \tag{1.20}$$

From above expressions, we found that the diffusion coefficient is inversely proportional to the masses of the charged particles. The electrons as the lightest particles in plasma diffuse at faster rate and leave an excess of positive ions behind them. This results in the creation of space charge electric field pointing towards the direction of particle diffusion. This electric field will accelerate the ions and retard the motion of electrons in order to maintain the local flux balance. If the effect of space charge electric field is negligible then the diffusion is known as free diffusion. In this case, the electrons and ions diffuse independently in the plasma. In this situation, the particle flux can be expressed in terms of the density gradient. However, as the density increases and sufficient space charge is produced, free diffusion changes into effective diffusion called the ambipolar diffusion. The ambipolar diffusion is greater than ion diffusion but less than the electron diffusion. The net electron flux resulting from electric field and diffusion is given by:

$$\Gamma_e = n_e \mu_e E - D_e \nabla n_e \tag{1.21}$$

where,

$$\mu_e = -\frac{e}{m_e \nu_e} \tag{1.22}$$

is called the electron mobility. Similarly, the net ion flux is given by,

$$\Gamma_i = n_i \mu_i E - D_i \nabla n_i \tag{1.23}$$

where,

$$\mu_i = \frac{e}{m_i \nu_i} \tag{1.24}$$

is called the ion mobility. Under quasineutrality assumption, $\Gamma_e = \Gamma_i = \Gamma_{ambipolar}$ and $n_e = n_i = n$, the ambipolar electric field is given by:

$$E_{ambipolar} = \frac{D_i - D_e}{\mu_i + \mu e} \frac{\triangledown n}{n} \tag{1.25}$$

Substituting this value of **E** into the common flux relation we get ambipolar diffusion as follows

$$\Gamma_{ambipolar} = -\frac{\mu_i D_e + \mu_e D_i}{\mu_i + \mu_e} \triangledown n \tag{1.26}$$

Based on the Fick's law $\Gamma = -D_a \triangledown n$

$$D_a = -\frac{\mu_i D_e + \mu_e D_i}{\mu_i + \mu_e} \tag{1.27}$$

This is known as ambipolar diffusion coefficient.

1.3 Electron Density Measurement Techniques

We briefly described the basic principle of some invasive and non-invasive plasma diagnostic techniques for measuring the electron density in plasma. The invasive techniques are Langmuir probes and resonance probes such as hairpin probe (HP) [36], plasma absorption probe (PAP) [42], plasma oscillation probe (POP) [43], wave-cutoff method (WCM) [44], LC resonance probe (LCRP) [45], and multipole resonance probe (MRP) [46] while the commonly used non-invasive techniques are optical emission spectroscopy [15, 47] and microwave interferometry [1, 48].

1.3.1 Langmuir Probe

A Langmuir probe [5, 19–21, 30, 49–52] can be defined as any small metallic object inserted into a plasma discharge whose potential is varied generally from -30V to +30V in order to draw either electron or ion current from the plasma ensemble. The plasma parameters such as electron temperature, electron density, and space potential of plasma can be calculated from the proper analysis of the measured voltage drops and currents. Mott-Smith and Langmuir [19] have done extensive study of the probe's current-voltage characteristics. The basic principle is based on how the local plasma particles response to a steady state and/or time varying perturbation imposed within the plasma. Therefore, the technique itself is based on the intrinsic property of the plasma.

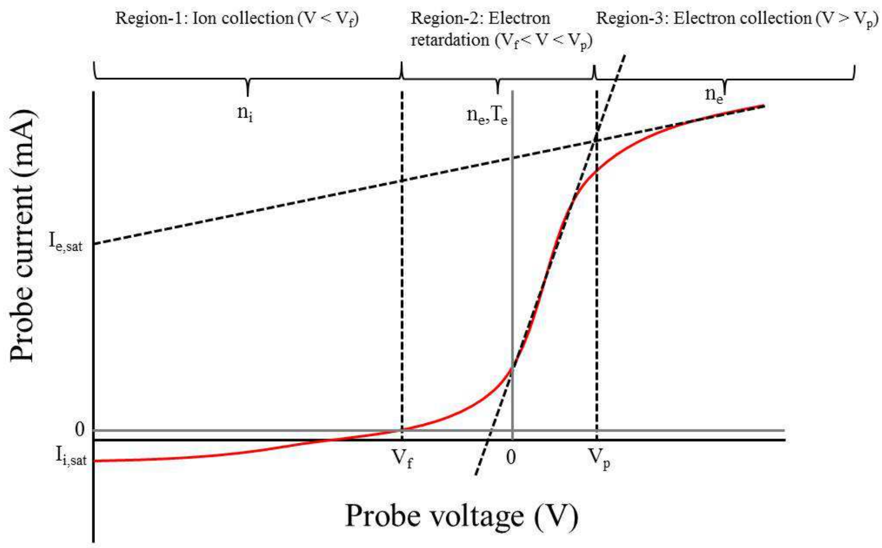

Figure 1.3: Current-voltage characteristics of Langmuir probe.

The typical trace of current-voltage characteristics with the use of Langmuir probe is shown in Fig. 1.3. It can be analyzed by considering three different regions as follows:

The region-1 is corresponding to the values of the potential less than V_f where floating potential V_f is defined as the potential at which the electron and ion flux towards the probe comes in an equilibrium and hence the net current from the plasma is zero. Due to large mass of ions this current is generally small and negative. The drawn current is mainly contributed by positive ions and gives ion density in plasma.

The region-2 is corresponding to values of potential between V_f and V_p, where V_p is the plasma potential or space potential. At the beginning of this region from V_p, the electrons are initially attracted to the positive potential of the probe and hence form a sheath in order to shield the electric field produced. After the formation of sheath, the probe surface becomes negatively charged so it will start attracting the positive ions and repels the electrons to preserve the quasi neutrality of the plasma. Since the electrons are mainly retarded therefore this region is called electron retardation region. The retardation process continues until the ion and electron fluxes become equal at floating potential.

The region-3 describes the situation where the potential is positive and greater than V_p. Therefore, the electrons will be accelerated and positive ions will be repelled from the probe. Increasing the bias will yield the electron saturation current such that increase in voltage does not increase the current. In experiments, it is difficult to achieve electron saturation current because of the increase of Debye length and hence the collection area of the probe (A_p). This results in large collection of current and also it creates significant perturbation in to the plasma. Since the electron density is calculated from this branch of current-voltage characteristics using the formula given by:

$$n_e = \frac{I_{e,sat}}{eA_p}\sqrt{\frac{2\pi m_e}{k_B T_e}} \tag{1.28}$$

Therefore, it can produce significant error in the measurements of electron density. In case of planar probes, the area of the probe is too large as compared to the sheath thickness such that effective area of the probe is independent of sheath thickness. This improves the measurement of $I_{e,sat}$. However, due to its large collection area and application of positive bias strongly perturbs the plasma. Thus the use of planer Langmuir probe is limited only to the measurement of ion density. The calculation of the other parameters is easily available in the literature [5, 19–21, 30, 49–52]. Here, we have shown only the concern of accurate electron density measurements from Langmuir probe. For cylindrical or spherical probe, the probe dimension should satisfy the following condition

$$a[\ln 1/2a] << \lambda_e, \lambda_e >> \lambda_D, I_p << I_d \quad (1.29)$$

where, a is the probe radius, $\lambda_{e,i}$ is the electron and ion mean free path and λ_d is the Debye length.

1.3.2 Resonance Probes

The plasma diagnostic based on resonance phenomenon is time honored idea [36, 53–56]. However, it has found renewed interest in last few decades where numbers of different approaches were realized for getting the information about the real state of plasma medium. They can be defined as the small conducting object (few cm in dimension) which is used to introduce a time varying local perturbation in to the plasma of frequency varies from MHz to GHz in order to determine the plasma permittivity from the relative shift in its resonance frequency. Due to lighter mass of electrons, they perform oscillations at a frequency either close to or equal to the plasma frequency, therefore by measuring the frequency one can get the value of plasma frequency and hence the electron density. The idea is similar to cavity resonance and interferometry method in the sense of introducing time-varying perturbation in plasma, but here the probes are developed for local measurement of electron density. The major advantage of resonance probes over electrical probes is to give local electron density without any need of temperature information. In this case, the frequency measurements are independent of thermal effects as the phase velocity of wave is much greater than the thermal velocity of particles in the plasma.

The dispersion relation of the electromagnetic waves propagating into the plasma with no dc magnetic field or of an ordinary wave in a dc magnetic field is given by [11]:

$$\omega^2 = \omega_{pe}^2 + c^2 k^2 \tag{1.30}$$

where, ω is the wave frequency, ω_{pe} is the plasma frequency, k is the wave number, and c is the speed of light in vacuum. The cold plasma permittivity κ_p is given by:

$$\kappa_p = n^2 = \frac{c^2 k^2}{\omega^2} = 1 - \frac{\omega_{pe}^2}{\omega^2} \tag{1.31}$$

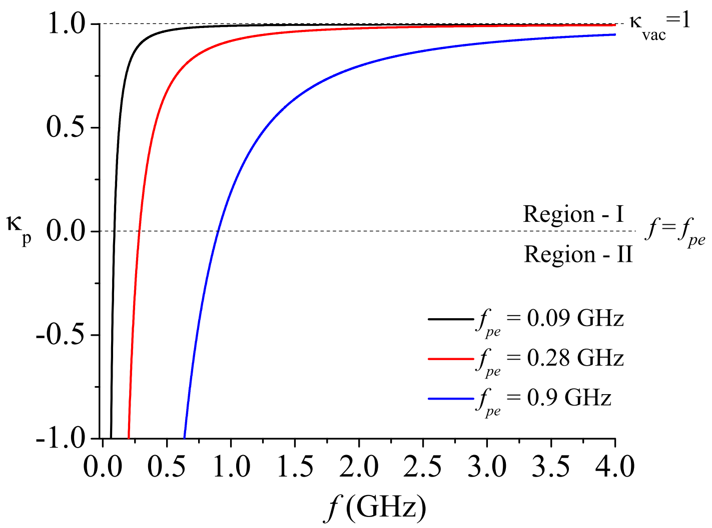

Figure 1.4: Plasma permittivity versus frequency applied electric field in plasma where region - I and region- II corresponds to the range of permittivity $0 \leq \kappa_p \leq 1$ and $-1 \leq \kappa_p < 0$ respectively.

By measuring the resonance frequency of the probe one can determine the cold plasma permittivity and the plasma frequency or electron density can be obtained. A plot of plasma permittivity versus f is shown in Fig. 1.4. The plot has two regions, the region-I and II. In the region-I the permittivity is in the range $0 \leq \kappa_p \leq 1$ while in the region-II is $-1 \leq \kappa_p < 0$.

The physical interpretation of the different regions is as follows: when the external frequency $f > f_{pe}$, the electrons respond in tune with the time-varying electric field unlike of ions and neutrals due to their significant difference in masses. Therefore, the plasma permittivity is similar to the permittivity of free space; hence κ_p is close to unity. As the frequency approaches the electron plasma frequency, the κ_p becomes zero and wave encounters cutoff. A wave gets reflected from the plasma medium at the plasma frequency, which gives the plasma frequency and hence the electron density. Generally, the diagnostic using resonance probes are mainly based on the frequency measurements either at cutoff condition or at frequency above the plasma frequency. However, there are some techniques such as plasma absorption probe [42] and plasma transmission probe [57] which works at a frequency below the plasma frequency. In this condition the introduced electromagnetic waves in the plasma becomes evanescent surface waves.

Among the different resonance probes [35, 36, 42–46], the HP is becoming increasingly popular for application in low temperature plasmas for measuring the electron density. The HP has been successfully applied in commercial plasma reactors which are routinely used in microelectronics industries [2, 27, 28, 58–73]. The detailed study about the operation of hairpin probe and its applications in reactive plasmas, high density plasmas, and in magnetized plasma will be discussed in the subsequent chapters of the thesis.

1.3.3 Optical Emission Spectroscopy

The basic principle of the technique is based on the detection of emission and absorption spectra of different wavelengths from atoms, molecules, and ions present in the plasma ensemble [15, 74, 75]. On this basis, the plasma spectroscopy is classified into passive method of emission spectroscopy and the active method of absorption spectroscopy. The population of species in an excited state depends on the various plasma parameters such as density and temperature of electrons and the heavy particles, radiating fields etc. Thus various population models such as corona model (CM), collisional radiative model (CRM) [76–78] are developed in order to understand the populating and depopulating processes for each individual energy level of particle. Precisely, the observables are shift, broadening, splitting, intensity ratios, intensity distribution, intensity, and the plasma parameters that can be obtain are ion velocity (v_i) from peak shifting, ion temperature (T_i) from Doppler broadening, magnetic field from Zeeman splitting, electric field from Stark splitting, electron temperature (T_e) and density (n_e) from intensity ratios, and ion density (n_i) from intensity.

Generally, the line-ratio technique is applied for measuring the electron density and temperature using OES [79]. In this technique, the dominant production and depopulation processes are considered in the population model for a given pair of excited levels which emit light of particular intensity. The model consists of set of rate balance equations of these two excited levels and therefore one can solve for population density ratio. By fitting the density ratio with the measured emission intensity, one can obtain the plasma parameters. Depending on the plasma discharge conditions, the technique is classified mainly into two kinds for measurements in argon plasmas. First method uses a CM for the plasma operates at low pressure and with low ionization ratio. Second method uses a CRM for the plasma operates at high pressure and relatively high ionization ratio. The accuracy of the results from OES depends on the quality of cross sections and rate coefficient data for the collisional-radiative processes.

The excited atom population distribution is generally affected by the electron density, electron temperature (T_e), and the gas temperature (T_g). However, the T_e and T_g are nearly constant for the low temperature collisionless plasmas. For instance, consider the higher excited levels such as Ar($3p_1$) and Ar($5p_5$) in low pressure argon plasma where the levels have very small excitation cross sections from the metastable since the angular momentum quantum number (J) is zero in this case. The governing electron-impact population transfer processes and rate equations can be found in the literature. One can obtain the electron density using the following relation [75]:

$$\frac{I_{Ar}(3p1)}{I_{Ar}(5p5)} = \frac{Q_{exc}^{Ar(3p1)}}{Q_{exc}^{Ar(5p5)}} \times \frac{1 + \frac{n_e}{n_{eC,5p5}}}{1 + \frac{n_e}{n_{eC,3p1}}} \tag{1.32}$$

Where, Q_{exc} is an effective rate coefficient of the electron-impact population excitation process and $n_{eC} = A/Q_{trans}$ is the characteristic electron density with A as Einstein coefficient and Q_{trans} electron-impact population transfer process. The n_{eC} is corresponding to the low energy electrons which contributes to the transfer process where as high energy electrons mainly contribute to the excitation. The above equation n_e values should be comparable with the n_{eC} otherwise the intensity would be independent of the electron density.

1.3.4 Microwave Interferometer

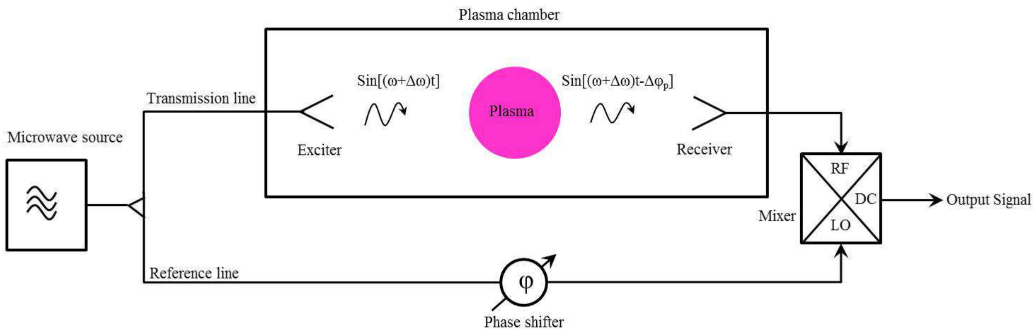

Figure 1.5: Block diagram of a conventional microwave interferometer [1] (RF is the phase shifted mw signal, LO is the reference signal from local oscillator, and DC indicates the voltage proportional to the detected phase shift).

The microwave interferometer [1, 9, 16, 17] is a device which is based on the principle of interference between two or more waves by coherent addition of electric fields. Depending on the type of interference whether constructive (in phase) or destructive (out of phase), the intensity will be modulated. The idea behind the measurement of electron density is to measure the phase shift of a microwave signal transmitting through the plasma and from the relative phase shift of the wave we can get the so-called line-integrated density [10, 16, 80].

The block diagram of the microwave interferometer setup is shown in Fig. 1.5. The arrangement is based on the Mach-Zehinder interferometer where the input signal is split into reference signal passed in the absence of plasma and transmitted signal passed through the plasma. The phase shift of the microwave signal happens in one arm due to plasma medium which is given by:

$$\nabla\phi = \int (k_{plasma} - k_o)dl = \int (N-1)\frac{\omega}{c}dl \tag{1.33}$$

where, $k_o = \omega/c$ and $k_{plasma} = N\omega/c$ are wave number in vacuum and in plasma respectively and N is the refractive index of plasma. Under cold plasma approximation for uniform magnetic field free plasma, the above expression can be simplified in terms of density over the path length L of mw signal as follows:

$$n_e = \frac{2cm_e\epsilon_o\omega_{mw}}{e^2L}\Delta\phi(rad) or\ n_e(cm^{-3}) = [7.3\times 10^{10}\times\Delta\phi(deg)]L(cm) \tag{1.34}$$

The advantage of this technique is being non-invasive and hence it does not require any information about the sheath. It is also unaffected by deposition or sputtering in particularly reactive plasmas. However, the major drawback of using interferometry is that it gives spatially averaged electron density in plasma. Besides, it requires complicated experimental setup as compare to the probe techniques.

1.4 The Resonance Hairpin Probe - Literature Review

Historically, the hairpin probe has been briefly introduced by Stenzel [35] in 1971, where local electron density in the magnetized plasma is obtained from the measurement of cold-plasma perpendicular dielectric constant using a small parallel wire resonator. Later on in 1976 [36], he presented the detailed paper about the technique where it was named as *microwave resonator probe*. Around that time there were other groups [26, 58, 81–84, 84–86] also involved in similar methods of measuring the electron density. This method of measuring electron density was considered to be superior to electrical probes because it gives electron density without any knowledge of electron temperature [36]. The method is found to be least perturbative since the probe works at a floating potential and also does not need any reference electrode. The measurements are also found to be independent of the sheath effects if proper attention is given to its design. Denisov et al [81] presented the detailed study of non-linear effects in a parallel wire conductor due to the pronounced localization of the electromagnetic field near the conductors. Kim et al [58, 82, 83] applied this probe for measuring spatially as well as temporally variation of electron density generated by a semiconductor bridge device for related input energy and electrode material probe. They termed as 'novel diagnostics technique employing a microwave resonator probe'. Kondrat'ev et al [84] revisited the theory by Denisov and showed that the probe operated in a non-linear mode could be useful for electron temperature measurements. One of the new applications of probe is for finding the negative ion density in conjunction with the laser photo-detachment technique is presented by Hebner et al [26]. Unlike the traditional microwave techniques, this method offers the possibility of spatially resolved negative ion density measurements. The probe operation was modified by implementing a hybrid system that used a coaxial cable loop antenna to excite the parallel wire resonator and a horn antenna as a sensor.

Looking at the literature, the technique is intermittently used until its revival in 2004 through pioneering work by Piejak et al [2, 60]. In his work, the probe theory and its new designs for determining the probes resonance frequency were explored and the probe is denominated as 'Hairpin resonator probe' because of its physical structural resemblance with the hairpin. The authors also accounted for the vacuum sheath around the resonator wires and proposed the modified electron density formula, which further enhanced the accuracy of the technique. There were two types of hairpin probes introduced in his work; one is based on transmission type and the other on reflection type operation. Precisely, these designs eliminate the bulky insulated bridge in Stenzel's probe design and the glass tube in Hebner's probe design, thus resulting in a compact design with reduced probe volume, smaller plasma perturbation, and less plasma depletion around the probe. However, the novel idea of reflection based hairpin probe comes from Prof. Hideo Sugai as per Piejak et al's expressed appreciation in his article [2]. Another paper by Haas et al [87] shows the study of electron and ion sheath effects on the resonant properties of HP.

At the same time, the development of floating probe is independently started by other groups [27, 57, 60, 63–67, 67–69, 71, 87] [Karkari et al, Booth et al, and Braithwaite et al]. Karkari et al showed one of the major contributions in doing the time resolved electron density measurement using floating hairpin probe in number of plasma reactors such as dual frequency CCP, DC magnetron discharge, Laser ablation plume similar to those that are commonly used in microelectronics industries. Recent work by Sirse and Conway [27, 28] has also shown HP as a useful device for negative ion diagnostic when used in conjunction with laser photo-detachment technique. Besides, the systematic study of probe resonances in strongly magnetized plasma by Gogna [73] showed for the first time the dual resonance property of the hairpin resonator. This will be subsequently discussed in details in the course of the thesis. The collaborative research work [71] of Curley et al and Gogna et al shows a hairpin probe as an important diagnostic tool for validating the results obtained using optical emission spectroscopy.

Recent studies on the application of hairpin probe in the collisional plasma from Sands and Sugai group [72, 88] widen the research area of investigation. Recently, Sugai and coworkers proposed a new compact design of hairpin probe called curling probe [89] for electron density measurements in reactive plasmas. In this case, the spiral slot instead of U-shaped hairpin is excited by a monopole antenna. The HP investigated in this thesis work is floating reflection type hairpin probe based on the work of Piejak [2].

1.5 Thesis Outline

The thesis is covered in total of six chapters that are outlined in this section. The chapter-1 provides a detailed statement of objectives of the study and describes the fundamentals of plasma physics on which the diagnostic theory is actually based for density measurements. The last part of the chapter provides research background and motivation behind studying the hairpin probe technique.

Chapter-2 reviews the basic theory behind the hairpin resonator probe. This includes the study of resonant properties of hairpin, ponderomotive effects, and principle of measuring the electron density. Apart from this, we presented the various designs of hairpin and its methods for detecting the resonance signal. Besides, the electric field distribution around the resonator and its resonant characteristics is obtained using FDTD simulation software. The results are compared with the experimental data. Furthermore, the preliminary density measurements by the probe are also presented.

Chapter-3 deals with the study of resonances of hairpin probe in the presence of adjunct dielectrics near its vicinity. The analytical models are proposed for correcting the electron density for two specific hairpin designs (1) Partially shielded hairpin (2) Hairpin covered with uniform dielectric sleeves. The models are experimentally verified.

Chapter-4 deals with the study of the resonant properties of the probe in presence of externally applied magnetic field. Due to anisotropic nature of the magnetized plasma, the probe measurements become direction dependent with respect to the magnetic field. The analysis of effective plasma permittivity observed by hairpin for specific probe orientation with respect to the magnetic field is presented. The influence of tunable parameters such as vacuum resonance frequency, plasma frequency, and gyro-frequency on the resonant properties of the probe is studied and experimental results are discussed.

Chapter-5 deals with the factors influencing the dispersion of the resonance signal. The hairpin resonator is theoretically studied based on its transmission line properties. Besides, the experimental results are discussed in support of the theory. The factors such as electron-neutral collisions, radiation losses, losses due to the excitation of the warm plasma modes at high densities and presence of strong magnetic field are qualitatively discussed. These factors act adversely on the sensitivity of the frequency measurements during the plasma operation.

Chapter-6 concludes the thesis work and presents the future recommendation of the resonance hairpin probe for plasma diagnostics.

CHAPTER 2

Fundamentals of Hairpin Resonator Probe

2.1 Introduction

The hairpin probe can be treated as a dipole antenna formed by joining two-quarter wavelength conductors joined back to back giving a total length of $\lambda/2$. This is conveniently formed by bending a piece of wire at the center in to the shape of a hairpin as shown in Fig. 2.1 [39–41].

The hairpin can be also visualized as two wire parallel wire transmission line with one end shorted while the other end is left open. When suitable frequency from a signal source is applied to the shorted-end, maximum coupling takes place at the specific frequency whose quarter wavelength equals the length of the pins. Under this condition the probe is said to be under resonance. This condition is characterized by observing maximum time-varying electric potential at the open end while maximum time-varying magnetic field is observed at the short-circuited end.

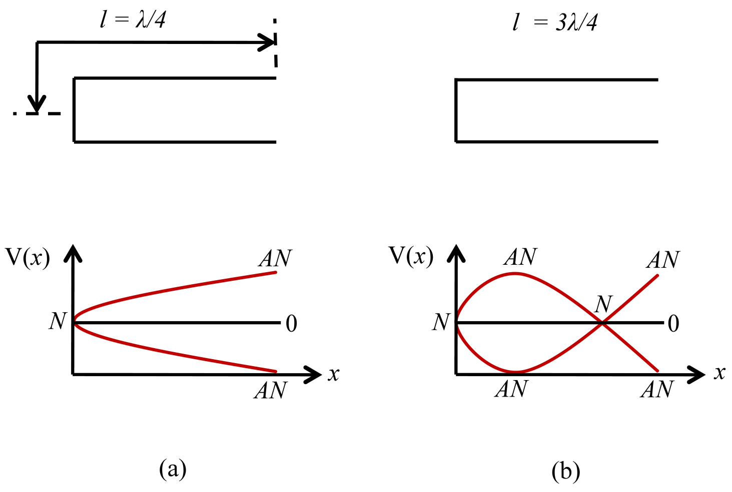

Figure 2.1: Standing wave formation in quarter-wavelength hairpin structure (a) $l = \lambda/4$ (b) $l = 3\lambda/4$.

Another way of looking at the hairpin is a waveguide supporting $l = \lambda/4$ standing wave. If an electromagnetic wave is excited from the short-circuit end, the energy propagates along the length of the probe at a speed determined by its dielectric permittivity ϵ of that characteristic medium surrounding the probe. The propagation constant k of the wave is given by [36]:

$$k = \frac{\omega}{c}\sqrt{\epsilon} = \frac{2\pi}{\lambda} \tag{2.1}$$

where, c is the speed of light in vacuum, ω is the angular frequency, and λ is the wavelength. For a given frequency, k is directly proportional to the background permittivity.

Section 2.2 discusses the physical mechanism of resonance condition. For detecting the resonance condition, a loop antenna is generally placed close to the short-circuited end which picks up the time-varying magnetic field. Section 2.3 and 2.4 presents various designs of hairpin probes and methods for detecting its resonance frequency respectively. Section 2.5 presents an FDTD simulation [90] used for of simulating the spatial electric field duration between the pins. The simulation is also used for benchmarks of experimental data in vacuum or air. This is followed with some practical examples of electron density measured in inductive coupled plasma reactor as presented in section 2.6. Summary is given in section 2.7.

2.2 Resonance of the Hairpin in Plasma Medium

By substituting $\lambda = 4L$ in Eq. 2.1, we can obtain the resonance frequency. This is expressed as [36]:

$$f_r = \frac{c}{4l\sqrt{\epsilon}} = \frac{f_o}{\sqrt{\epsilon}} \tag{2.2}$$

where, $f_o = c/4l$ is the resonance frequency in vacuum ($\epsilon = 1$), which is inversely related with the hairpin length (l). When the space between the pins is filled with dielectrics the resonance frequency tends to shift to a lower value than in vacuum since the relative permittivity of dielectric is greater than unity.

Plasma can also be treated as dielectric. If the thermal motion of electrons can be considered weak as compared to the electric field set-up between the pins, then one can model the plasma permittivity based on cold plasma approximation, which ignores the thermal motion of electrons. At low pressures, the electron neutral mean free path can be larger than the separation between the pins. Hence plasma permittivity is given by [11]:

$$\epsilon_p = 1 - \frac{f_{pe}^2}{f^2} \tag{2.3}$$

Plot of plasma permittivity as a function of frequency is shown in Fig. 1.4. At very high frequency plasma, permittivity approaches to 1.0 (as in case of vacuum). While it has negative values for frequencies $f < f_{pe}$ and singularity at $f = f_{pe}$. For $f > f_{pe}$, we observe that the frequency dependent plasma permittivity is less than 1.0. Therefore, Eq. 2.2 suggests that the resonance frequency expected to shift to a higher value as compared to that in vacuum.

This can also be understood from the concept of wave velocity in a medium from the given equation:

$$v = \frac{c}{\sqrt{\epsilon_p}} = f\lambda \tag{2.4}$$

The above equation can be further simplified in terms of wavelength as follows:

$$\lambda = 4l = \frac{c}{f\sqrt{1-\frac{f_{pe}^2}{f^2}}} \tag{2.5}$$

The above equation suggest that the electromagnetic wave gets elongated to infinite as the applied frequency approaches the plasma frequency. This is particularly the case of plasma absorption phenomenon where the incident wave suffer full absorption of its energy in the plasma. Therefore, the plasma frequency acts like a cutoff frequency below which wave cannot propagates.

On substituting Eq. 2.3 in Eq. 2.2 and replacing f with f_r, we obtain the dispersion relation given by:

$$f_r^2 = f_o^2 + f_{pe}^2 \tag{2.6}$$

The above equation can be simplified to obtain the electron number density [6, 11] as given by:

$$n_e[10^{10}cm^{-3}] = \frac{m_e\epsilon_o\omega_{pe}^2}{e^2} = 1.23\left[\left(\frac{f_r}{GHz}\right)^2 - \left(\frac{f_o}{GHz}\right)^2\right] \tag{2.7}$$

The electron density formula can also be expressed in the following form:

$$n_e[10^{10}cm^{-3}] = 1.23\left(\frac{f_o}{GHz}\right)^2\left(\frac{1}{\epsilon_p} - 1\right) \tag{2.8}$$

where, m_e is the mass of electron, e is the electronic charge and ϵ_o is the electric constant. The above analysis also holds for the magnetized plasma as long as $f_{ce} << f_r$, where f_{ce} is the electron gyro-frequency. The effect of strong magnetic field on the probe's resonance frequency is dealt in chapter-4 of the thesis.

2.3 Design and Construction of Hairpin Probe

The hairpin probe has three key elements: (1) 50 Ω coaxial line feed through, (2) Loop antenna and (3) the hairpin. These are schematically shown in Figs. 2.2 and 2.3.

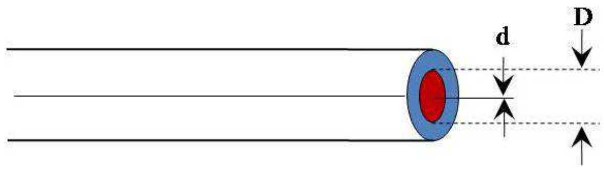

Figure 2.2: 50 Ohm Coaxial Line for Hairpin Probe.

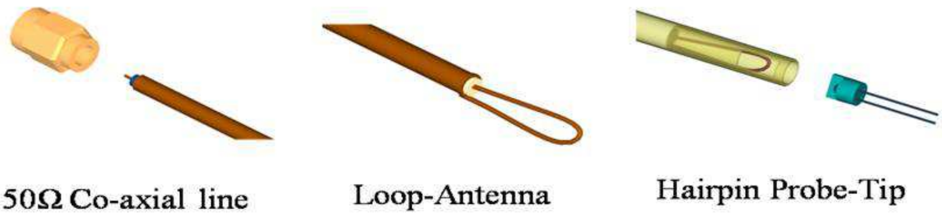

Figure 2.3: Assembly of Hairpin probe.

1. 50 Ω coaxial line feed-through

   The function of the coaxial line is to carry the microwave (a few dbm power) from the signal source to the loop antenna. This is commonly made of semi-rigid coaxial cable or can be constructed using refractory materials such as quartz, tungsten wire and copper tube to with stand high heat during operation in plasma environment.

   For 50 Ohm coaxial, the dimensions are related according:

$$Z_o = \frac{138}{\epsilon^{0.5}} \log(D/d) \tag{2.9}$$

where, d is diameter of center conductor, D is inner diameter of cable shield and ϵ is dielectric constant. The coaxial is encased inside ceramic tubing which protects the outer conductor, usually copper from being exposed to plasma. One end of the coax is fitted with the SMA (Sub-Miniature version A) for feeding in microwave signal from the generator.

2. The loop-antenna

   The center conductor at the open end of the above 50 Ω coaxial line is formed as a loop and soldered to the outer conductor. Typical size of the loop antenna may vary from 2.0 to 3.0 mm depending on the size of the hairpin. In some cases dual loop antenna are used, one for carrying the signal from the source while the other is used for detecting the resonance signal as shown in figure below:

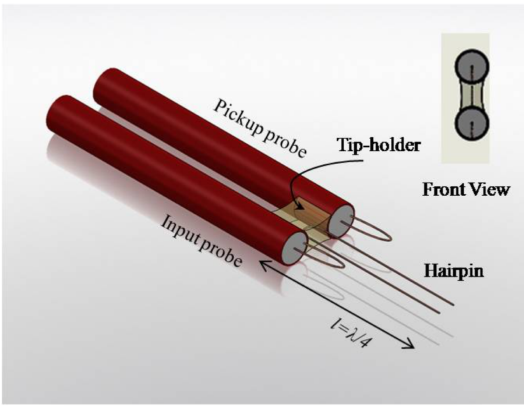

Figure 2.4: Stenzel's transmission type hairpin probe.

   Dual loop antenna attached to individual coaxial are commonly described as transmission type hairpin probe. While single loop system used for both transmitting the signal to the loop antenna as well detecting the resonance is known as reflection type hairpin probe. This shall be discussed in the next section.

3. The hairpin

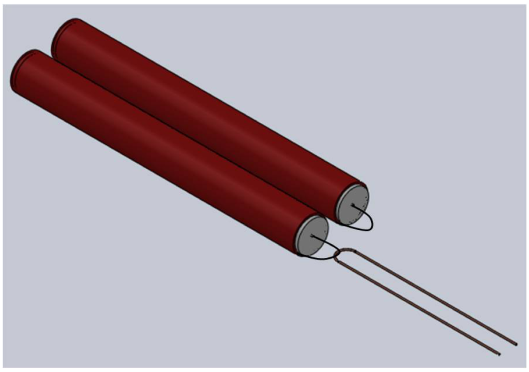

Figure 2.5: Piejak's transmission type hairpin probe [2].

The hairpin is formed by bending a piece of wire to form a U-shape structure. The short circuited end is placed close to the loop where a fixture is used to hold it with the 50 Ω coaxial feed-through structure. The wires of the hairpin resonator are generally made of tungsten with typical length between 10.0 mm to 30.0 mm long and separation between the pins of usually 3.0 mm to 4.0 mm.

Typical hairpin probes are as follows:

Transmission type hairpin probe

The transmission types are shown in Figs. 2.4 and 2.5. They were originally used by Stenzel [36]. In this case one loop is used for exciting the hairpin while the other loop is used for detecting the emf generated the time-varying current flowing through the hairpin at the point of resonance.

In a slight modification from Stenzel's design, Peijak soldered the hairpin directly to the input loop antenna used for exciting the resonator while the other is used for the detection of the resonance. This compacts the design as compared with Stenzel's probe.

Reflection type hairpin probe

A further simplification of hairpin probe design was proposed by Peijak [2] who used the same loop antenna for excitation as well as for the detection of the resonance signal. Hence single coaxial line and a loop antenna are used. The hairpin was directly attached to the loop antenna. This revolutionized the application of hairpin since 2004.

Following that several groups researched in to various design aspects of the hairpin to make it electrically isolated from the loop antenna. Important ones are those published by Briathwaite [59], Karkari [65, 68], and Booth [67]. Because the probe is floating, it allows the probe to be used in high amplitude rf plasmas typically used for plasma processing in micro-electronic industries.

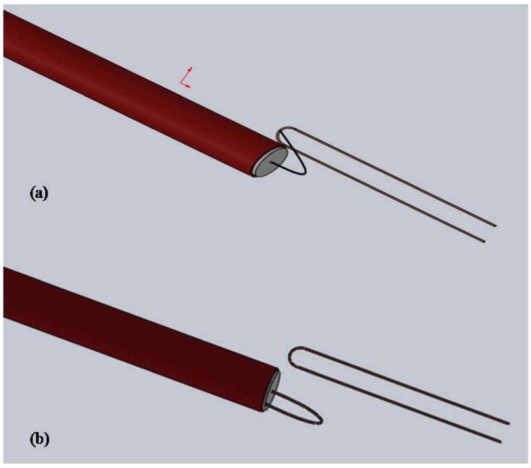

Figure 2.6: Piejak's reflection type hairpin probe [2]: (a) dc coupled hairpin probe (b) fully floating hairpin probe.

The floating hairpin has advantage because the sheath around the pins is smaller. Because of this reason, the fully floating reflection type hairpin probe is investigated in our thesis work. In this thesis work, we shall be using the reflection probe for the study. The measurement of resonance peak is discussed in the next section.

2.4 Resonance Signal Detection and Data Processing Methods

Main components for the detection of resonance signal is the variable frequency source (2.0 to 8.0 GHz), a directional coupler, and a zero-bias Schottky diode as shown in Fig. 2.7.

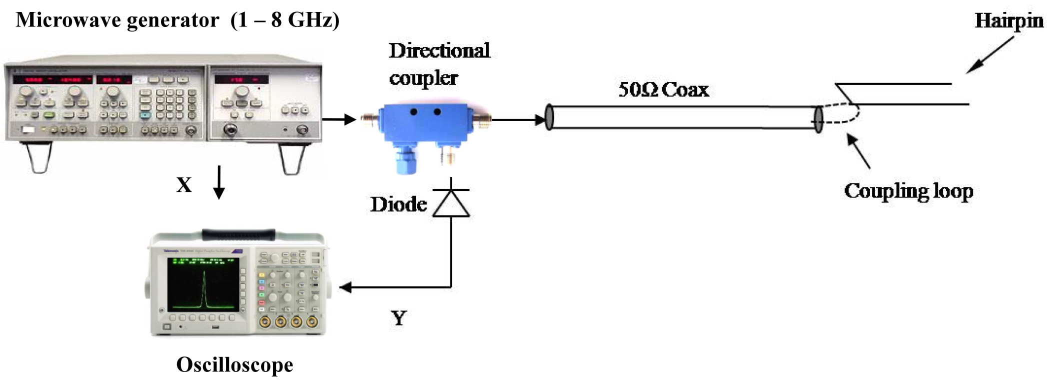

Figure 2.7: Hairpin probe setup for detecting the resonance frequency signal.

The directional coupler is positioned between the microwave source and the hairpin. It allows to measure the reflected power emerging from the closed end of the 50 ohm coaxial line terminated by the loop-antenna. The amplitude (r.m.s value obtained using the Schottky diode) of the reflected signal at all frequency is monitored on the oscilloscope. If the input signal frequency approaches the resonance frequency, maximum power coupling takes place between the loop and the hairpin. Therefore the reflected signal amplitude drops drastically. This is shown in the Fig. 2.8. When immersed in plasma the probes resonance frequency shift to higher frequency as shown in Fig. 2.9, since the relative dielectric constant of plasma is less than that of the vacuum.

In some cases imperfection in SMA connection of the feed-through may result in unwanted reflected wave interferences in the background signal. This can be eliminated by subtracting the reflected signal obtained at one time in vacuum from

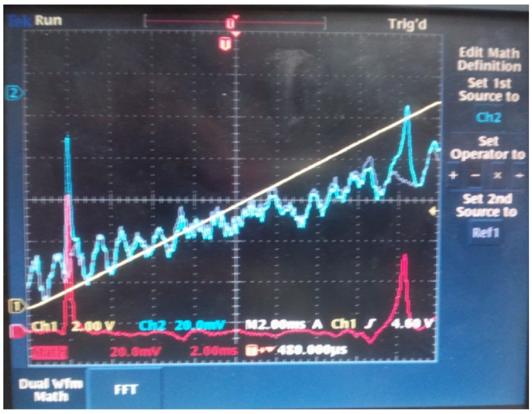

Figure 2.8: Resonance frequency signal in vacuum.

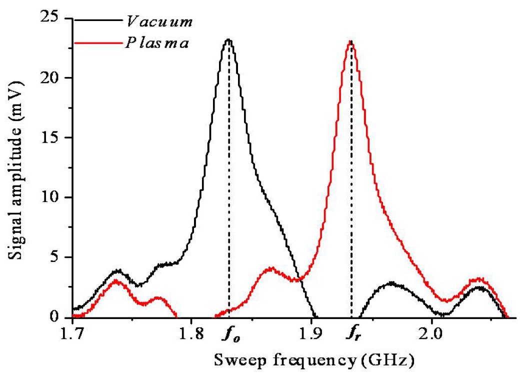

Figure 2.9: Resonance frequency signal in vacuum and in plasma.

that obtained in plasma. An example of this is shown in Fig. 2.8 where the first peak corresponds to the fundamental frequency ($l = \lambda/4$) of the hairpin whereas other is its harmonic ($l = 3\lambda/4$). The subtraction is applied with the hairpin on and removed from the vicinity of the loop in order to obtain the common-mode background.

2.5 Simulation of Hairpin Resonator

In this section, the electromagnetic field simulation of the hairpin using CST MICROWAVE STUDIO [90] based on the FDTD (finite difference in time domain) is presented. The software simulates the microwave signal transmitted in and reflected from the hairpin probe. The primary objective is the simulation of electric field distribution around the hairpin. Secondary is to perform comparative study of probe's resonance signal in simulation and in experiments.

2.5.1 Model of Hairpin Resonator

The diagram of the hairpin resonator and coupling loop antenna is shown in Fig. 2.10. The length of the hairpin is shown by L, separation between wires by w, and

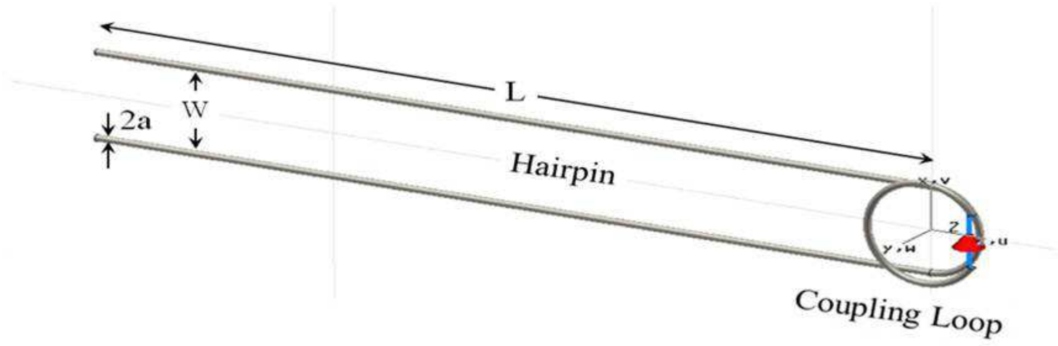

Figure 2.10: Simulation model of hairpin resonator probe.

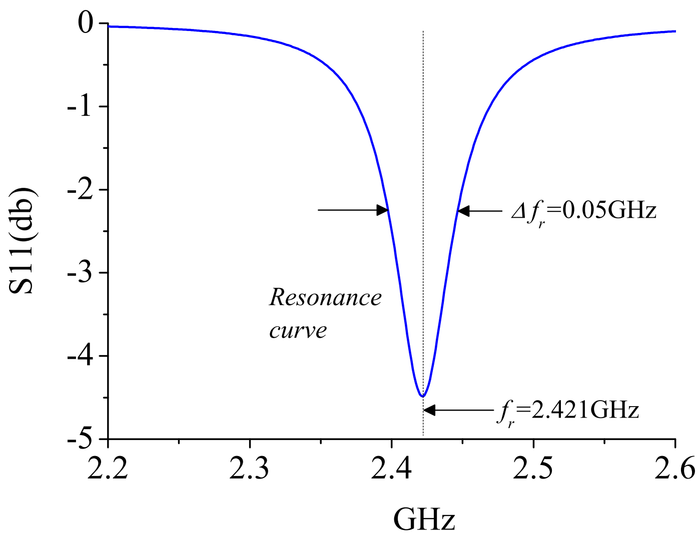

Figure 2.11: Typical resonance curve showing resonance frequency and signal width (FWHM).

radius of the wire is a. The microwave power near the closed end of hairpin is supplied by defining the port type, impedance, location, and excitation signal. The coupling loop antenna is completely isolated from the hairpin in order to act hairpin as floating.

A small microwave power is fed to the closed end of hairpin and the reflected signal from the input port given by S-parameter S(1,1) is measured. At resonance, the reflected signal goes to minimum, which result in full transfer of microwave energy into the hairpin resonator. Typical resonance signal obtained in the simulation is shown in Fig. 2.11. The central frequency of the resonance curve is the resonance frequency and full width at half maxima (FWHM) Δf is signal width. The parameter that defines the quality of the resonance curve is called the Q-factor. It is defined as the ratio of the central frequency to the signal width. For instance, a broader peak has smaller value of Q-factor. The detailed discussion about the signal width of the probe signal is discussed in chapter-5 of the thesis.

2.5.2 Electric Field around Hairpin Resonator

Different E-field regions around hairpin resonator

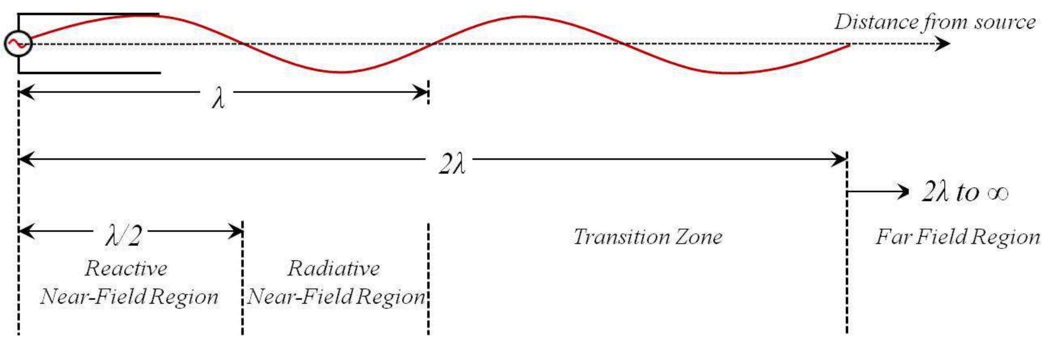

Figure 2.12: Different field regions around the hairpin resonator.

The antenna [40, 41] can be used for two main purposes: one is for the energy propagation into a medium and the second is for storing energy in a small volume. On this basis, the field regions of the antenna are characterized as *reactive field* and *ra-*

diative field. The reactive field is the region where the standing (stationary) waves exist which represents the stored energy. The radiation field is the region where the propagating waves transfer energy from one point to another. There is another intermediate region called Radiative Near-field or Fresnel region where the radiation fields are dominant and the field distribution is dependent on the distance from the antenna. The Far-field also called Fraunhofer region where the field distribution is independent of the distance from the antenna i.e. for the propagating waves. The region between the far-field and near-field is the transition zone. Although the hairpin resonator supports standing waves, the part of the energy can be dissipated via radiation in the medium. The regions around the hairpin are sketched in Fig. 2.12.

E-field distribution in the near field region of hairpin

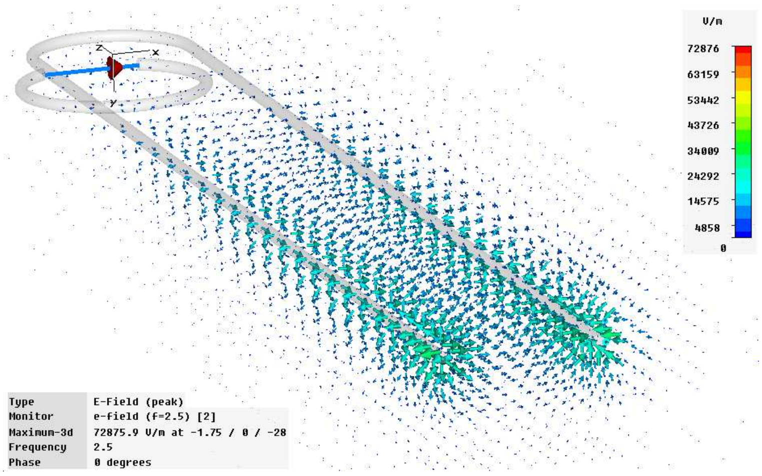

Figure 2.13: Vector plot of E-field around the hairpin resonator.

In the simulation, the electric field distribution around the hairpin resonator is obtained. The vector plot of field is shown in Fig. 2.13. It is obvious that the electric field is mainly concentrated between the wires. In addition to the field component in the plane of the hairpin it also has strong fringing field components. The absolute value of E-field and one of the strongest x-component for different cut-planes are presented from Figs. 2.14 to 2.19. On the basis of these results, we can

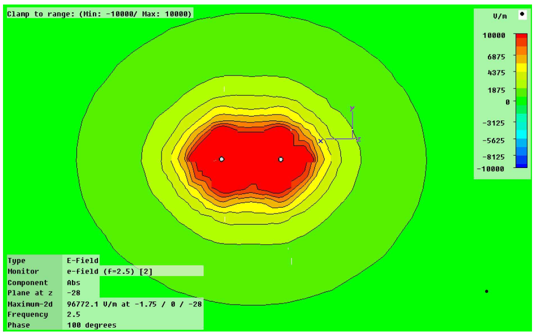

Figure 2.14: Absolute value of E-field from front.

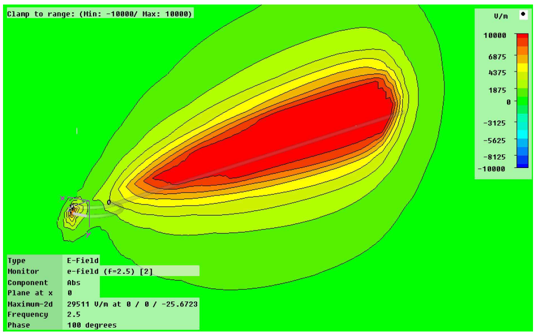

Figure 2.15: Absolute value of E-field in mid-plane.

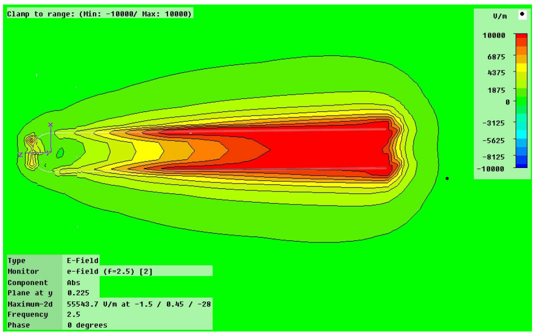

Figure 2.16: Absolute value of E-field from top.

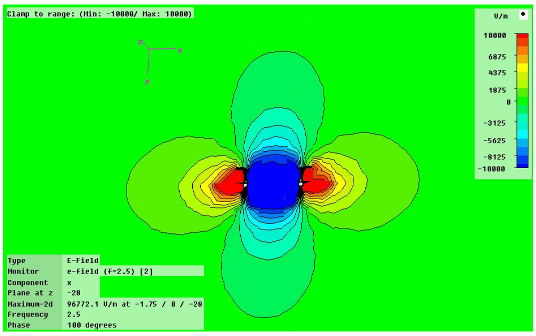

Figure 2.17: E_x component of field from front.

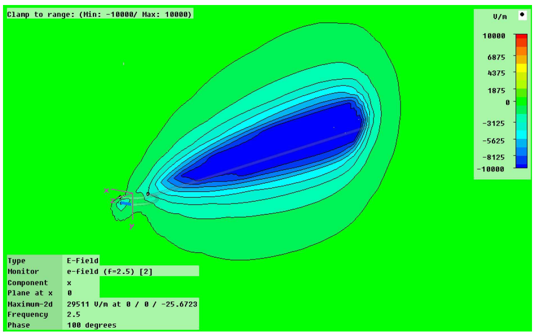

Figure 2.18: E_x component of field in mid-plane.

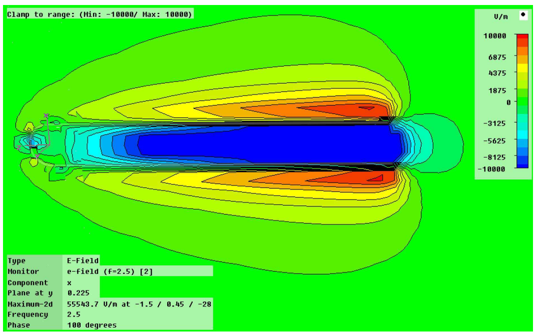

Figure 2.19: E_x component of field from top.

say that the spatial resolution of the hairpin is roughly given by its dimensions as the electric field is mainly concentrated between the wires. The typical dimensions of the hairpin are 25 mm in length and 3 mm of wire separations. Therefore, if the plasma has a steep gradient in electron density smaller than the dimension of hairpin then the probe gives average of the electron density near its vicinity.

2.5.3 Typical Characteristics of Hairpin Resonance Signal

Effect of hairpin dimensions on the resonance frequency

The resonance frequency is ideally obtained when the effective path length $2L+w = \lambda/2$. In most cases the $L >> w$ therefore it is assumed that $L \approx \lambda/4$. However for shorter hairpin the finite width cannot be ignored. This is shown in the Fig. 2.20.

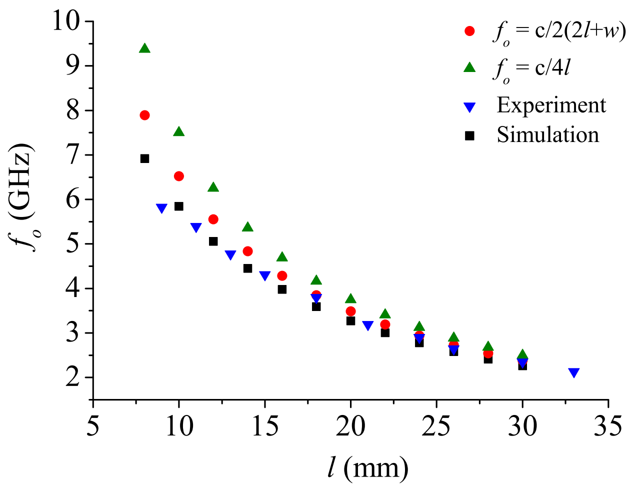

Figure 2.20: Resonance frequency versus length of hairpin (w = 3.0 mm).

For longer hairpins, all the results match very well. For shorter hairpins $f_o = c/4L$ gives an overestimated value of resonance frequency because of ignoring the finite width. The typical resonance signals obtained for different length of hairpins in simulation and experiment are shown in Figs. 2.21 and 2.22 respectively. The

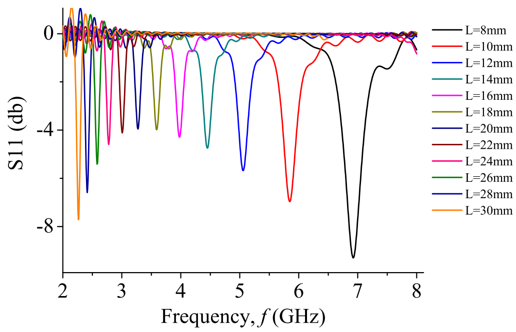

Figure 2.21: Typical resonance signal obtained in simulation for different lengths of hairpin.

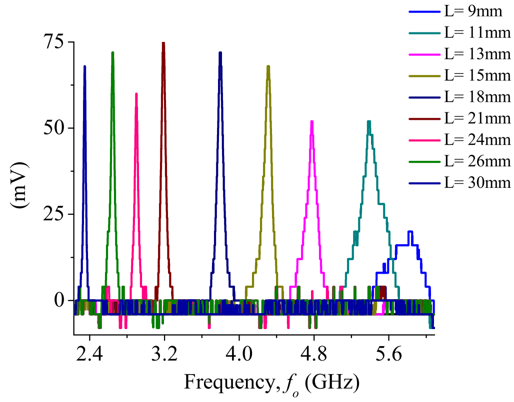

Figure 2.22: Typical resonance signal obtained in experiment for different lengths of hairpin.

signal amplitudes and their widths are found to be dependent on the resonance frequency. The signal widths are calculated for each signal and they are plotted in Fig. 2.23. The Q-factor of the resonance signal defined as $fcenter/\Delta f$ is plotted in Fig. 2.24. Increase in the signal width results in the decrease of Q. Lower values of Q implies lossy signal as the energy stored in the resonator is dissipated by Ohmic heating of the wire. However, the comparison between simulated and experimental values of quality factor in Fig. 2.24 indicates that the experimental Q is greater than the simulation one. The simulation could have been improved to give the better quality factor by increasing the amount of microwave energy coupled into the hairpin structure. Besides, the physical trends of the Q-factor on increasing the length are in good agreements with each other. In our present study, the numerical values of Q does not have significant importance as our primary concern is to study the physical factors influencing the Q-factor of probe.

The Ohmic resistance in ohm per meter depends on the wire radius, the electrical conductivity (σ_{line}) of the wire material and inversely proportional to the skin depth which depends on the frequency. The resistance is hence defined as [91]:

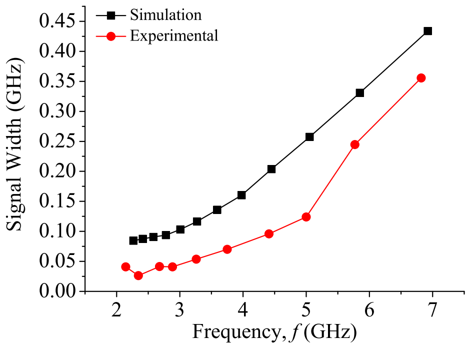

Figure 2.23: Signal width vs probe frequency.

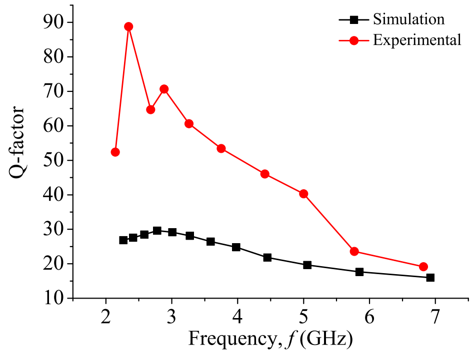

Figure 2.24: Q-factor vs probe frequency.

$$R = \frac{1}{2\pi a \sigma_{line} \delta} \tag{2.10}$$

The skin depth of the conductor is given by $\delta = \sqrt{\frac{2\rho}{\omega \mu_o \mu_r}}$ where, $\rho =$ is bulk resistivity (ohm-meter), ω = frequency (Hertz), μ_o is permeability constant (Henry/meter) $=4\pi \times 10^{-7}$, and μ_r is relative permeability (usually one). Therefore the resistance offered will increase with operating frequency. Hence lower values of Q is expected when at higher frequencies. This fact is consistent with the experimental observation in Fig. 2.24. The relative plots of the resonance signal for different frequencies in Fig. 2.25 show that the amplitude of the signal drastically reduced at 5.86 GHz as compared to 2.346 GHz. Therefore it is important to work with longer hairpin for achieving better signal to noise ratio.

The quality-factor of the resonance signal also depends on the type of resistive material used for making the hairpin. Figs. 2.26 and 2.27 below shows typical resonance curves for different wire material such as copper (A), molybdenum (B), Nichrome (C), and Aluchorme (D).

The signal width and Q-factor as a function of probe resistivity is presented in Figs. 2.26 and 2.27 respectively. The simulations results are found to be in good agreement with the experiments.

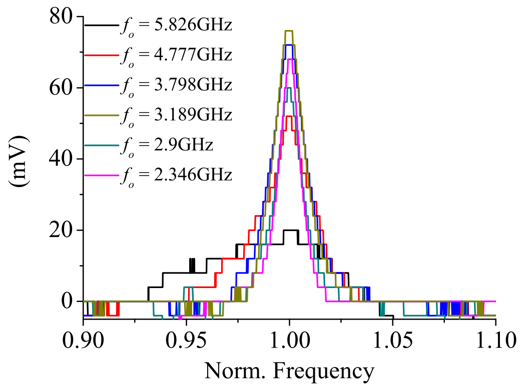

Figure 2.25: Normalized resonance signal for difference resonance frequencies where the normalization is done by dividing the frequency axis by resonance frequency of individual signal.

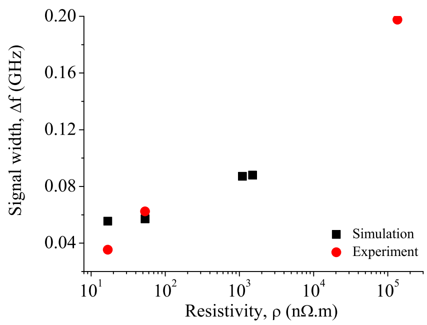

Figure 2.26: Signal width versus probe resistivity.

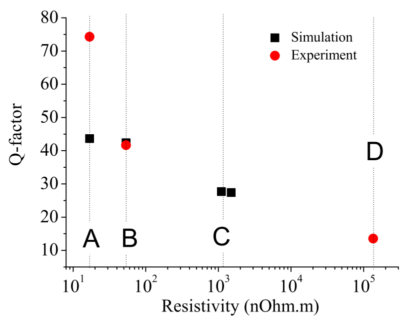

Figure 2.27: Q-factor versus probe resistivity.

Measurement of dielectric constant of a medium using resonance frequency shift of hairpin

In principle, the hairpin measures the effective permittivity surrounding the pins. This can be expressed in the form,

$$\epsilon = \frac{f_o^2}{f_r^2} \tag{2.11}$$

where, f_o and f_r are the resonances measured in vacuum and in the medium. In order to verify the above formula we devised an experiment in which the hairpin was immersed in silicone oil of known permittivity 2.55 as shown in Fig. 2.28.

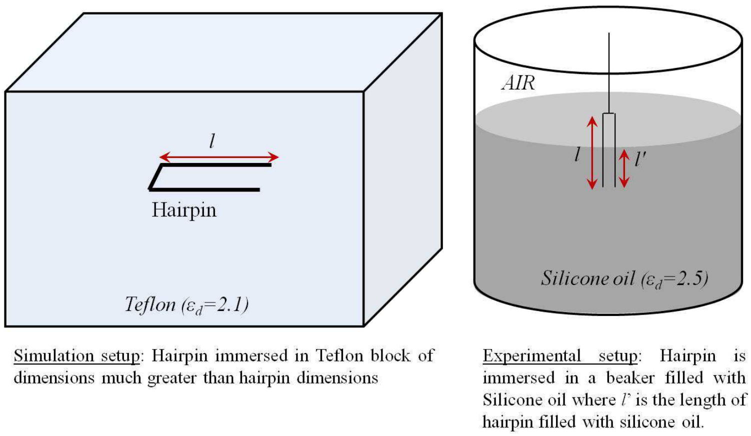

Figure 2.28: Setup for measuring the dielectric constant of the medium surrounding the hairpin using resonance frequency shifts.

When the hairpin is partially immersed in the silicone well, it sees an effective permittivity due to air and oil. The effective permittivity approaches the dielectric constant of the silicone (2.55) when the probe is fully immersed in the oil as shown in Fig. 2.29. A similar feature is also observed in simulation where the hairpin is completely filled with a Teflon dielectric (ϵ = 2.1) register a shift which gives an dielectric constant of Teflon as shown in Fig. 2.30.

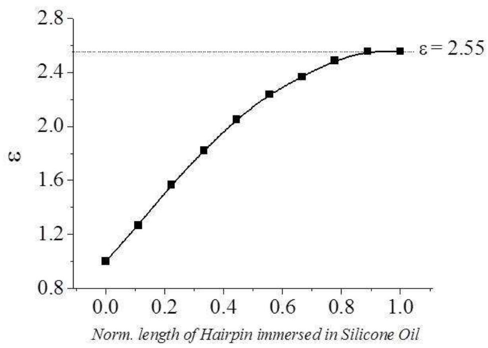

Figure 2.29: Experimentally measured effective dielectric constant for hairpin surrounded by air and silicone oil as shown in Fig. 2.28.

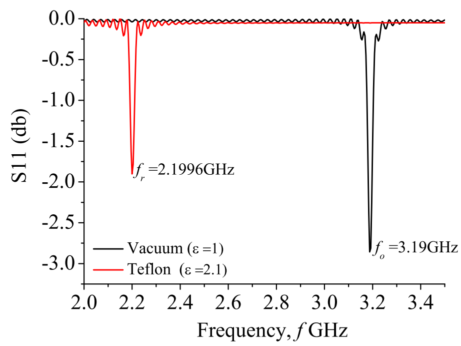

Figure 2.30: Typical resonance signals obtained for the cases when hairpin is surrounded by only vacuum (black peak) or Teflon medium (red peak).

Effect of mutual coupling on the probe's resonance signal

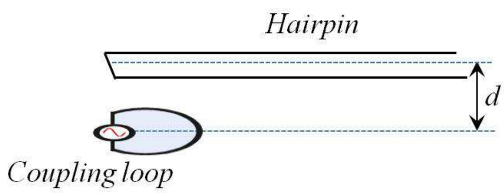

Figure 2.31: Picture shows the hairpin and coupling loop antenna where d is the separation between them.

The position of the loop antenna from the hairpin has dramatic influence on the resonance frequency. For systematically studying this effect, we performed an experiment by fixing the position of the loop while the hairpin was moved away from the loop and the corresponding resonance signal was recorded. Schematic of the setup is shown in Fig. 2.31 while the experimental and simulation results are shown in Figs. 2.32 and 2.33 respectively.

The deviation from the actual resonance due to change in the position of the loop are plotted in Figs. 2.34 and 2.35. Both simulation and experimental results points

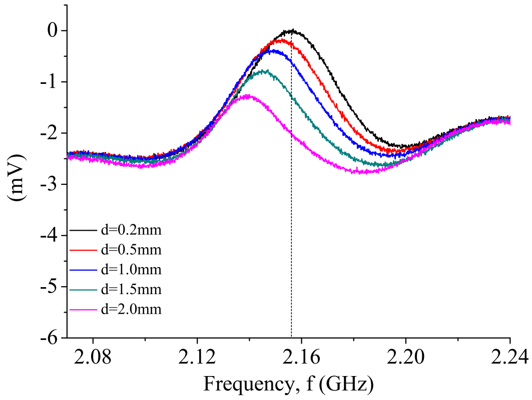

Figure 2.32: Resonance signals obtained for different separation (d) between loop and hairpin in experiments.

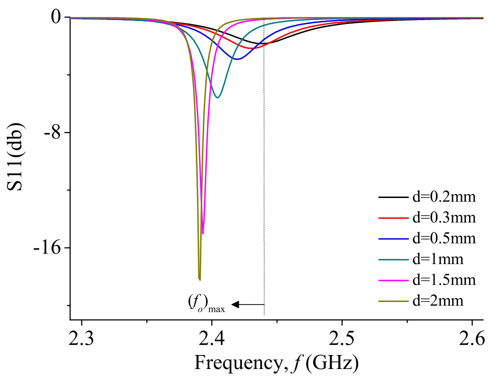

Figure 2.33: Resonance signals obtained for different separation (d) between loop and hairpin in simulation.

towards similar effect, while in the simulation the drop is 1.9 % as compared to 0.7 % as obtained from experiment. Similarly, the percentage change in magnitude of signal width in simulation is 87 % and in experiments it is 30 %.

Drop in signal amplitude is due to decrease in the coupled microwave energy into the hairpin. On the other hand, shift of resonance frequency towards the lower side is due to the increase in effective capacitance of the hairpin as the separation between loop and hairpin increases.

2.6 Electron Density Measurements and Typical Resonance Signals in Plasma

For measuring electron density in plasma, the hairpin was introduced in an inductive radio-frequency source. The typical resonance signals in plasma are shown in Fig. 2.36. The background noise is subtracted from the data. The amplitude of the resonance peak is found to decrease with the increase in electron density. This may

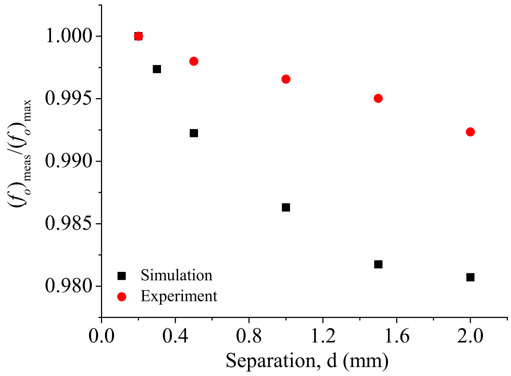

Figure 2.34: Normalized vacuum resonance frequency versus separation between coupling loop and hairpin where $(f_o)_{max}$ is the frequency corresponding to best coupling case.

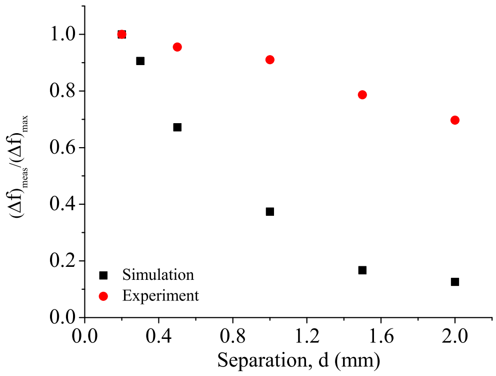

Figure 2.35: Normalized signal width versus separation between coupling loop and hairpin, where Δf_{max} is the frequency corresponding to best coupling case.

be attributed to losses due to radiation, Ohmic heating and dielectric losses in the presence of plasma. At very high densities typically $10^{12} cm^{-3}$, we observed complete loss of the resonance signal against the background noise. A comprehensive study of the factors influencing the quality of resonance signal is presented in chapter-5.

As expected the electron density is found to scale with the discharge power as plotted in Fig. 2.37. Fig. 2.38 shows the electron density as a function of discharge power for two dimensions of hairpin with wider and smaller separations such that total physical length i.e. $2l+w$ remain fixed. The density measured using the various probes are found to be independent of hairpin dimension. Similar results obtained for high and low Q probe as well as hairpins of two different resistive materials in Figs. 2.39 and 2.40 respectively. The high and low Q probe in Fig. 2.39 have been designed by changing the separation between the coupling loop antenna and the hairpin resonator.

The variation in the shape of the hairpin can result in shifting the vacuum frequency as the resultant of inductance and capacitance is slightly modified. However

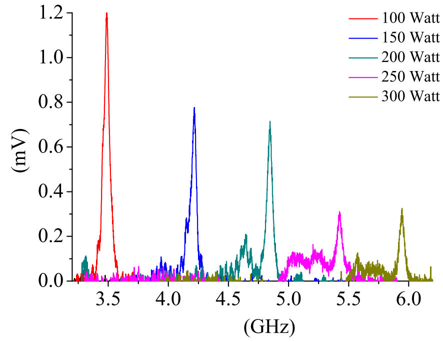

Figure 2.36: Resonance signal obtained for different powers in argon discharge at 10mTorr.

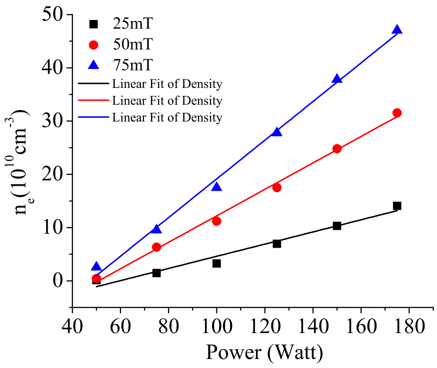

Figure 2.37: Density versus discharge power for different operating pressures.

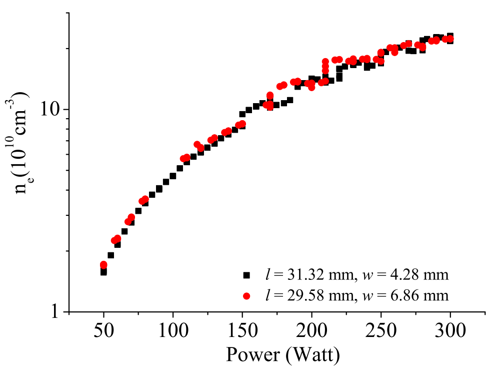

Figure 2.38: Density versus discharge power measured using two hairpins of different widths.

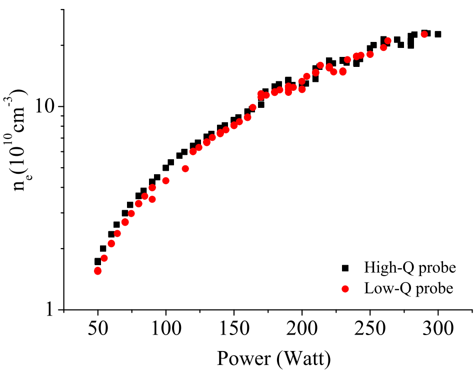

Figure 2.39: Density versus discharge power for two hairpins having low and high signal to noise ratio.

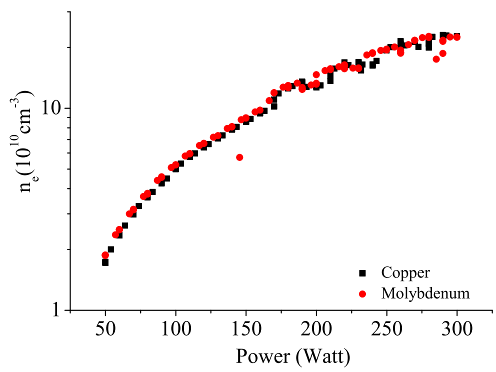

Figure 2.40: Density versus power for two different material of hairpin of length = 31.61mm, width = 4.69mm, and f_o = 2.232 GHz.

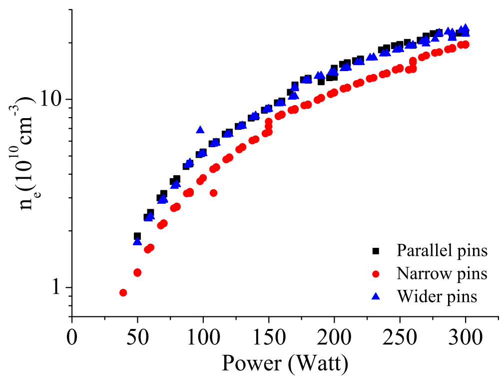

Figure 2.41: Density versus power, where f_o of hairpin having parallel pins, narrow pins and wider pins are 2.2986 GHz, 2.2326 GHz, and 2.3586 GHz respectively.

no significant difference in the measured density is observed as shown in Fig. 2.41. In the case when pins are tapered towards the end, it may be likely that the overlapping sheaths of both pins can result in measuring an under-estimated density as compared with the ideal or the wider case.

2.7 Summary and Conclusion

We have described the fundamental property of the hairpin resonator and its principle of measuring electron density measurement. A comprehensive experimental and simulation study is presented which highlights some of the important aspect about the performance of hairpin which is directly linked with the plasma properties and the basic construction of the hairpin. Besides, we have presented the brief description about the various designs of hairpin probe used by different research groups and effective method for detecting resonance signal. The hairpin probe investigated in this thesis is fully floating and based on the reflection mode operation.

CHAPTER 3

Electron Density Measurement with Fully-Shielded and Semi-Shielded Hairpins

Ideally the hairpin should be a perfectly parallel conductor with its pins immersed in the plasma completely. However, if an additional dielectric with relative permittivity, $\kappa_d > 1$, is attached or placed adjacent to the hairpin, it effectively modifies the permittivity. Therefore, the characteristic resonance frequency tends to shift towards the lower frequency f_o^* as compared with the ideal probe in vacuum f_o ($\kappa_d = 1$). This can be understood from the following relation,

$$f_o^* = \frac{f_o}{\sqrt{\kappa_d}} \tag{3.1}$$

If Δf_o is the shift in vacuum frequency from the ideal scenario, we can write,

$$f_o^* = f_o - \Delta f_o \tag{3.2}$$

With the same probe placed in plasma, it is expected that the resultant effect would be cumulative. Hence the shifted resonance frequency f_r^* in plasma is given by,

$$f_r^* = f_r - \Delta f_r \tag{3.3}$$

Plugging Eq. 3.2 and Eq. 3.3 in electron density formula given in Eq. 2.8 we obtain,

$$n_e(10^{10}cm^{-3}) = 1.23[(f_r^2 - f_o^2) + error] \tag{3.4}$$

where, the *error* term is expressed as,

$$Error = (\Delta f_r)^2 - (\Delta f_o)^2 - 2[f_r(\Delta f_r) - f_o(\Delta f_o)]. \tag{3.5}$$

Typically the non-zero Error term in the above equation is negative. This leads to underestimated electron density measured by such hairpins.
The presence of adjunct dielectrics is a practical problem while designing the support structure for the hairpin probe. The first important case addressed in this chapter is related to the probe-tip holder. Typically a dielectric fixture as shown in Fig. 3.1 helps in attaching the short-circuited end to the 50Ω coaxial. In certain cases, the hairpin is directly glued to the probes feed-through using castable ceramic or glassy material that supports the short-circuited end of the hairpin [2, 36, 62]. This is required for keeping the hairpin at the pre-calibrated position giving maximum coupling from the loop antenna.

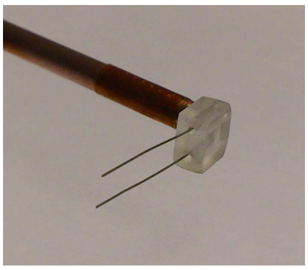

Figure 3.1: Partially shielded probe (PSP) using perspex.

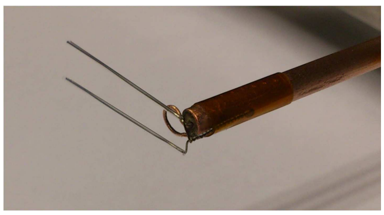

Figure 3.2: Hairpin with uniform dielectric quartz sleeves.

Another practical application requires the surface of the metallic pins to be insulated from the plasma using suitable dielectric coatings that helps in protecting the metal body exposed to reactive etch plasmas. This can be achieved by introducing quartz or ceramic sleeves as shown in Fig. 3.2. Covering the outer surface can improve the longevity of the pins; improve the quality of the resonance signal while maintaining the plasma clean.

In both of the above examples, the semi-shielded or fully-shielded hairpins ends up measuring underestimated electron density. We address these specific cases in the following sections.

In section 3.1 we present the experimental setup used for the study of external dielectrics on probes resonance frequency. In section 3.2 and 3.3 we take specific cases required for the calibration of measured electron densities for the semi-shielded hairpin and the resonator pins with insulating sleeves. Summary and conclusion is presented in section 3.4.

3.1 Experimental Setup

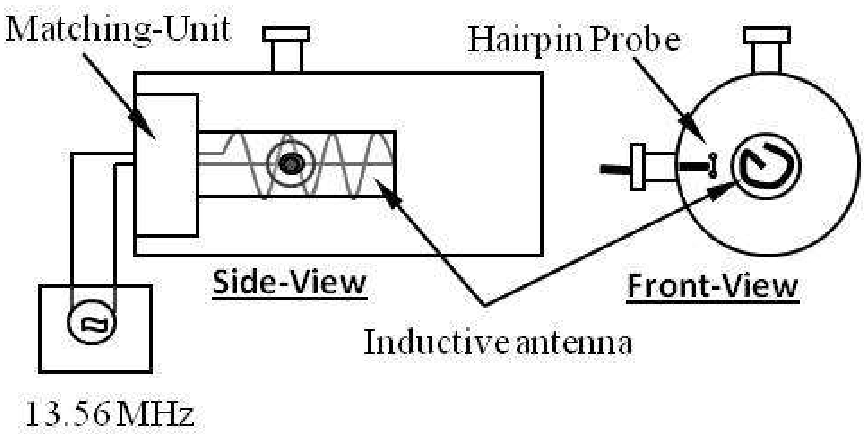

Figure 3.3: Basic Radio frequency Ion Source (BARIS).

The experimental device used for the systematic study of hairpin properties is carried in the Basic Radio Frequency Inductive Source (BARIS) [92–94] as shown in Fig.

3.3. The source consists of a helical antenna enclosed in a glass tube and mounted on the axis of a 90.0 cm long stainless steel cylindrical discharge chamber with internal diameter of 20.0 cm. One end of the reactor is closed with a 1.5 cm thick Pyrex window and the other with a stainless steel flange. The helical antenna is inserted through the flange that has a 5.0 cm port. The antenna is driven at 13.56 MHz through an automated impedance matching unit. All experiments were carried out with the argon at pressures 10 mTorr and 20 mTorr. The rf power was varied from 50 Watt to 500 Watt. The flow rate is maintained constant at about 50 sccm using mass flow controller. The plasma parameters of the reactor are very reproducible.

The plasma profile has a gradient in electron density along the radius but is uniform density along the radial plane. Therefore we positioned the pins such that they lay exactly in the same plane and pointing towards the axis of the chamber. Because the plasma in the device is highly reproducible, we used a manually operated gate valve for inserting and replacing with dielectric probes without disrupting the vacuum. For experimenting with semi-shielded hairpins, dual bore Teflon ($\kappa_d = 2.1$) and Perspex ($\kappa_d = 3.42$) blocks were used. Three different lengths designated as Perspex-1, 2, 3 and Teflon-1, 2, 3 respectively for 7.0 mm, 15.0 mm, and 18.0 mm was used in the experiment. The dimension of the hairpin is about 25.41 mm, width of 3.0 mm and wire diameter of 0.25 mm.

For experimentation with dielectric sleeves three different dimensions (in mm) of quartz sleeves S1, S2, and S3 are $0.4 \times 0.55, 0.6 \times 0.84$, and 0.9×1.1 respectively were used for covering the entire surface of the pins. The chosen length of the hairpin is 25.0 mm and the width is 4.0 mm.

3.2 Characteristics of Semi-Shielded Hairpin Probes

A systematic experiment was carried out to study the effect of fractional coverage of the hairpin inside the dielectric on its characteristic resonances in vacuum. This was

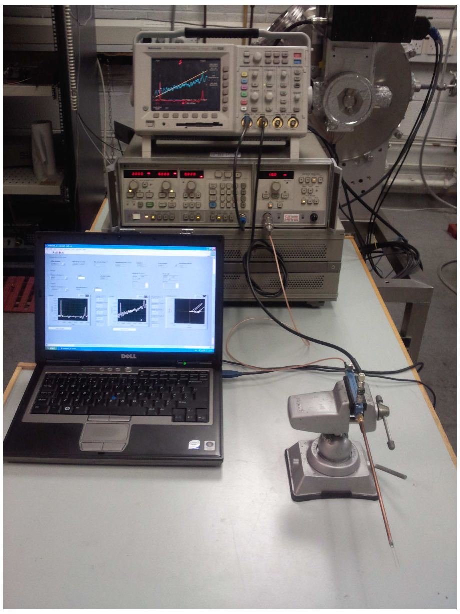

Figure 3.4: Arrangement for the study of additional dielectrics affects on the resonance frequency of the hairpin.

achieved by inserting the dielectric blocks of Teflon and Perspex on to the hairpin. We varied the covering length both from the short-circuited end as well from the open ends as shown in Fig. 3.4. The results are presented in section 3.2.1. In section 3.2.2 we present a method for the calibration of electron density obtained by the semi-shielded hairpin. The results are discussed in section 3.2.3.

3.2.1 Experimental Results

Fig. 3.5 shows typical resonance signals with the partially shielded probes as compared with those obtained in vacuum. The Perspex having higher value of $\kappa_d = 3.42$ as compared with Teflon $\kappa_d = 2.1$ shows more shifting of the resonance frequency towards the lower frequency according to Eq. 3.1.

In Fig. 3.6, when the dielectric was systematically placed from the short-circuited (SC) end we observe its influence to be significant above 20% coverage. A factor of 2.0 drop in the resonance frequency is observed for fully shielded hairpin. The effect

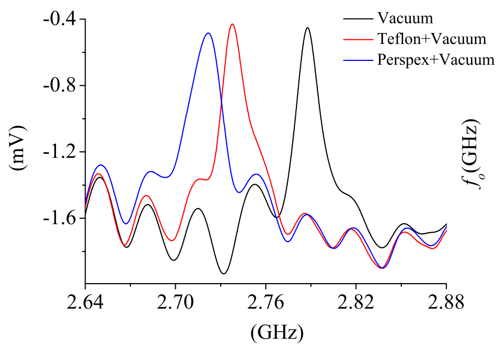

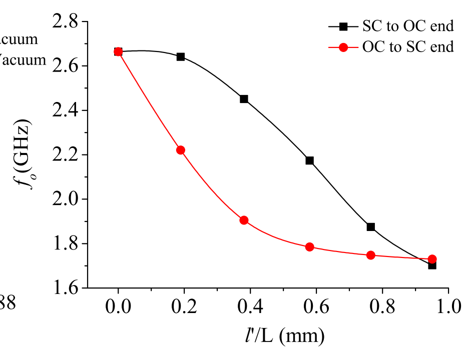

Figure 3.5: Resonance signal by semi-shielded hairpin using Teflon-1 and Perspex-1.

Figure 3.6: Resonance frequency versus normalized shielding length using Teflon-1, where SC is short-circuited end and OC is open-circuited end of hairpin.

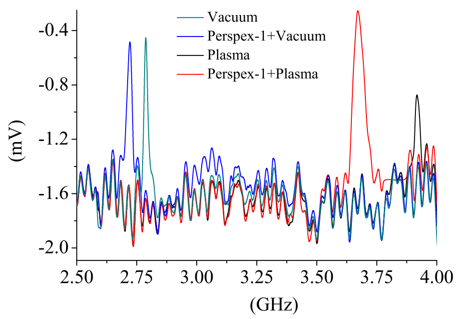

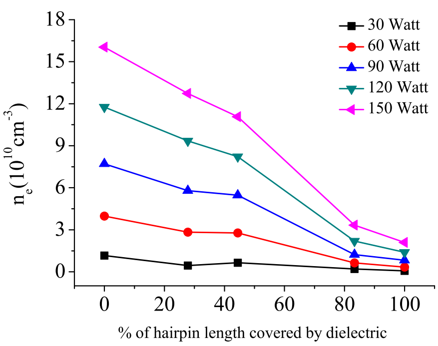

Figure 3.7: Resonance frequency signal obtained using semi-shielded hairpin using Perspex-1 in vacuum and in the argon plasma at 200 W and 10 mTorr.

Figure 3.8: Electron density measured in argon discharge at 10 mTorr using semi-shielded hairpin ($l = 18mm, w = 3.75mm$) covered by Teflon blocks.

is higher in the case when the dielectric is introduced from the open end as the open end that the short-circuited end because of the electric field is more pronounced at the open ends.

Also observed in Fig. 3.7 that the relative shifts in the resonance signals with the addition of dielectric performed in vacuum are not proportionate as obtained in plasma. The results indicate that the electron density measured by shielded hairpins can significantly underestimate the electron density. Fig. 3.8 shows electron density obtained using various dielectric shielded probes as compared to those obtained with the dielectric free probe at different operating powers of the discharge. The results clearly suggests that the probe gives underestimation in density if the contribution of dielectric material in the measured resonance frequencies is not taken into account.

3.2.2 Method of Calibration of Density for the Semi-Shielded Probe

The equation that relates the effective dielectric permittivity with the relative shifts in the resonance frequencies in presence of vacuum/air (f_o) and dielectric (f_r) can be written as:

$$\kappa^{eff} = \frac{f_o^2}{f_r^2} \tag{3.6}$$

Consider a simple geometry by considering the short-circuited end is covered inside a dielectric with permittivity κ_d as shown in Fig. 3.9. We use the nomenclature f_o^m for the measured resonance in vacuum and f_r^m for the plasma. The original vacuum frequency $f_o = c/(2l + w)$ which can be easily calculated knowing the physical dimension of the hairpin.

Considering Eq. 3.6, one can obtain an effective permittivity κ_v^{eff} of the hairpin in vacuum as follows:

$$\kappa_v^{eff} = \frac{(f_o)^2}{(f_o^m)^2} \tag{3.7}$$

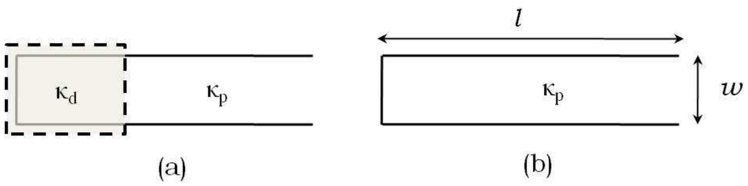

Figure 3.9: (a) semi-shielded probe (PSP) (b) reference probe (RP).

similarly in plasma,

$$\kappa_p^{eff} = \frac{(f_o)^2}{(f_r^m)^2} \tag{3.8}$$

The effective dielectric permittivity observed by hairpin is obtained by considering weighted average of the dielectric constants. The method of expressing the cumulative dielectric in this form has also been applied in microstrip resonator for measuring permittivity on substrates having horizontal and vertical dielectric permittivity components [95–97]. It is also applied for calculating the surface impedance of the dielectric [98]. Thus, the effective permittivity observed by semi-shielded hairpin in vacuum and in plasma may be expressed as:

$$\kappa_v^{eff} = \frac{\zeta\kappa_d + \kappa_v(=1)}{\zeta + 1} \tag{3.9}$$

$$\kappa_p^{eff} = \frac{\zeta\kappa_d + \kappa_p}{\zeta + 1} \tag{3.10}$$

where, ζ is an weighted factor that takes the values anything between 0.0 and 1.0. The value of $\zeta = 0$ indicates absence of dielectric while, ζ =1 is the situation when the hairpin is completely covered inside the dielectric.

From Eq. 3.7 and Eq. 3.9, the value of ζ can be obtained in terms of f_o's and κ_d as

$$\zeta = \frac{\frac{(f_o)^2}{(f_o^m)^2} - 1}{\kappa_d - \frac{(f_o)^2}{(f_o^m)^2}} \tag{3.11}$$

Similarly, by equating Eq. 3.8 and Eq. 3.10 the plasma permittivity can be written as:

$$\kappa_p = (\zeta + 1)\frac{(f_o)^2}{(f_r^m)^2} - \zeta\kappa_d \tag{3.12}$$

The above equation gives the relation of cold plasma permittivity as a function of resonance frequency, weighted factor, and the dielectric constant of the material. Using equation $f_r = f_o/\sqrt{\kappa_p}$, the cold plasma permittivity can also be written as:

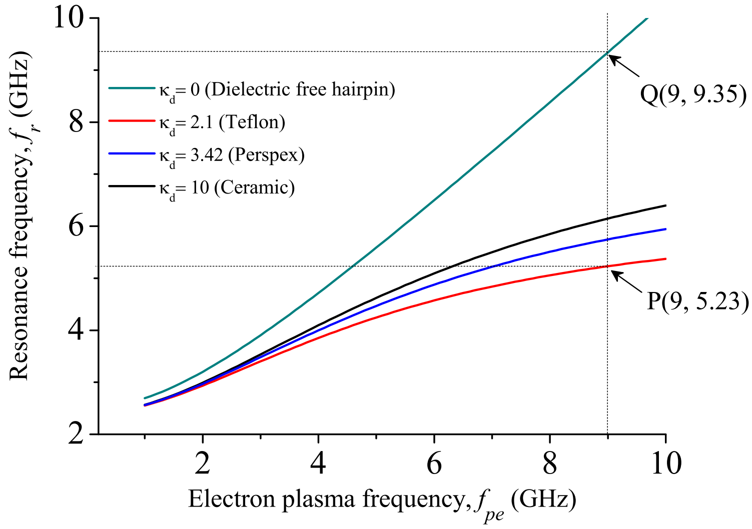

Figure 3.10: Plots of resonance frequency versus electron plasma frequency where resonance frequencies are calculated using Eq. 2.6 for dielectric free hairpin and Eq. 3.16 for semi-shielded hairpin).

$$\kappa_p = \frac{1}{1 + \frac{f_{pe}^2}{f_o^2}} \tag{3.13}$$

Therefore, equating equations 3.12 and 3.13 one can obtain the corrected plasma frequency from that the electron density as follows:

$$n_e[10^{10}cm^{-3}] = 1.23\left[(f_r^m)^2 - (f_o^m)^2\right] \times C.F. \tag{3.14}$$

where, C.F. is the correction factor given by

$$C.F. = \frac{(\kappa_d - 1)(f_o)^4}{\kappa_d\{(f_r^m)^2\,[(f_o^m)^2 - (f_o)^2] + (f_o)^2(f_o^m)^2\} - (f_o)^2(f_o^m)^2}. \tag{3.15}$$

If $\kappa_d = 0$, we find that the Eq. 3.14 reduces to its ideal form given by Eq. 2.7. Also Eq. 3.14 can be expressed in following form:

$$(f_r^m)^2 = \frac{(\kappa_d - 1)(f_o)^2(f_o^m)^2}{(\kappa_d - 1)f_o^4 - \kappa_d f_{pe}^2[(f_o^m)^2 - (f_o)^2]}(f_o^2 + f_{pe}^2) = C.F. \times (f_o^2 + f_{pe}^2) \tag{3.16}$$

Inspecting equations 3.14 and 3.16, it suggests that C.F. is sensitive to the background electron density, the dielectric constant of the material and the vacuum resonance frequency modified by the presence of external dielectric. The relationship between the measured resonance frequencies corresponding with electron density is shown for various cases in Fig. 3.10.

An important advantage of using a semi-shielded probe suggests higher plasma densities can be measured at reduced frequency. Generally, the suitable range of frequency measurements is from 2.0 GHz to 6.0 GHz. Therefore partially shielded probes can help in covering wide range of plasma densities that are otherwise limited to $10^{12} cm^{-3}$.

3.2.3 Results and Discussion of Semi-Shielded Probe

The values of the weighting factor ζ as a function of normalized length (l'/L) are plotted in Fig. 3.11, where l' is the length of the dielectric block. The experiments are systematically done for different hairpins of lengths 15.0 mm, 20.0 mm, 25.0 mm, and 29.0 mm. A sharp rise in the ζ values is observed on increasing the shielding length. Equation 3.11 suggests that the value of parameter ζ depends on hairpin dimensions, dielectric constant of the material used for shielding the hairpin, and volume occupied by dielectric material in the vicinity of hairpin. For a given hairpin dimension, the sharp rise in ζ value is observed in case of material with smaller dielectric constant. Therefore, it is recommended to use material of higher

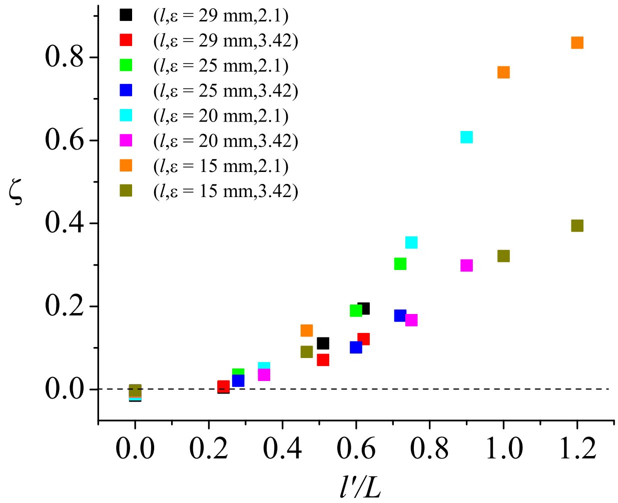

Figure 3.11: ζ versus normalized length of dielectric (l') by hairpin length (L) for Teflon ($\kappa_d = 2.1$) and Perspex ($\kappa_d = 3.42$).

dielectric constant such as Al_2O_3 for partial shielding of the hairpin. Practically, if the value of ζ is close to zero means smaller affect of adjunct dielectric on frequency measurements.

The Perspex blocks are used for the experimental verification of the analytical model for partially shielded hairpin presented in previous section. The hairpin used has length = 25.0mm and width = 4.0mm. The blocks of length l'=7mm, 15mm, 18mm having width = 7mm and height = 4mm are typically used in experiments. The corresponding measured resonances in vacuum are f_o^m= 2.777GHz, 2.694GHz, 2.512GHz, and 2.386GHz respectively which is lower than theoretical f_o (2.777GHz) calculated using the formula $f_o = c/(2l + w)$.

For demonstrating the model, the experiment is performed in argon plasma by varying the rf power to reach a highest possible density of $3.0 \times 10^{11} cm^{-3}$ at approximately 3.0 cm away from the inductive antenna of the BARIS.

Figs. 3.12 to 3.14 shows the electron density measured by the semi-shielded probe (PSP) and the reference probe (ref-probe) that is close to give actual density.

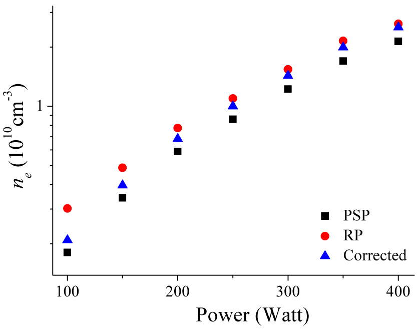

Figure 3.12: Plot of n_e versus power, where l'=7mm (28% of hairpin length) and pressure is 5×10^{-3} mbar.

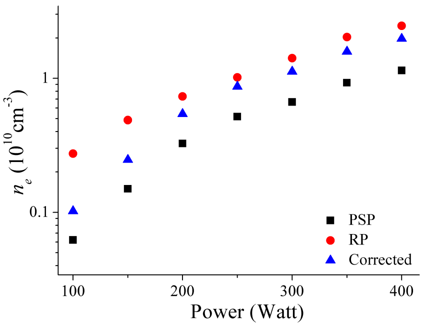

Figure 3.13: Plot of n_e versus power, where l'=15mm (60% of hairpin length) and pressure is 5×10^{-3} mbar.

The partially shielded probe shows lower density than those measured by the ref-probe. However by applying the correction formula the shielded probe data matches reasonably well with that obtained from the ref-probe. There is a small discrepancy at lower densities $\approx 10^{10} cm^{-3}$. This may be because of sheaths created around the insulating block that the model does not take in to account.

Using the above model, it is shown in Fig. 3.15 that the electron densities can be reliably obtained with the partially shielded hairpins up to 60% to 80% embedded inside the dielectric.

Fig. 3.16 shows the graph of density measured using hairpin shielded with Teflon-1 and Perspex-1. The corrected densities for both Teflon and Perspex are in good agreement with the density measured by the ideal ref-probe. This highlights the fact that the model is independent of the choice of dielectric.

Based on the above observations it is reasonable to conclude that the model can be applied for correcting densities greater than $10^{10} cm^{-3}$. It may be improved to work at lower densities as well by suitably incorporating the sheath effects. The semi-shielded probe can be promising for measuring higher plasma densities.

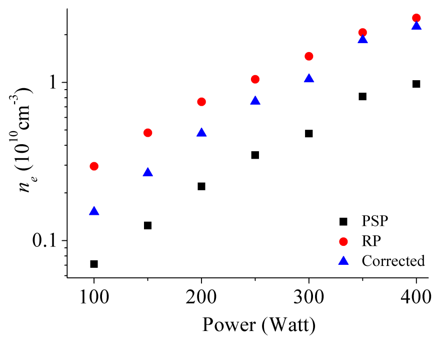

Figure 3.14: Plot of n_e versus power, where l'=18mm (72% of hairpin length) and pressure is 5×10^{-3} mbar.

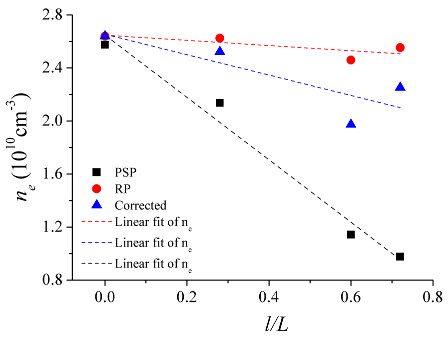

Figure 3.15: Plot of n_e versus normalized length of dielectric in Argon plasma at 400 W and 5×10^{-3} mbar.

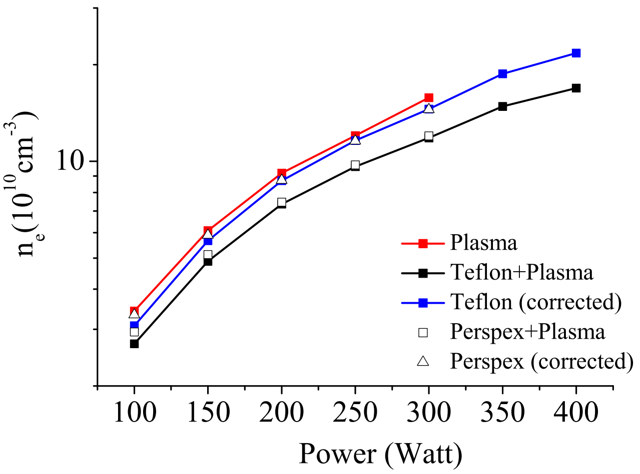

Figure 3.16: Plot of n_e versus rf power in Argon plasma at 10mT using hairpin covered with Teflon-1 and Perspex-1.

3.3 Investigation of Hairpin Resonator with Uniform Dielectric Sleeves

In this section we present the influence of dielectric sleeves on the performance of hairpin probe. Just as in the case of semi-shielded hairpin, the introduction of sleeves over the pins will result in the shift of vacuum resonance towards the lower frequency. In section 3.3.1, we present a model for correcting the electron density in the case of dielectric column of arbitrary thicknesses covering the entire surface of the pins. This is followed by experimental data and discussion in the section 3.3.2.

3.3.1 Model for Density Correction

Consider the case when a thin dielectric sleeve ($\kappa_d = 3.8$) is introduced over the pins as shown in Fig. 3.17. Because $\kappa_d > 1$, the new characteristic resonance falls below f_o. When such a probe is immersed in a plasma the measured resonance peak will be also lower compared to the dielectric-free hairpin. Substituting f_r in Eq. 2.7 leads to erroneous measurement of the electron density. We address this problem by modeling the effective capacitance of the sleeve and the plasma. In the first approximation, we ignore the sheath contribution to the effective dielectric permittivity. We choose the quartz as the dielectric material because of its high secondary electron emission yield. This has the advantage in reducing the sheath width which forms around the hairpin wires.

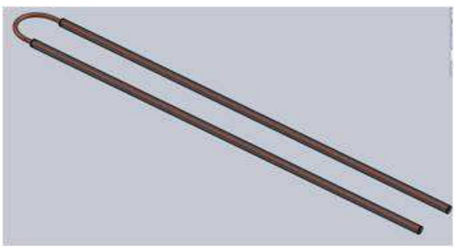

Figure 3.17: Hairpin covered with uniform dielectric sleeves.

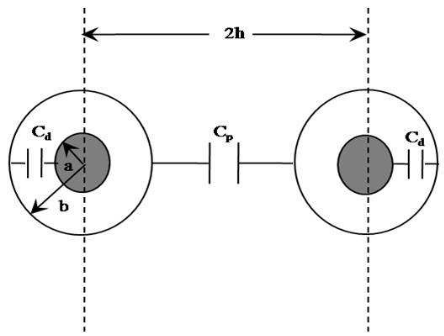

Figure 3.18: Hairpin probe covered with the dielectric sleeves (a is wire radius, b, is sleeve outer radius and 2h is the separation between the wires).

This will result in an additional capacitance between the individual pins with respect to the mid-plane. Fig. 3.18 shows schematic of the different capacitances associated with the hairpin on introducing the dielectric sleeves. The additional dielectric shifts the resonance signal from f_o and f_r to some lower values, denoted by f_o^m and f_r^m in vacuum and in plasma respectively. Therefore, f_o^m is given by:

$$f_o^m = \frac{c}{2(2l + w)\sqrt{\kappa_v^{eff}}} = \frac{f_o}{\sqrt{\kappa_v^{eff}}} \tag{3.17}$$

where, κ_v^{eff} is the effective dielectric permittivity due to vacuum and sleeves. Similarly, for the plasma:

$$f_r^m = \frac{c}{2(2l + w)\sqrt{\kappa_p^{eff}}} = \frac{f_o}{\sqrt{\kappa_p^{eff}}} \tag{3.18}$$

where, κ_p^{eff} is the effective permittivity due to plasma and the sleeve.
Considering a first approximation of homogeneous plasma around the hairpin, the total capacitance per unit length can be written as:

$$C_T = \frac{\pi \epsilon_o \kappa_p^{eff}}{\ln(h/a + \sqrt{(h/a)^2 - 1})} \tag{3.19}$$

where, a is the probe tip radius and $2h$ is the separation between the axis of wires. Assuming that dielectric sleeve is perfectly fitted on the hairpin wires we can write the total capacitance of the system as two capacitors connected in series: capacitance C_d due to the dielectric sleeve with inner radius a and outer radius b and the capacitance C_p due to the plasma. The C_d and C_p can be written as:

$$C_d = \frac{2\pi\varepsilon_o\kappa_d}{\ln(b/a)} \tag{3.20}$$

$$C_p = \frac{\pi\varepsilon_o\kappa_p}{\ln(h/b + \sqrt{(h/b)^2 - 1})} \tag{3.21}$$

where, κ_p is given by Eq. 2.3. The total capacitance is given by the series combination of C_d and C_p. Substituting the values of capacitances from Eq. 3.20 and Eq. 3.21 we obtain:

$$C_T = \pi\epsilon_o \frac{\kappa_d\kappa_p}{\kappa_d \ln(h/b + \sqrt{(h/b)^2 - 1}) + \kappa_p \ln(b/a)} \tag{3.22}$$

Equating Eq. 3.19 and Eq. 3.22, one can solve for f_{pe}^2, alternatively, the plasma frequency corrected in the presence of a dielectric sleeve may be directly expressed as:

$$f_{pe}^2 = \frac{(f_r^m)^2 - \frac{f_o^2}{A}\left\{\frac{\ln(b/a)}{\kappa_d} + B\right\}}{1 - \frac{f_o^2}{(f_r^m)^2} \times \frac{\ln(b/a)}{\kappa_d A}} \tag{3.23}$$

where, $A = \ln(h/a + \sqrt{(h/a)^2 - 1})$, $B = \ln(h/b + \sqrt{(h/b)^2 - 1})$, and the plasma density can be found directly from relation, $n_e = \frac{m_e\pi}{e^2} f_{pe}^2$.

3.3.2 Results and Discussion

The experiment was performed using the set-up discussed in section 3.1. The measurements were done systematically at one time with the ideal hairpin containing no dielectric sleeves followed by introducing quartz sleeves on the same probe. The density measurement was repeated at a different time but without disrupting the vacuum or the chamber condition to ensure the plasma is reproducible.

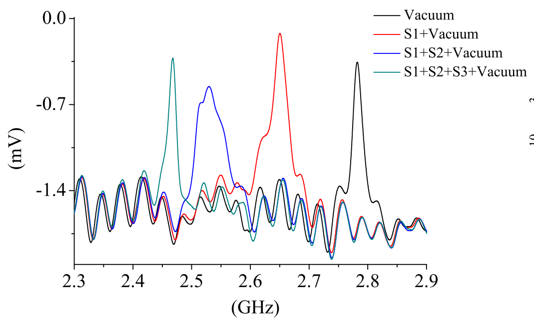

Figure 3.19: Resonance signals of hairpin covered with sleeves S1, S2, and S3.

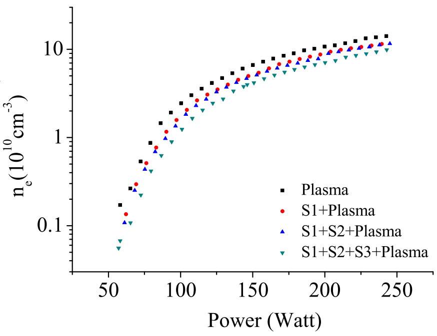

Figure 3.20: Electron density measured in argon discharge at 10mTorr using uniformly covered hairpin with quartz sleeves.

In the experiment the rf power is varied up to 250W at a given pressure of about 10mTorr with constant flow rate of about 50 sccm. In first case, the measurements were taken with the ref-probe, followed by introducing quartz sleeves of different thicknesses over the reference probe. The plasma densities are recorded as a function of the RF power at a given operating pressure. The hairpin resonator used in the experiment has length (l) of 29.5 mm, width (w) of 3.65 mm, and wire diameter (2a) of 0.25 mm. Different sleeves S1, S2, and S3 of standard thickness (ID×OD) in mm $0.4 \times 0.55, 0.6 \times 0.84$, and 0.9×1.1 respectively are used in the experiment, where S2 and S3 are added on top of S1.

The electron density using standard formula given in Eq. 2.7 is calculated for the dielectric probe then compared with that obtained with the ref-probe. However, the corrected densities are calculated using Eq. 3.23.

Fig. 3.19 shows some typical resonances obtained with different quartz sleeves ($\kappa_d = 3.8$) introduced to the ref-probe. Contribution of quartz sleeve on the effective permittivity increased with the thickness giving rise to larger shift from f_o towards the lower frequency as expected.

Plots of density measured with different probes on the log scale in Fig. 3.20 shows that the probe having maximum contribution of the dielectric measures lower density as compared with the ref-probe without any sleeves.

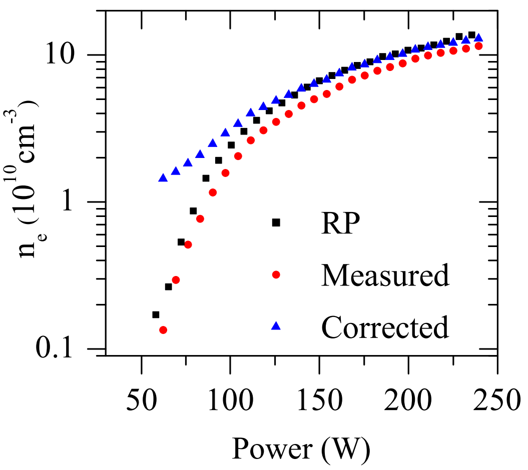

Figure 3.21: Plot of n_e versus discharge power at 10 mTorr for hairpin covered with quartz sleeve S1.

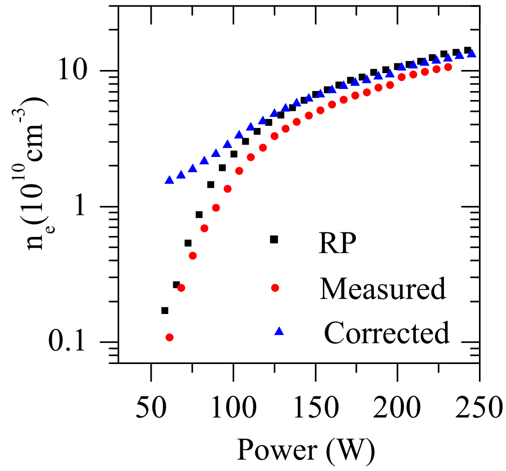

Figure 3.22: Plot of n_e versus discharge power at 10 mTorr for hairpin covered with quartz sleeve S1 and S2.

Density measured using individual sleeves S1 and S1+S2 is plotted in Figs. 3.21 to 3.24 with those measured by the ref-probe for 10 mTorr and 20 mTorr over a range of operating powers.

Consistently the density measured with the dielectric probe is lower than the ref-probe. However, n_e obtained using new formula is found to match very well with those obtained from the ref-probe. This result is consistent for different sleeve thicknesses except for lower densities.

Fig. 3.25 shows the plot of densities as a function of b for the same plasma conditions. It shows that without applying correction model, the density begins to fall significantly with increasing b. However, by applying the new formula, the corrected electron density remain almost constant for $b/w \approx 0.08$. For $b/w > 0.08$, the model is not so accurate as the sheaths around the dielectrics can be influential.

For the practical application of the model, one needs to choose the hairpin width larger than the effective sheath radius. The sheath radius is relatively larger at

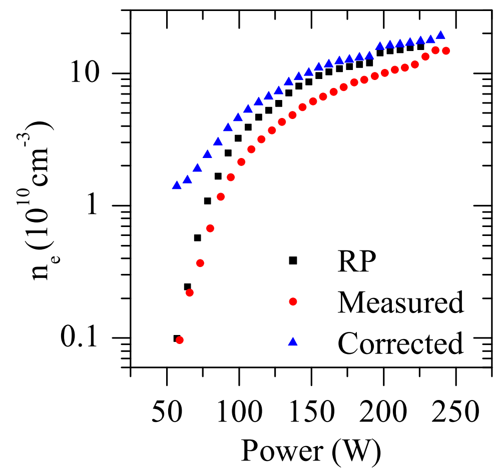

Figure 3.23: Plot of n_e versus discharge power at 20 mTorr for hairpin covered with quartz sleeve S1.

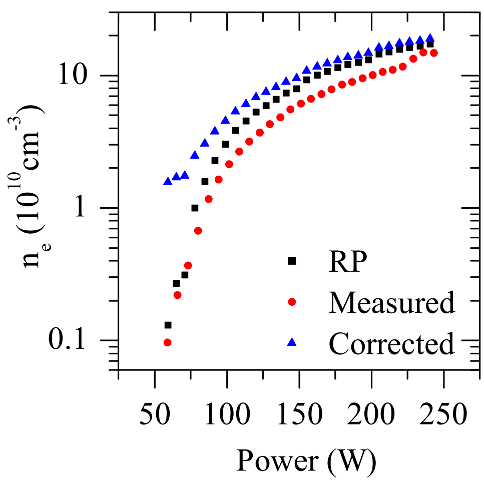

Figure 3.24: Plot of n_e versus discharge power at 20 mTorr for hairpin covered with quartz sleeve S1 and S2.

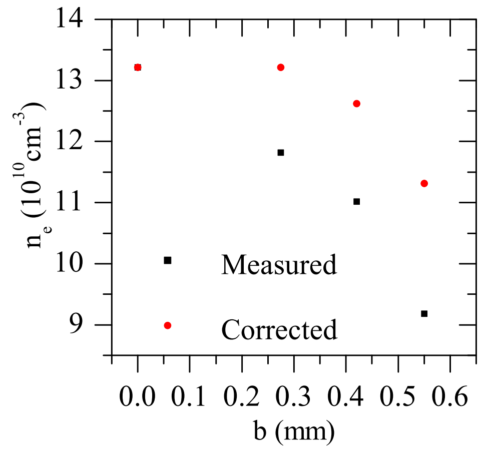

Figure 3.25: Plot of n_e versus quartz sleeve radius at 241 W and 10 mTorr.

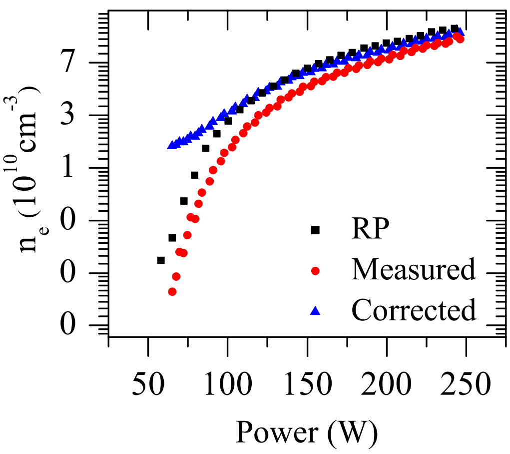

Figure 3.26: Plot of n_e versus discharge power at 10 mTorr for hairpin covered with Al_2O_3 sleeve having $\kappa_d = 10$.

lower densities hence occupying significant portion of the space between the pins. Therefore the correction overestimates the densities in Figs. 3.21 to 3.24 at lower operating powers since rf rectification resulting in greater sheath width is higher at lower plasma densities. In principle the sheath effect may be incorporated in the model by considering the additional capacitance in series with the capacitance due to plasma and dielectric sleeves provided electron temperature of the plasma is measured independently using a Langmuir probe as demonstrated by Piejak et al [2]. Fig. 3.26 shows the plot of n_e as a function of discharge power measured using hairpin covered with Al_2O_3 sleeve having dielectric constant 10. The sleeve dimensions (mm) are (ID×OD) 0.4×0.55. We found that the present model gives reasonable density corrections even for high dielectric material. However, no significant reduction in overestimation of electron density by model is found at lower discharge powers as compared to the quartz sleeve case presented in Figs. 3.21 to 3.24. The main factor responsible for the density overestimation at lower discharge powers is the sleeve dimensions as compare to wire radius and width of the probe. Therefore, it is suggested to include sheath effects in the present model in order to work at lower densities.

3.4 Summary

Two types of dielectric shielded hairpin probes are presented and their practical application to plasmas are discussed in this chapter. The presence of adjunct dielectrics in the vicinity of hairpin resulted in modifying the effective permittivity as seen by the probe. As a result the electron density measured by the dielectric probes show an underestimated density as compared with the ideal reference probe.

For correcting the electron density, suitable models are proposed for dealing with specific cases. For the semi-shielded probe, the model allows to rectify the underestimated density up to 40% covered inside the dielectric which resulted in lowering of the resonance frequency by almost a factor of 2.0 allowing the device to operate at lower frequency range. Operating the device at lower frequency range below f_{pe} is important for avoiding excitation of warm plasma modes resulting in losses of the signal amplitude. Besides, the method can be a promising tool for application of the hairpin in very high density plasmas which are currently limited to densities less than $10^{12} cm^{-3}$. The validity and precision of the present model and dielectric covered hairpin probe shall be also tested for reactive gases such as O_2/N_2 and SF_6 in the plasma for further expansion of the present research. The dielectric shielded probes can be very useful in reactive plasmas. It helps to safeguard the probe and well minimize interference to the plasma.

CHAPTER 4

The Effects of External Magnetic Field on Probe's Resonance Frequency

4.1 Motivation

So far we have considered the case of magnetic field free plasma. In presence of external magnetic field the electrons start gyrating in the plane perpendicular to the magnetic field while free streaming along the field lines, resulting in helical orbits. The plasma electrons are said to be magnetized when the electron on an average completes at least one gyration around the magnetic field before getting deflected by collision with another neutral or ion, such that $\omega_{ce}/\gamma_m > 1$; where ω_{ce} is the electron gyro-frequency and γ_m is the electron collision rate. In general, electrons can be magnetized easily as compared with ions. For strongly magnetized plasmas, radial diffusion to adjacent field line can only take place via collisions.

Because of constrained electron motion perpendicular to the field lines, the plasma permittivity becomes anisotropic resulting in two separate components, $\kappa_{||}$

along the direction of B-field while $\kappa_\times$ and $\kappa_\perp$ are the components in the plane transverse to the magnetic field lines [11]. The behavior of $\kappa_{||}$ is the same as in the case of non-magnetized plasmas, however the transverse components are modified due to the contribution of ω_{ce}. Therefore resonance conditions are strictly dependent on the orientation of the probe with respect to the field lines.

The primary objective is to investigate the dispersion relation valid in the case of a hairpin immersed in magnetized plasmas and understand the effect of magnetic field on the resonant properties of the probe.
Section 4.2 discusses the dispersion formula applicable for an electromagnetic wave in a magnetized plasma [99–101] and its application in the context of a hairpin probe placed at different orientations with respect to the magnetic field lines. Section 4.3 describes the experimental setup. This is followed by experimental results and discussion in section 4.4 and 4.5 respectively. The summary and conclusion is presented in section 4.6.

4.2 Analysis of Cold Plasma Permittivity in Presence of External Magnetic Field

When magnetic field is present, the electron dynamics in plasma is modified due to cyclotron motion superimposed with freely streaming electrons along the field lines. This results in a change in effective permittivity of the plasma surrounding the hairpin. For satisfying the resonance condition the length of the resonator has to be equal to a quarter wavelength. Therefore, the resonance frequency will vary in response to the permittivities $\kappa_{||}$, $\kappa_\times$ and $\kappa_\perp$. The contribution of each component on propagation vector $\vec{k}$ will be sensitive to how the probe is oriented with respect to the B-field. Analysis of each case is therefore necessary which is considered in the following section.

4.2.1 Effective Plasma Permittivity for Propagating Waves in Magnetized Plasma

Consider the hairpin immersed in a homogeneous plasma with an external magnetic field. The electromagnetic field traveling along the pins composed of mutually perpendicular time varying components $\vec{E}(\vec{r},t)$, $\vec{B}(\vec{r},t)$. The propagation constant in the presence of a magnetic field is given by,

$$k = \frac{\omega}{c}\sqrt{\tilde{\epsilon_p}} = \frac{2\pi}{\lambda} \tag{4.1}$$

where, $\tilde{\epsilon_p}$ is the plasma permittivity tensor.
Fig. 4.1 gives the schematic of the direction of different components of permittivity $\kappa_{||}$,$\kappa_\times$ and $\kappa_\perp$ with respect to the magnetic field considered along z-axis.

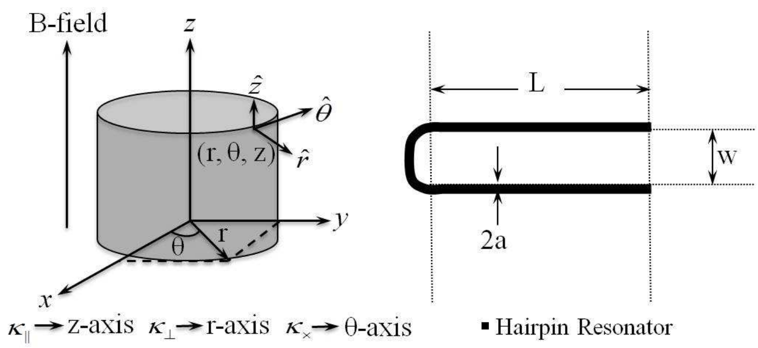

Figure 4.1: The components of plasma permittivity with respect to the direction of magnetic field are shown in cylindrical coordinate system.

The dielectric permittivity of the magnetized plasma can be represented as a tensor given by [11, 100]:

$$\tilde{\epsilon_p} = \epsilon_o \tilde{\kappa_p} = \epsilon_o \begin{pmatrix} \kappa_\perp & -j\kappa_\times & 0 \\ j\kappa_\times & \kappa_\perp & 0 \\ 0 & 0 & \kappa_{||} \end{pmatrix} \tag{4.2}$$

Under the cold plasma approximation [6, 7, 11], requiring the phase velocity to be much greater than the thermal velocity, one may neglect the effect of thermal motion of the electrons. This is generally applicable when the plasma pressure and absorption are negligible. In this case, the loss of plasma wave energy to the plasma particle medium is negligible. Plasma absorption is the physical phenomenon which happens in the situation when an electromagnetic wave propagates through a plasma medium and accelerates the electron motion due to electromagnetic forces. If the electrons make significant collisions with other particles then the net energy will be absorbed from the wave. For collisionless plasmas, the plasma permittivity components are given by the following equations [11]:

$$\kappa_{||} = 1 - \frac{f_{pe}^2}{f^2} \tag{4.3}$$

$$\kappa_{\perp} = 1 - \frac{f_{pe}^2}{f^2 - f_{ce}^2} \tag{4.4}$$

$$\kappa_{\times} = \frac{f_{ce}}{f} \frac{f_{pe}^2}{f^2 - f_{ce}^2} \tag{4.5}$$

The component $\kappa_{\times}$ is in the azimuthal direction with respect to the magnetic field. Because it is an imaginary quantity it contributes to the attenuation of the wave and broadens the resonance signal [99, 100]. A detailed discussion on the effect of $\kappa_{\times}$ on the attenuation of the resonance signal is discussed in chapter-5 which deals with the dispersion of resonance signal in the plasma.

If the electromagnetic wave is allowed to propagate for a distance much greater than its characteristic wavelength a variety of possible plasma wave modes can appear because of the wave phase velocity dependence on the wave frequency and the angle between the wave vector with respect to the B-field. A general expression for the effective permittivity [11], $\kappa_p^{eff} = n^2$, can be written in terms of the permittivity components as given below:

$$tan^2\theta = -\frac{\kappa_{||}(n^2 - \kappa_r)(n^2 - \kappa_l)}{(n^2 - \kappa_{||})(\kappa_\perp n^2 - \kappa_r \kappa_l)} \tag{4.6}$$

where,

$$\kappa_r = \kappa_\perp - \kappa_\times \tag{4.7}$$

$$\kappa_l = \kappa_\perp + \kappa_\times \tag{4.8}$$

In Eq. 4.6, θ is the angle between the wave vector and the applied magnetic field strength. Eqs. 4.7 and 4.8 gives rise to right (RCP) and left hand circularly polarized (LCP) wave modes for the electrons and ions respectively [6, 7]. These modes are obtained when the wave is propagating along the B-field such that the time-varying electric vector is perpendicular to the magnetic field, which gives rise to azimuthal components. In addition to circular polarization, other important wave modes are the ordinary (O-mode) and extraordinary (X-mode). These modes are observed when the magnetic field is perpendicular to the wave-vector. Therefore, EM waves in plasma in the presence of external B-field give rise to a variety of plasma wave modes. However in context of the hairpin, only a few of these modes are applicable. This is because the physical length of the hairpin terminates at $\lambda/4$. Hence wave modes resulting from the $\kappa_\times$ component responsible for circular polarization in the near field region of hairpin may not be realistic in the case of hairpin. However these modes can be excited in the far field region from the hairpin. Therefore, the only relevant components contributing to the effective permittivity are $\kappa_{||}$ and $\kappa_\perp$.

For simplicity we consider two primary cases, (i) $\vec{k}||\vec{B}$ and (ii) $\vec{k} \perp \vec{B}$. In the $\vec{k}||\vec{B}$ case, the pins point along the direction of the B-field while for $\vec{k} \perp \vec{B}$ case the probe cuts across the external field lines. The effects due to different probe orientations on probe's resonance frequency are discussed in the following section.

4.2.2 Effective Plasma Permittivity as Observed by Hairpin

Case-1: $\vec{k}||\vec{B}$

Fig. 4.2 shows the condition when $\vec{k}||\vec{B}$. This results in the transverse electric field in the x-y plane for all azimuthal angles of the plane with respect to $\vec{k}$. Because the time varying $\vec{E}$ and $\vec{B}$ are mutually perpendicular, this gives rise to circular polarization of the wave as given in Eqs. 4.7 and 4.8.

The effective plasma permittivity for the $\vec{k}||\vec{B}$ is given by [11];

$$\kappa_p^{eff} = \kappa_r = \kappa_\perp - \kappa_\times = 1 - \frac{f_{pe}^2}{f(f - f_{ce})} \tag{4.9}$$

$$\kappa_p^{eff} = \kappa_l = \kappa_\perp + \kappa_\times = 1 - \frac{f_{pe}^2}{f(f + f_{ce})} \tag{4.10}$$

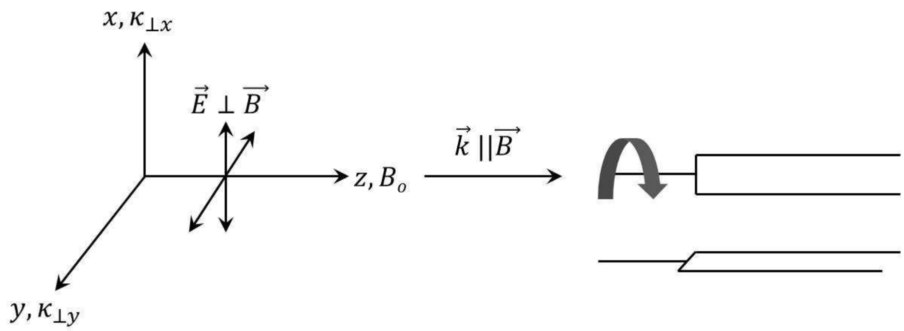

Figure 4.2: Figure showing the mutually orthogonal electric and magnetic field components of the hairpin with respect to the external B-field for the case $\vec{k}||\vec{B}$.

We assume that in the near field approximation, the circular polarization is not effective within the $\lambda/4$ distance. The only contributions are from the components κ_r and κ_l, which reduce to $\kappa_\perp$ as given by Eq. 4.4.

Case-2: $\vec{k}\perp\vec{B}$

Assuming the hairpin points across the external magnetic field, the time-varying $\vec{E}$ field generated during resonance in this case can either be parallel (i) $\vec{E}||\vec{B}$ or perpendicular (ii) $\vec{E}\perp\vec{B}$ to the external field as shown in Fig. 4.3.

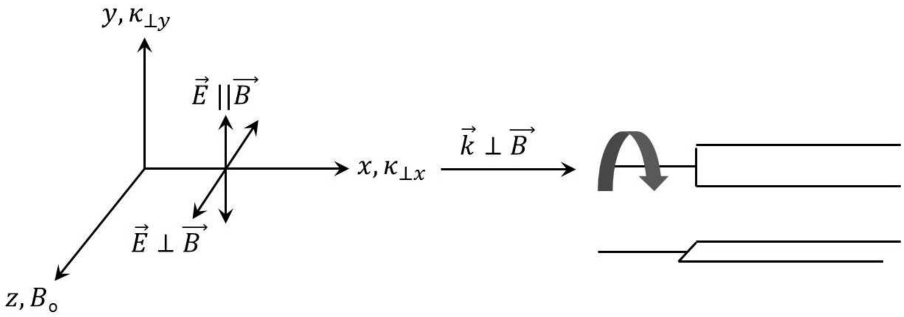

Figure 4.3: Figure showing the electric field components of the hairpin with respect to the B-field for the case $\vec{k}\perp\vec{B}$.

The electrons which are present in the plane where $\vec{E}||\vec{B}$ does not suffers $\vec{E}\times\vec{B}$ force . Therefore plasma electrons contributing to the permittivity in this volume is independent of the external magnetic field.
Considering that the electromagnetic wave is propagating perpendicular to B_o, this is the case of O-mode, which has the same dispersion relation for a non-magnetized plasma. On the other hand, we are left with those electrons which experience Lorentz force because of the crossed electric and magnetic field components in the remaining volume. This interaction leads to a longitudinal component of the E-field in the direction of propagation $\vec{k}$. This is the X-mode. The wave becomes partially longitudinal and partially transverse resulting in elliptical polarization. The effective plasma permittivity is given by [11]:

$$\kappa_p^{eff} = \frac{\kappa_r\kappa_l}{\kappa_\perp} = \frac{\kappa_\perp^2 - \kappa_\times^2}{\kappa_\perp} = \frac{f^2(f^2 - f_{ce}^2) - 2f^2f_{pe}^2 + f_{pe}^4}{f^2(f^2 - f_{ce}^2 - f_{pe}^2)} \tag{4.11}$$

Again these modes are only possible in the far field region. Therefore the plasma permittivity in presence of B-field is reduced to $\kappa_\perp$ component only for both $\vec{E}||\vec{B}$ and $\vec{E}\perp\vec{B}$ cases respectively. In fact the majority of the electron population in the vicinity of the hairpin experience an $\vec{E}\times\vec{B}$ force due to fringing E-field set-up by the hairpin. Thus, Eq. 4.11 also reduces to $\kappa_\perp$ when the $\kappa_\times$ component is ignored. This is discussed in the following section.

4.2.3 Spatial Electric field Distribution around the Hairpin Resonator

A sketch of the electric field lines between the pins is shown in Fig. 4.4. Above the plane containing the pins, the curvilinear electric field lines can be resolved in to two components, (i) the E_x component - this is the component of electric field directed between the pins; and (ii) E_y component - the component normal to the plane containing the pins. At the mid-plane the dominant component is the E_x component whereas at all other regions, the electric field component is the resultant of the components, E_x and E_y.

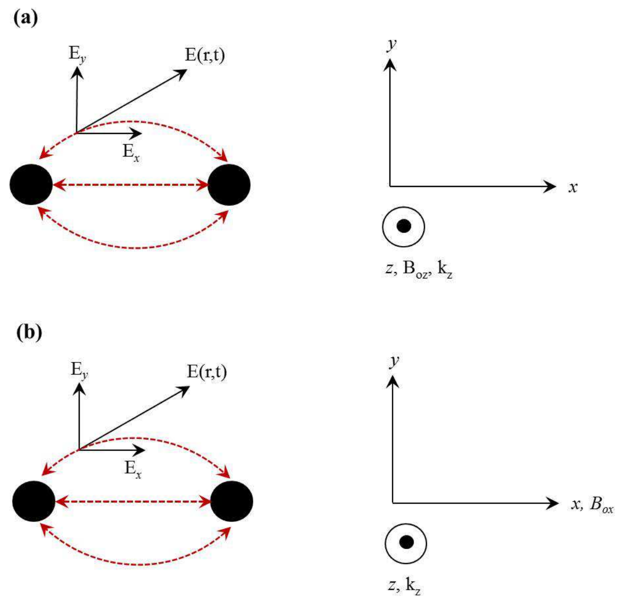

Figure 4.4: Drawing shows the electric field components with respect to the B-field for (a) $\vec{k}||\vec{B}$ (b) $\vec{k}\perp\vec{B}$.

When $\vec{k}||\vec{B}$, both E_x and E_y components are normal to B_o. Hence all the electrons contribute to $\kappa_\perp$. On the other hand, when $\vec{k}\perp\vec{B}$ as shown in Fig. 4.4(b), we have following situations: (i) The E_x component is parallel to B-field - In this condition those electrons present between the pins are not affected by the B-field, however the major population of electrons above the plane of the hairpin are influenced by $\vec{E}\times\vec{B}$. Hence their effective permittivity is given by $\kappa_\perp$. (ii) When the plane of the probe is rotated by 90^o, this merely interchanges E_x and E_y, therefore the permittivity remains same in all cases.

In conclusion, $\kappa_\perp$ is a reasonable approximation for dealing with the plasma permittivity in the presence of an external magnetic field. This is mainly because propagating em-waves are only observable in the far field region away from the source when the effective path length is much greater than the wavelength of the EM wave. This is unlikely for the hairpin whose physical length is limited to $\lambda/4$.

When the hairpin is orientated in the fashion $\vec{k}||\vec{B}$, we observe that most of the tangential component of spatial electric field $\vec{E}(\vec{r},t)$ at any a particular location is tangential to $\kappa_\times$ which is the imaginary component which is attenuated. Hence a large dispersion of the resonance is observed by orienting the probe $\vec{k}||\vec{B}$. Therefore $\vec{k}\perp\vec{B}$ will be experimentally investigated in details.

4.2.4 Resonance Frequency Response in Presence of Magnetic Field

The effective plasma permittivity for $\vec{k}\perp\vec{B}$ is given by Eq. 4.11. Substituting κ_{eff} in Eq. 4.11 in Eq. 2.2, we get a bi-quadratic equation of f_r in terms of three independent variables f_{ce}, f_{pe} and f_o as follows:

$$f_r^4 - f_r^2(f_{ce}^2 + 2f_{pe}^2 + f_o^2) + f_{pe}^2(f_{pe}^2 + f_o^2) = 0 \tag{4.12}$$

There are four real roots of f_r. Out of these, two roots are unphysical as they are negative. The positive roots of f_r are f_{r1} and f_{r2} given by,

$$f_{r1,r2} = \sqrt{(F/2) \pm \sqrt{(F/2)^2 - f_{pe}^2(f_o^2 + f_{pe}^2)}} \tag{4.13}$$

where, F $= (f_o^2 + 2f_{pe}^2 + f_{ce}^2)$.

On neglecting $\kappa_\times$ in Eq. 4.11, we find κ_{eff} reduces to $\kappa_\perp$. Substituting this in the principal Eq. 2.2 for probes resonance frequency we get a modified bi-quadratic equation,

$$f_r^4 - f_r^2(f_o^2 + f_{ce}^2 + f_{pe}^2) + f_{ce}^2 f_o^2 = 0 \tag{4.14}$$

This also gives four real roots of f_r. The positive roots of f_r are f_{r1} and f_{r2} given by,

$$f_{r1,r2} = \sqrt{(F/2) \pm \sqrt{(F/2)^2 - f_o^2 f_{ce}^2}} \tag{4.15}$$

where, F $= (f_o^2 + f_{ce}^2 + f_{pe}^2)$.

Solving Eq. 4.14 in terms of f_{pe} as a function of f_r, f_{ce} and f_o we obtain,

$$n_e[10^{10} cm^{-3}] = 1.23(1 - f_{ce}^2/f_r^2)(f_r^2 - f_o^2) \tag{4.16}$$

In Eq. 4.16, the electron density has positive values only when both bracketed terms carry the same sign. Therefore the probe will resonate at a frequency greater than f_o provided if it satisfies the condition $f_r > f_{ce}$. Otherwise the resonance frequency shall fall below the vacuum frequency $f_r < f_o$.

4.3 Experimental Setup

4.3.1 Description of Plasma Reactor

For the systematic study of the effect of magnetic field on probes resonance frequency, we install the hairpin in an inductive RF source [102, 103] which comprises a plasma production region or the source, and a diffusion region. The plasma is created by an inductive discharge by applying 13.6 MHz RF frequency to a three turn air cooled antenna wound on a quartz tube. The external diameter of the quartz tube is 10 cm, wall thickness of 1.0 cm and a length of 15.0 cm. Using a matching network, a maximum power is transferred to the antenna by matching its impedance to the generator output impedance of 50 Ohm. The match box is positioned in a manner that allows direct connection of the antenna to the output capacitor of the matching network. This reduces the ohmic power loss at the antenna side of the matching network. The match box is used in an automatic matching mode so that the power delivered to the discharge remains constant. The diffusion chamber comprises a stainless steel cylinder with internal diameter 41 cm, length 29 cm terminated at both ends with stainless steel plates. The chamber is shielded using aluminum electrostatic shields which enclose the tube and antenna to prevent RF radiation.

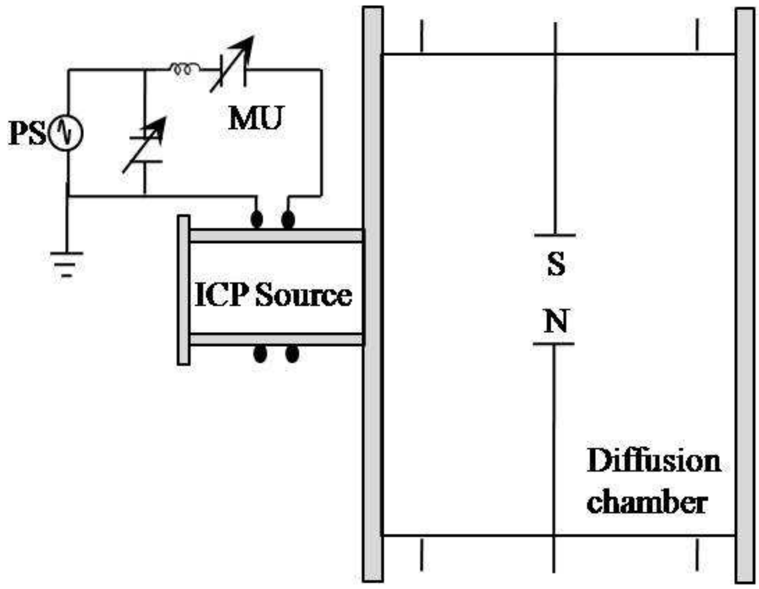

Figure 4.5: Applied Radio Frequency (13.56MHz) Inductive source: NS are poles of Magnets, PS is Power supply and MU is matching unit.

The plasma is formed in a capacitive mode by applying the large rf voltage on the antenna. When the plasma density increases adequately the discharge transit into an inductive mode which is maintained by the time varying magnetic field associated with the rf currents through the antenna. Predominantly, the experiments were performed in the range of 100 W to 500 W where the rf power coupling was stable with little or no reflected power. Some specific experiments were performed at higher powers of up to 700 W depending on the subject under study. The pressure (in microbar) varied in a range from 1.0 to 8.0.

4.3.2 Magnetic Field Configuration

For a systematic study of the effect of magnetic field on the probe's resonance frequency, we used two cubical shaped permanent magnets with pole strengths of 0.43 Tesla each having dimension (in cm) $5 \times 5 \times 2.5$. They are installed inside the chamber from the diametrically opposite ports as shown in Fig. 4.5. They are positioned inside the chamber using a vacuum feed-through arrangement with a holder for the magnets. The other end is completely vacuum sealed. By moving the feed-throughs, the separation between the magnets can be easily adjusted and thus the magnetic field strength at the center of the chamber can be varied systematically during the experiments. The holder is also useful to keep the strong magnets separated as per requirement. The spatial field strength was measured using a Hall probe designed prior to producing the plasma. The picture of the hall probe used for the magnetic field measurements is shown in Fig. 4.8.
In Fig. 4.6, the magnetic lines of force around the two permanent bar magnets are shown where they are facing opposite poles to each other. One can see that the field strength between the magnets is quite uniform where the measurements were performed. In Fig. 4.7, the magnetic field strength measured at the center is plotted as a function of separation (x) between the magnets. The magnets could be moved closer or further from each other with the help of the feed-through.

4.3.3 Magnetic Field Sensor (Hall Probe)

To measure the magnetic field strength, a measurement probe is a need i.e. a magnetic field sensor. The magnetic field sensor is composed of a hollow ceramic

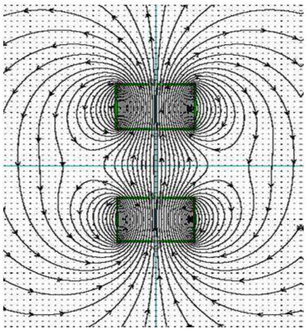

Figure 4.6: Magnetic lines of force around two bar magnets.

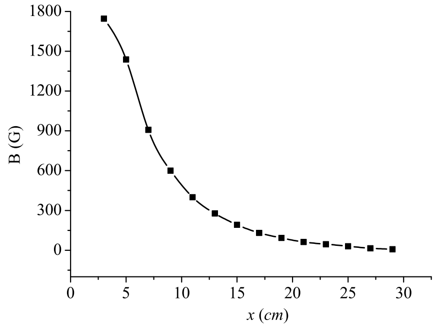

Figure 4.7: Magnetic field strength at the center of chamber where x is the separation between the magnets.

rod, a battery, and a multimeter. These parts are sketched in Fig. 4.9.

Figure 4.8: Hall probe for the measurement of magnetic field strength.

The hollow rod is made of ceramic with a hall effect transducer chip [104] at one end (shown as the circle on the right hand end with three pins coming out of it). The chip produces a voltage that is linear with the magnetic field. The Amplifier (battery) is contained in a small box and allows measuring a greater range of magnetic field strengths. The multimeter gives the reading of the voltage with and without the magnetic field. The magnetic field strength can be directly calculated from the following formula:

$$B(inGauss) = \frac{(V_{withB-field} - V_{withoutB-field}) \times 1000}{1.3} \tag{4.17}$$

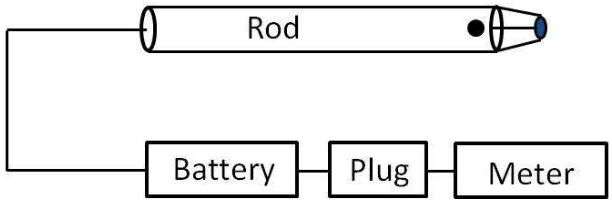

Figure 4.9: Schematic of Hall probe.

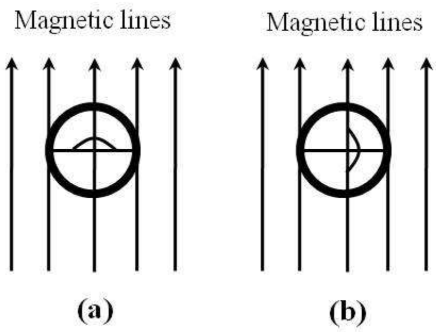

Figure 4.10: Sensor position: (a) orientation for maximum reading (b) orientation for zero reading.

The maximum output of the chip occurs when the area vector of the hump on the sensor points directly toward a magnetic south pole, as shown in Fig. 4.10.

4.3.4 Installation of Hairpin Probe and Spherical Langmuir Probe

The hairpin is introduced from the top port pointing perpendicular to the magnetic field lines such that $\vec{k}\perp\vec{B}$ as shown in Fig. 4.11. The hairpin floats at the center of chamber, in the region of the uniform B-field region. The magnetic field at the center is altered by simply changing the separation between the permanent magnets. The spatial magnetic field strength is measured using the Hall probe prior to producing the plasma. Using this setup, we achieved a local maximum electron density of about $5 \times 10^{10} cm^{-3}$ at approximately 15.0 cm away from the plasma source region where the hairpin is situated. On increasing the B-field the local electron density decreases between the poles of the magnets due to the limited cross-field diffusion of electrons across the magnetic field lines.

In order to keep the electron density the same in the region between the poles of the magnet during variation of the field, we relied on a spherical probe (SP) shown in Fig. 4.11 which was constantly biased at -30.0 Volts and the corresponding ion current variation indicates the local change in plasma density on changing the magnetic field strength.

The two probes are physically separated by a distance of 3.0 mm. Also, the SP is kept in the consecutive magnetic flux tube with respect to the hairpin so that there should not be any influence on the hairpin measurements due to shadowing effect by SP. Both probes are placed in the uniform magnetic field region of plasma. Throughout the entire experiment, the current was maintained constant at $I_{+} = 280\mu A$ by adjusting the RF power (100 W to 900 W) and slightly varying the background gas pressure (5.0×10^{-3} mbar to 8.0×10^{-3} mbar). The wires of the hairpin resonator were made of Platinum Rhodium alloy with radius 0.125 mm, typical length about 20.0 mm to 30.0 mm and separation of about 3.0 mm to 4.0 mm.

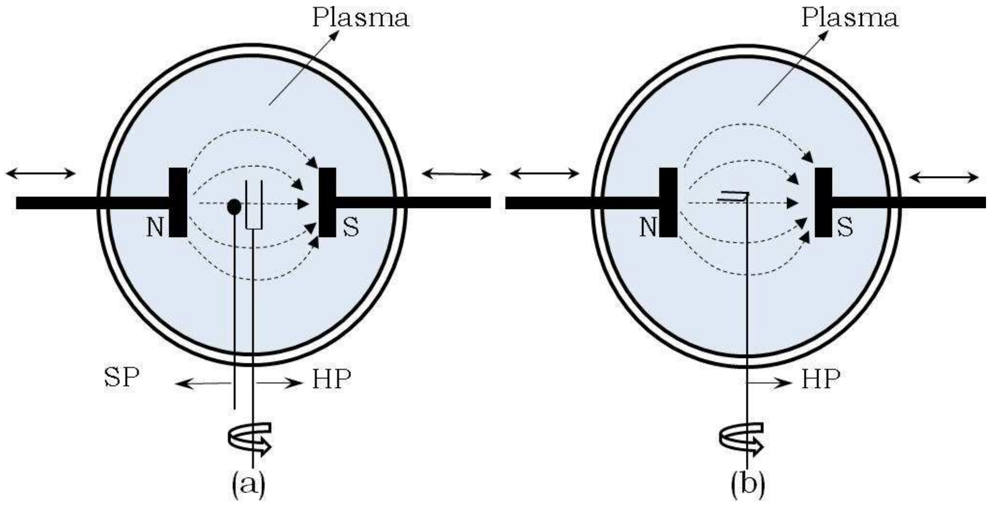

Figure 4.11: Front view of the ARIS: (a) SP (spherical probe) and HP (hairpin probe) installed normal to magnetic axis i.e. $\vec{k}\perp\vec{B}$ and (b) HP installed along the magnetic axis i.e. $\vec{k}||\vec{B}$.

4.4 Experimental Results

4.4.1 Typical Spectrum of Resonance Signals in Presence of Magnetic Field

The typical resonance signals for $\vec{k}\perp\vec{B}$ and $\vec{k}||\vec{B}$ are shown in Figs. 4.12 and 4.13. Unlike non-magnetized plasmas we observe that the hairpin displays dual resonances namely f_{r1} and f_{r2}, where, $f_{r1} > f_o$ and $f_{r2} < f_o$. Both resonance frequencies shift away from the vacuum frequency f_o with the increase in electron density. This is shown in Figs. 4.14 and 4.15. One basic characteristic difference found that the f_{r2} tends to saturate at f_{ce} when f_o value is chosen below f_{ce}. Whereas, in Fig. 4.15 both f_r's responded to increase in discharge power from 100 W to 500 W by moving away from f_o.

Similar behavior is also observed for the case $\vec{k}||\vec{B}$ as shown in Fig. 4.16 and 4.17. However, when $f_o > f_{ce}$ we found that f_{r2} falls outside the starting frequency, which is 2.0 GHz. Therefore f_{r2} is not present in the spectrum. Hence we only

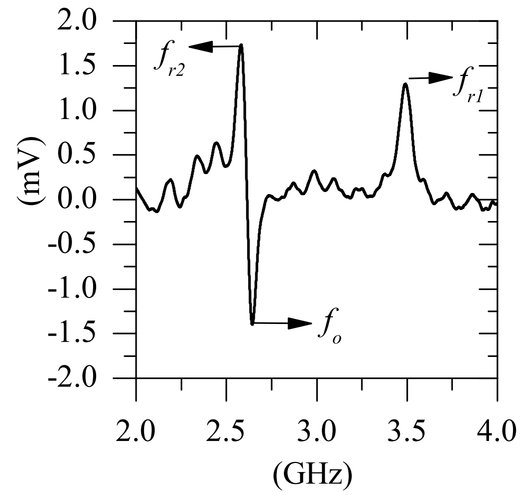

Figure 4.12: Resonance signal for $\vec{k}\perp\vec{B}$ case where $f_o = 2.625GHz$.

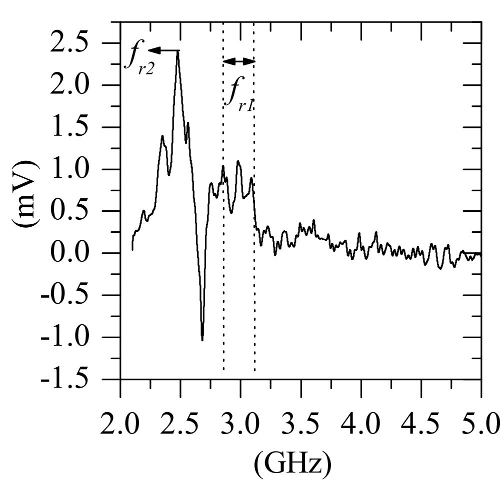

Figure 4.13: Resonance signal for $\vec{k}||\vec{B}$ case where $f_o = 2.68GHz$.

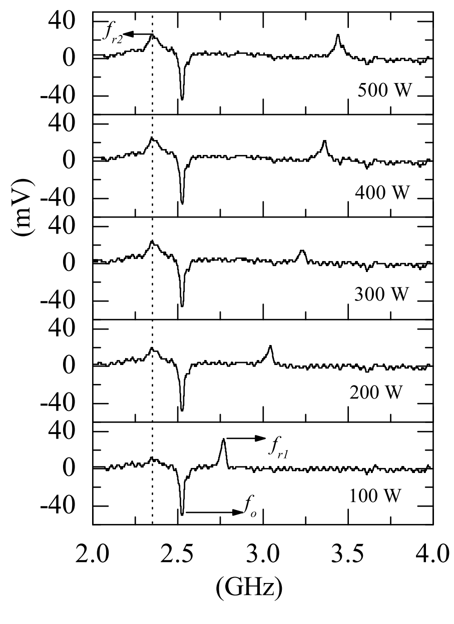

Figure 4.14: Resonance signals of hairpin obtained in plasma for case $\vec{k}\perp\vec{B}$ and $f_o > f_{ce}$, where $f_o = 2.52GHz$ and $f_{ce} = 2.3GHz$.

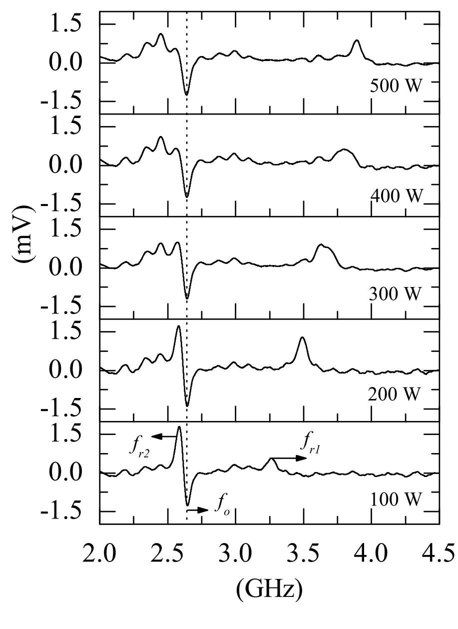

Figure 4.15: Resonance signals of hairpin obtained in plasma for case $\vec{k}\perp\vec{B}$ and $f_o < f_{ce}$, where $f_o = 2.64GHz$ and $f_{ce} = 2.8GHz$.

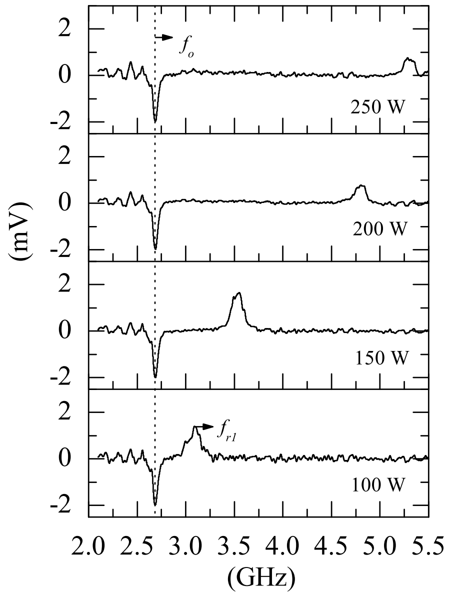

Figure 4.16: Resonance signals of hairpin obtained in plasma for case $\vec{k}||\vec{B}$ and $f_o > f_{ce}$, where $f_o = 2.68GHz$ and $f_{ce} = 1.0GHz$.

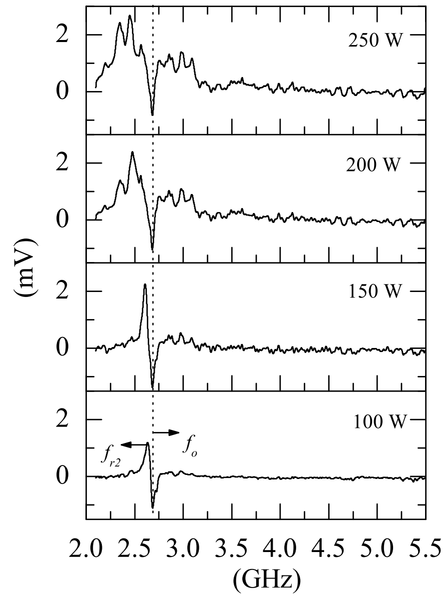

Figure 4.17: Resonance signals of hairpin obtained in plasma for case $\vec{k}||\vec{B}$ and $f_o < f_{ce}$, where $f_o = 2.68GHz$ and $f_{ce} = 3.14GHz$.

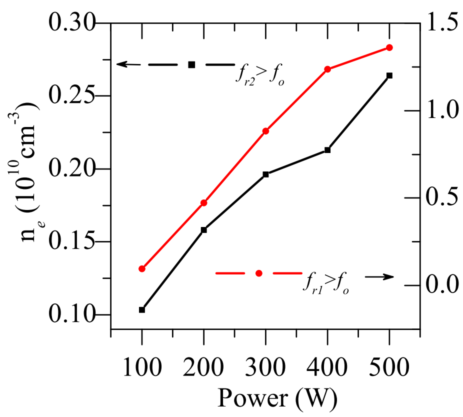

Figure 4.18: n_e vs power. Conditions: $\vec{k}\perp\vec{B}$, 6.4×10^{-3}mbar, B = 0.1T, f_o = 2.4871GHz.

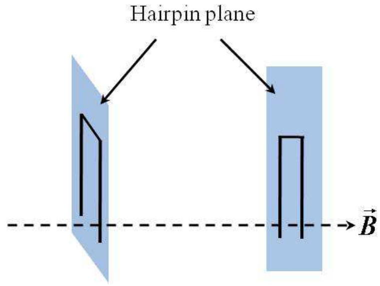

Figure 4.19: Hairpin rotation sketch with respect to B-field.

observe f_{r1} shifting with discharge power. On the other hand, when $f_o < f_{ce}$ we find that f_{r2} is present within the range of scanning frequency and it moves apart from f_o as we increase the plasma density by increasing the discharge power from 100 W to 250 W. However, in this case we observed that f_{r1} resonance signal is found to be strongly attenuated and not responding significantly to the change in background plasma density.

In Fig. 4.18, we plotted the electron densities calculated using f_{r1} and f_{r2} for a range of discharge powers for a case when $\vec{k} \perp \vec{B}$ and $f_o < f_{ce}$. The electron density is calculated using a revised formula given in Eq. 4.16 for a given value of $f_{ce} = 2.8$ GHz. The reason for discrepancy in the electron densities using two resonances is discussed in section 4.5.

4.4.2 Effect of Probe Rotation on Resonance Signal

For the $\vec{k} \perp \vec{B}$ case, we investigated the effect of hairpin's plane rotation with respect to the B-field on the resonance frequency. The schematic of the set-up is as shown in Fig. 4.19. Here, we defined θ as an angle between the plane of hairpin and magnetic field.

In order to avoid spatial inhomogeneity of electron density introduced by the magnetic field, we limited the field strengths from B = 10 mT to 59 mT. It is found from Figs. 4.20 and 4.21 that the difference is less than 2%, indicating no significant effects introduced due to the rotation of the probe relative to the field.

Therefore, the estimate of the electron density remains largely unaffected as shown in Fig. 4.21. This rotation of the probe by 90^o merely interchanges E_x and E_y as discussed in section 4.2.3. However if magnetic field is strongly non-uniform compared with the probe length, then one may need to take in to account the spatially varying density around the resonator.

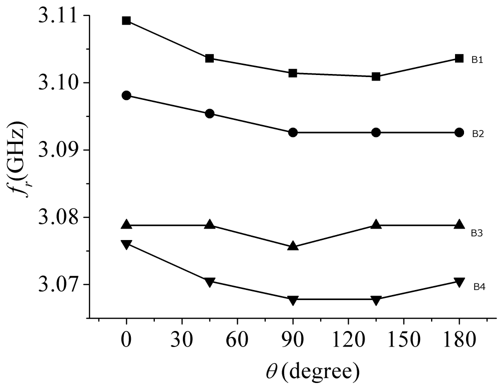

Figure 4.20: Resonance frequency versus different rotation of hairpin plane w.r.t B-field where B1 = 0.01T, B2 = 0.017T, B3 = 0.03T and B4 = 0.059T.

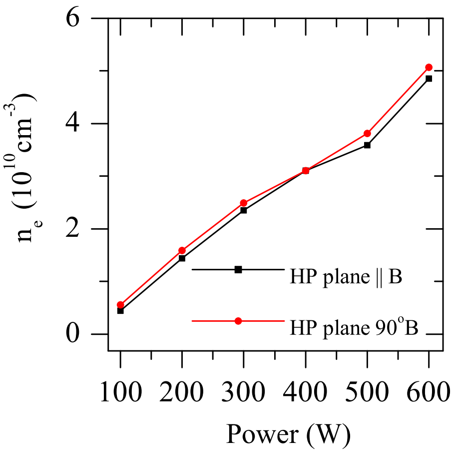

Figure 4.21: Electron density calculated using f_{r1} vs discharge power for two rotation of hairpin plane w.r.t B-field (0.08T) in Argon plasma 6.4×10^{-3}mbar, f_{ce} = 2.24GHz and f_o = 2.5269GHz.

4.4.3 Effective Plasma Permittivity Measured by Hairpin

The effective permittivity in the presence of magnetic field is given by $\kappa_\perp$. In order to verify this fact, we systematically vary f_{ce} by varying the magnetic field over a wide range of field strengths 0.01T to 0.15T while keeping the background plasma density (or f_{pe}) constant.

In Fig. 4.22, we present the resonance frequency f_r verses f_{ce} normalized to f_o. On the same plot we show the numerical values of f_r's obtained using Eqs. 4.13 and 4.15.

The results shows that the measured f_r values match very well with the calculated ones based on considering $\kappa_\perp$. Therefore the role of $\kappa_\times$ can be neglected. Therefore, $\kappa_\perp$ is found to be a good approximation for calculating the electron density in case of magnetized plasma. Similar results are obtained for the case when

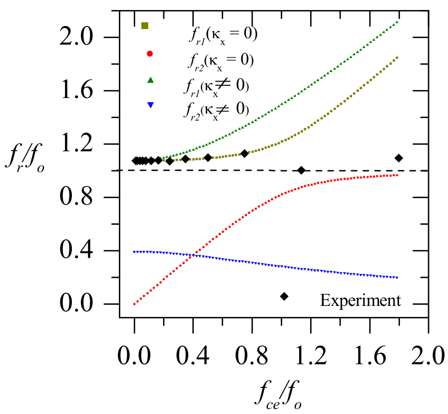

Figure 4.22: Plot of f_r vs f_{ce} where the hairpin plane is position along the B-field (f_o=2.24GHz and f_{pe}=0.8871GHz).

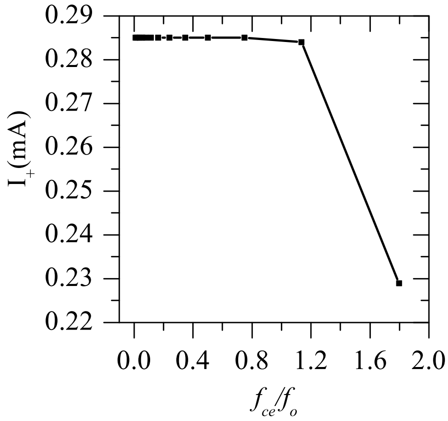

Figure 4.23: Positive ion current corresponding to the experimental data shown in Fig. 4.22.

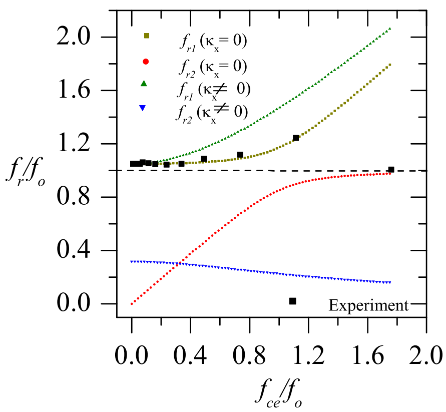

Figure 4.24: Plot of f_r vs f_{ce} where the hairpin plane is position normal the B-field (f_o=2.284GHz and f_{pe}=0.73GHz).

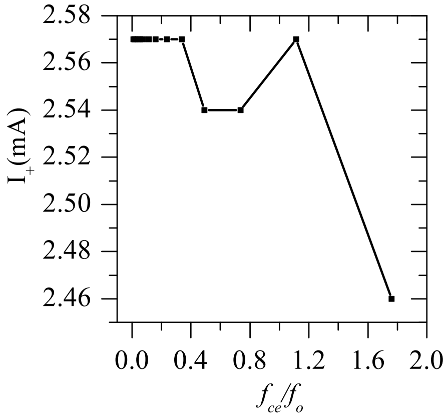

Figure 4.25: Positive ion current corresponding to the experimental data shown in Fig. 4.24.

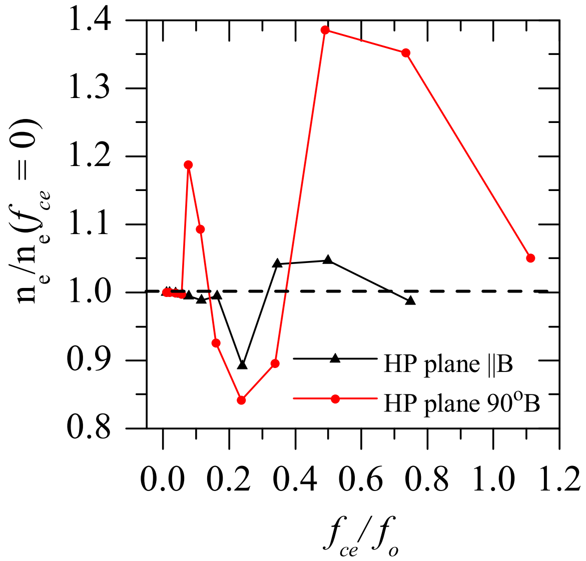

Figure 4.26: n_e versus f_{ce}, where density is normalized with the measured density when $f_{ce} = 0$ and f_{ce} by f_o.

the hairpin plane is placed normal to the field lines as shown in Fig. 4.24.

During the above experiments, constant plasma density was maintained by adjusting the background neutral pressure and power applied to the discharge. This is indicated from the plot of ion-saturation current verses f_{ce} in Figs. 4.23 and 4.25. The ion saturation current is nearly flat except for strong magnetic field greater than 0.1T as very high discharge powers was required for keeping the density constant.

Fig. 4.26 shows the normalized electron density $n_e/n_e(f_{ce} = 0)$ as a function of f_{ce}/f_o. Plasma density is found to be nearly constant as expected within reasonable experimental error. The error is caused due to slight deviation of experimental conditions when discharge power and pressure is varied for keeping the ion saturation current constant during changing the field strength.

4.5 Discussion

One of the important observations presented in previous section is the excitation of dual resonances due to the presence of external magnetic field. When the resonance frequency is below f_o, it suggests that the plasma electrons behaving similar to a dielectric material which are characterized by permittivity $\kappa > 1$. On the other hand, permittivity $\kappa < 1$ is generally observed in the case of non-magnetized plasma. Therefore plasma electrons behave differently at distinct resonance frequencies due to because of the intrinsic nature of $\kappa_\perp$.

Using Eq. 4.4, we observe the resultant permittivity of the plasma, $\kappa_\perp > 1$ for all resonance frequencies which are below the cyclotron frequency ($f_r < f_{ce}$). The electrons are considered to be strongly magnetized as the oscillating field between the probe is slower than the gyration.

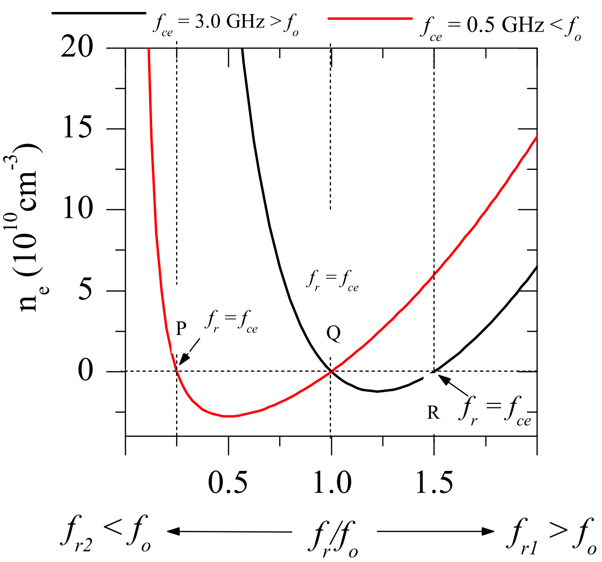

Figure 4.27: Electron density (n_e) as a function of f_r normalized to f_o for a given magnetic field strengths. The exclusion frequency at which $n_e < 0$ stretches between f_{ce} and f_o. These are indicated between the points PQ and QR respectively for the red and black curves.

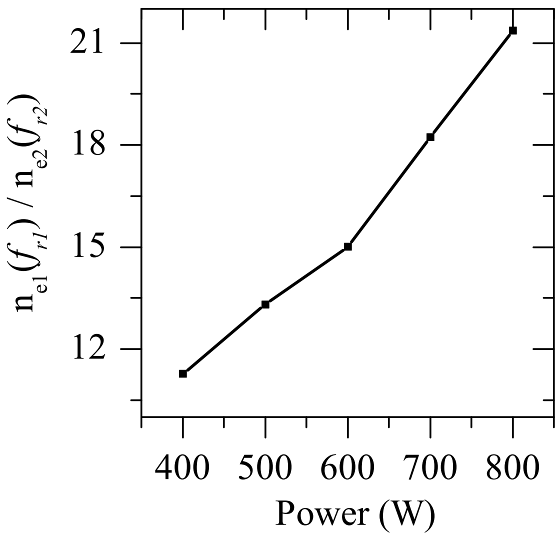

Figure 4.28: Ratio of the electron densities calculated using f_{r1} and f_{r2} as a function of discharge power.

On the other hand when $f_r > f_{ce}$ the electron response is governed by both time-varying electric field and the static magnetic field. In Fig. 4.27, we present the characteristic density curves as a function of normalized resonance frequency according to Eq. 4.16. We considered two magnetic field parameters, in one case the chosen value of $f_o < f_{ce}$ (red curve), in second case it is $f_o > f_{ce}$(black curve). We observe that for the same value of electron density satisfying two resonance frequencies, one f_{r1} appearing above f_o and f_{ce} while the second resonance frequency f_{r2} below f_o and f_{ce} respectively.

An exclusion range is obtained for frequencies giving negative values of n_e. These are unphysical therefore no resonances can be observed. For the red curve, the lower limit of the exclusion region is f_{ce} as indicated by P while the upper limit at Q corresponds to the vacuum resonance f_o. This swaps in the case for black curve as the lower limit of the exclusion region is f_o while the upper limit at R is f_{ce}. At these points, the electron density is zero. However, the same condition is satisfied at one single point Q if $f_o = f_{ce}$.

Physically, when $f_r = f_o$ means no plasma electrons are present between the pins. Therefore, the resonance frequency will be same as that observed in the case of vacuum. This is the point Q on the graph. On the other hand $n_e = 0$ at points P and R corresponds to $f_r = f_{ce}$. This above situation is paradoxical as the existence of f_{ce} must be associated with electrons present in the system. Practically, this is only possible if $f_{pe} << f_{ce}$. The electrons are strongly magnetized such that the characteristic electron plasma frequency practically disappears as compared with the gyro motion. In order to observe shift in f_{r2}, sufficient electron density is required such that $f_{pe} > f_{ce}$. This is also evident from Fig. 4.14 in which f_{r2} is not changing with the background plasma density. On the other hand f_{r1} monotonically increases with density. This corresponds to the right hand branch of the curve for all values $f_r > f_o$.

When f_o is chosen to be lower than f_{ce}, we also find a similar behavior shown by black curve. Therefore we observe both resonances f_{r1} and f_{r2} responding to the change in background electron density by departing away from f_o. This is consistent with the observation in Fig. 4.15.

According to above discussion one expects to obtain same electron densities using f_{r1} and f_{r2}. However, this is not the case as found from Fig. 4.28. The discrepancy in electron density increases with the discharge power.

A possible reason for observing this anomalous effect may be due to local depletion of electrons around the resonator when the probe is resonating close to f_{ce}. This can lead to to strong $\vec{E} \times \vec{B}$ interaction between the oscillating field of the probe and the external electric field cause the electrons to be pushed away from the vicinity of the probe. The electric field is in resonance with the cyclotron motion of electrons at f_{ce}.

When $f_o \approx f_{ce}$ in Fig. 4.27, both f_{r1} and f_{r2} move away from f_{ce}. On the other hand choosing the vacuum frequency much below the cyclotron frequency as in the case of the black curve, will make the f_{r1} component relatively closer to f_{ce} than f_{r2} for a given density. In this case we expect that f_{r2} will give a better estimate of density than f_{r1}. The above fact is supported from the experimental data shown in Fig. 4.17 for the case $f_{ce} >> f_o$. In this case we observe pronounced peak of f_{r2} as compared with f_{r1}.

We found that the probe can resonate at a frequency smaller or greater than its vacuum resonance for the same electron population. For a given magnetic field, the electrons are bounded by the magnetic field irrespective of the orientation of the probe with respect to the field lines. However ponderomotive force can act on certain population of electrons because of spatially varying oscillating E-field and static magnetic field. In that sense there can be distinct population of electrons affected by the external magnetic field inside probes surroundings. However, it is hard to pursue that the observed (two) resonances are due to different populations of electrons. The dispersion relation $\kappa_\perp$ is valid for all electrons and it results in two roots that corresponds to same density. Since one of the roots is closer to f_{ce}, the interaction leads to pushing electrons away from the probe (resonance heating) resulting in the underestimated density as observed in the case of f_{r2} in Fig. 4.28. On the other hand the upper root f_{r1} is much above the cyclotron frequency, hence secondary effects due to electron cyclotron heating are small. Hence f_{r1} is better for the calculation of electron density. In order to avoid this discrepancy, one should aim in keeping f_o well above the f_{ce} value. This can be possible by simply reducing the length of the hairpin so that probe resonate at frequency much above the gyration rate of electrons.

4.6 Summary and Conclusion

In this chapter, we presented the theoretical and experimental study of hairpin probe in magnetized plasma. The first part focused on an analytical model that describes various dispersion relations depending upon the angle between probe's wave vector ($\vec{k}$) and the applied magnetic field strength. The second part focused on the experimental method to verify the dispersion relation valid in the case of a hairpin immersed in a magnetized plasma. However, the experiments were performed for the specific case when $\vec{k}\perp\vec{B}$. The variation in resonance frequency of the hairpin is studied as a function of applied magnetic field strength and the electron density. In presence of a magnetic field, the time varying electric field between the pins drives electron motion perpendicular to the magnetic field. This makes the plasma anisotropic in nature and results in a direction dependent plasma permittivity with respect to the magnetic field.

The spatial distribution of the electric field around the hairpin is not confined to a single plane due to its three dimensional geometry. Therefore, it observes an effective plasma permittivity and gives an average electron density. For a sufficiently strong magnetic field, the probe resonance condition is found to be satisfied at two distinct frequencies. A second resonance appears, unlike in the case of a magnetic field free plasma, which is below the resonance frequency in air/vacuum. This suggests that the plasma electrons are tied to the field lines and are strongly coupled similar to the electrons present in dielectrics. Under such conditions, the resonant properties are found to be strongly influenced by the factors such as probe dimensions, electron density, applied magnetic field and unknown particle trajectories in the vicinity of the probe. Both resonances show two distinct plasma properties that stands for the presence of bounded and free electrons near the vicinity of the hairpin. Absolute values of densities calculated using two resonances depends on how the applied fields sample the electron population near the hairpin. Precisely, the accurate density depends on the spatial distribution of both electric and magnetic fields.

Systematic experiments for investigating the probe properties in the presence of an external magnetic field were performed in the radio frequency inductively coupled plasma source. The dispersion relation for calculating the electron density is verified experimentally. A modified formula is proposed for obtaining the electron density directly from the relative shift of resonance signal in plasma from that in vacuum for a known magnetic field strength. However, the n_e measurements are found to be unaffected by the probe rotation for $\vec{k}\perp\vec{B}$ under given experimental conditions. The experimental study of the dispersion relation for the case when the hairpin is placed in a non-uniform magnetic field region is not included in our present investigations and recommended for future investigation.

CHAPTER 5

The Study of Q-Factor of the Resonance Signal

5.1 Motivation

In section 2.5, we presented an experimental and simulation study of the characteristics of the resonance signal in air/vacuum. The peaked-ness of the resonance signal defined as the Quality-factor ($Q = f_{central}/\Delta f_{FWHM}$) is an important criteria [105–107] for determining the central frequency of the resonance signal with accuracy. Uncertainty in finding the exact value of $f_{central}$ can lead to error in the calculation of absolute density by hairpin.

The sharpness of the resonance peak is adversely affected by the dissipative factors. These are due to the resistivity of the wire and the position of the loop antenna with respect to the hairpin. Resistive elements are contributed from the probe wire, electron-neutral collisions in plasma, radiation and through wave-particle interaction such as Landau-damping phenomenon. If the plasma has an external magnetic field then the electron dynamics in the presence of a static magnetic field and the probe's oscillating electric field further complicate the situation.

In this chapter we specifically deal with these aspects in plasma. For the basic understanding of the Q-factor, we discuss the transmission line model of hairpin resonator in section 5.2. Section 5.3 describes the factors influencing the signal width in non-magnetized plasma. The experimental results are presented and discussed in section 5.4. Section 5.5 presents a summary and conclusion of the chapter.

5.2 Transmission Line Properties of Hairpin Resonator

The hairpin probe can be simplified by considering it as a two-wire parallel transmission line. In this model, one end of the transmission line is shorted while the other end is open. A wave initiating from the closed end reach the open end of the hairpin. Because of the impedance mismatch the wave is reflected back resulting in standing wave pattern along the length of the transmission line. For $L = \lambda/4$, (quarter wave-length) an anti-node of the wave is created at the open end yielding the greatest potential difference, while a node is formed at the short-circuited end of the hairpin.

Under the above condition the transmission line is said to be under resonance. During this event, the adjacent conductors carry currents at every point and they are out-of-phase with each other. In one branch the current flows to the left, while in the other the current flows to the right. Based on the above model, Warne et al of Sandia National Laboratory [108] and the Sugai group [72, 88] of Chubu University, presented a model of the hairpin circuit for the free-space. They compared their analytical results with those simulated using FDTD simulation similar to the one we presented in chapter-2. In this chapter we present comparison of the transmission line model with our experiments. Before that we present an overview of the model based on that of Sugai et al [72, 88] who proposed a theory for collisional plasmas.

5.2.1 General Criteria for the Resonance

The transmission line model of the hairpin is based upon distributed capacitance per unit length between the wires and inductance per unit length along its length. These elements contribute to reactive impedances namely, $X_C = 1/\omega C$ and $X_L = \omega L$. The X_C opposes dynamic voltage while X_L oppose the time-varying current. During the resonance, these reactive impedances are equal ($X_C = X_L$) allowing maximum transfer of the power from the source to the load end. This happens at a particular angular frequency ω_r termed as the resonance frequency given by [91],

$$\omega_r = \frac{1}{\sqrt{LC}} \tag{5.1}$$

The input impedance of the transmission line can be simplified to an RLC circuit as follows:

$$Z_{in} = \frac{V}{I} = R + j\omega L + \frac{1}{j\omega C} = R + j\left(\omega L - \frac{1}{\omega C}\right) \tag{5.2}$$

At resonance, the only opposition to the flow of current is due to the resistance i.e. $I_r = E/R$ instead of $I_r = E/Z$. The voltage will be at 90^o out of phase with the current in the circuit. The current in the 'tuned' or resonant series circuit is indicated at the peak of the resonance curve of Fig. 5.1. The effect of resistance is to reduce the resonant energy of the circuit. The energy lost per cycle is (Power)×(time for a cycle) $= I_{RMS}^2 R \times \frac{2\pi}{\omega_R} = I_{max}^2 R \times \frac{2\pi}{\omega_R}$. Therefore as the resistance increases, the resonance curve is broader and flatter due to reduction in circuit energy.

The magnitude of the impedance is minimal at the resonance frequency ω_r for which $Z_{in} = R$. At $\omega = \omega_r + \Delta\omega_r$, we get:

$$Z_{in} = R + j(\omega_r + \Delta\omega_r)L + \frac{1}{j(\omega_r + \Delta\omega_r)C} \tag{5.3}$$

where, $2\Delta\omega_r$ is the broadening of the resonance signal commonly known as signal width.

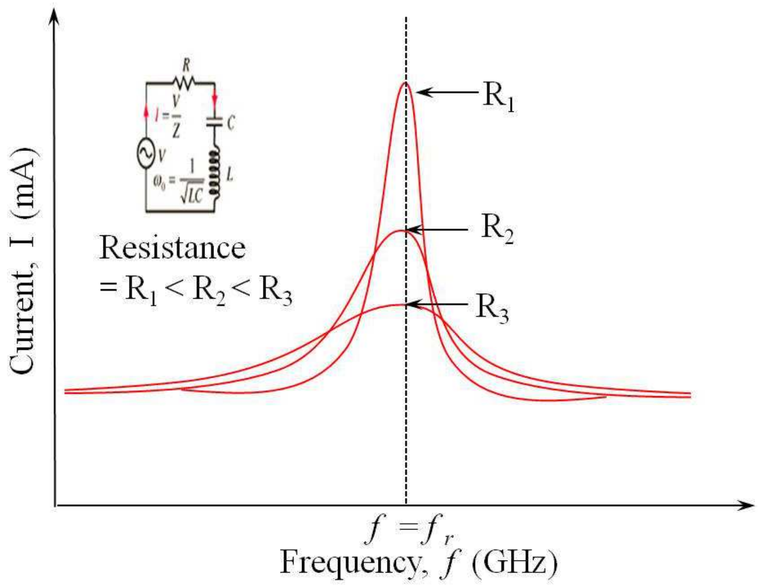

Figure 5.1: Series RLC-circuit and resonance curves for different resistance of the circuit.

$$Z_{in} = R + j\omega_o + j\Delta\omega_o L + \frac{1}{j\omega_o C}\left(1 + \frac{\Delta\omega_o}{\omega_o}\right)^{-1} \tag{5.4}$$

Applying binomial expansion and neglecting higher order terms of $\frac{\Delta\omega_r}{\omega_r}$ we get:

$$Z_{in} = R + j\omega_o + j\Delta\omega_o L + \frac{1}{j\omega_o C}\left(1 - \frac{\Delta\omega_o}{\omega_o}\right) \tag{5.5}$$

$$Z_{in} \cong R + j\Delta\omega_o L - \left(\frac{\Delta\omega_o}{j\omega_o C}\right) = R + 2j\Delta\omega_o L \tag{5.6}$$

Therefore, the impedance of the LCR circuit is proportional to the signal width, resistance of the wire and the inductance. However, the components R, L, and C of transmission line can be considered lumped or distributed constants. The lumped circuit refers to the assumption that the entire circuit (or system) is at a point (or in one lump), so that the dimensions of the system components (e.g. individual resistors or capacitors) are not important. The typical lumped elements are inductor, resistor, and capacitor. In other words, the circuit element is said to be lumped if the instantaneous current entering one of its terminals is equal to the instantaneous current throughout the element and leaving the other terminal. The lumped element model is valid whenever $L_c << \lambda$, where L_c denotes the circuit's characteristic length, and λ denotes the circuit's operating wavelength [91]. The dependent variables such as current and voltage are a function of time only. This means doing circuit analysis by solving a set of ordinary differential equations.

5.2.2 Analysis of Factors Responsible for the Determination of Signal Quality-Q

In the case of a distributed element model or a transmission line model of electrical circuits we assume that the attributes of the circuit (resistance, capacitance, and inductance) are distributed across the whole geometry. All dependent variables are functions of time and one or more spatial variables. This means doing circuit analysis by solving a set of partial differential equations. Unlike the lumped element model, it assumes non-uniform current along each branch and non-uniform voltage along each node. The model is used at high frequencies where the wavelength approaches the physical dimensions of the circuit, so the lumped element model used at higher frequencies becomes inaccurate. Therefore, we start our study with the distributed resonance model to do circuit analysis of quarter wavelength hairpin structure.

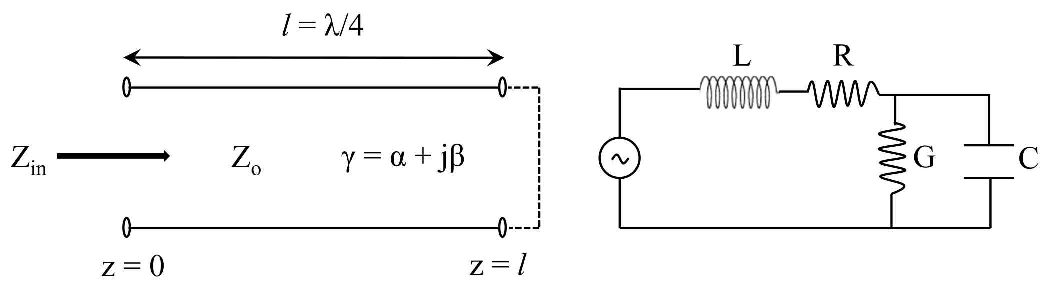

Figure 5.2: Equivalent circuit of hairpin.

Let $z = 0$ be the position of the short-circuited end while the open end is situated at

$z = l$ as shown in Fig. 5.2 [72, 88, 91]. Let Z_o represent the characteristic impedance of the line with the propagation constant $k = \alpha + j\beta$, where α is the attenuation constant and β is the phase constant of the standing wave. Based on distributed element LCR model, the voltage reflection coefficient $\Gamma(z)$ and impedance $Z(z)$ at the position z can be expressed as [91]:

$$Z(z) = Z_o \frac{e^{-\alpha z}e^{-j\beta z} + \Gamma_o e^{\alpha z}e^{j\beta z}}{e^{-\alpha z}e^{-j\beta z} - \Gamma_o e^{\alpha z}e^{j\beta z}} \tag{5.7}$$

where, the reflection coefficient $\Gamma(l) = -1$ which is the condition when open circuited load completely reflect an incident microwave signal.
For the length $l = \lambda/4$ at $\omega = \omega_o$, where $\lambda_o = 2\pi c/\omega$ with c is the speed of light in free space. In general, $\lambda = 2\pi c/\omega$, satisfy:

$$\beta l = \frac{2\pi}{\lambda} l = \frac{2\pi\lambda_o}{4\lambda} = \frac{\pi\omega}{2\omega_o} = \frac{\pi(\omega_o + \Delta\omega_o)}{2\omega_o} \tag{5.8}$$

$$e^{\pm j\beta l} = -e^{\pm j\frac{\pi(\omega_o + \Delta\omega_o)}{2\omega_o}} = \pm j e^{\pm(\frac{\pi\Delta\omega_o}{2\omega_o})} \tag{5.9}$$

On substituting above in Eq. 5.7 we obtained the following expression:

$$Z_{in}(l) \cong Z_o \frac{1 - e^{-2\alpha l}}{1 + e^{-2\alpha l}} \left[1 + j \frac{e^{-2\alpha l}}{1 - e^{-2\alpha l}} \frac{\pi\Delta\omega}{\omega_o} \right] \tag{5.10}$$

$$Z_{in}(l) \cong R_{eq} \left(1 + j2Q\frac{\Delta\omega}{\omega_o} \right) = R_{eq} + j2L_{eq}\Delta\omega \tag{5.11}$$

Comparing above equation with Eq. 5.6 of lumped series LCR circuit at a frequency of $\omega_o + \Delta\omega$, we get

$$R_{eq} = Z_o \frac{1 - e^{-2\alpha l}}{1 + e^{-2\alpha l}} \tag{5.12}$$

$$L_{eq} = \frac{\pi Z_o e^{-2\alpha l}}{2\omega_o(1 + e^{-2\alpha l})} \tag{5.13}$$

$$C_{eq} = \frac{2(1+e^{-2\alpha l})}{\pi Z_o \omega_o e^{-2\alpha l}} \tag{5.14}$$

$$Q = \frac{1}{\omega_o R_{eq} C_{eq}} = \frac{\pi e^{-2\alpha l}}{2(1-e^{-2\alpha l})} \tag{5.15}$$

And the bandwidth of the equivalent series LCR circuit is defined as $2\Delta\omega$

$$2Q\frac{\Delta\omega}{\omega_o} = 1 \tag{5.16}$$

$$\frac{\Delta f}{f_o} = \frac{2}{\pi}(e^{2\alpha l} - 1) \tag{5.17}$$

By solving phasor transmission line current and voltage equations for the RLCG distributed elements one can obtain simplified relation for the attenuation constant for the resonance frequency, $\omega_r = 1/\sqrt{(}LC)$ as follows:

$$\alpha = \frac{1}{\sqrt{2}}\sqrt{RG - 1 + \sqrt{(R^2 + L/C)(G^2 + C/L)}} \tag{5.18}$$

where G is the conductance of the medium between the parallel wires. For loss-less line, we consider $RG \approx 0$ and above equation can be simplified as follows:

$$\alpha \approx 0.5\left[R\sqrt{(C/L)} + G\sqrt{(L/C)}\right] \tag{5.19}$$

On the other hand, the phase constant of the parallel wire transmission line in terms of the applied frequency is given by:

$$\beta = \frac{2\pi}{\lambda} = \frac{\omega}{c}\sqrt{\epsilon} \tag{5.20}$$

Therefore, for the quarter wavelength transmission line $l = \lambda/4$ we can write the resonance frequency as follows:

$$f_r = \frac{c}{4l\sqrt{\epsilon}} \tag{5.21}$$

The equivalent circuit elements of hairpin structure with radius of wire a, length l and separation of wires w is given as follows:

- **Inductance**

The inductance per unit length (Henry per meter) depends on separation between the conductors (w), diameter (2a) of the wire and magnetic properties of the material surrounding the conductors.

$$L = (\mu_o/\pi)\lg\left(\left(\frac{w}{2a}\right) + \sqrt{\left(\frac{w}{2a}\right)^2 - 1}\right) \tag{5.22}$$

- **Resistance**

The series resistance per unit length (ohm per meter) depends on the shape, dimensions and electrical conductivity of the conductors and the frequency of operation.

$$R = \frac{1}{2\pi a\sigma_{line}\delta} \tag{5.23}$$

The skin depth of the conductor is given by $\delta = \sqrt{\frac{2\rho}{\omega\mu_o\mu_r}}$ where,
$\rho =$ bulk resistivity (ohm-meter)
$\omega =$ frequency (Hertz)
$\mu_o =$ permeability constant (Henries/meter) $=4\pi \times 10^{-7}$
$\mu_r =$ relative permeability (usually one)

- **Capacitance**

The capacitance per unit length (farad per meter) depends on the separation between the conductors, physical dimension and permittivity of the medium surrounding the conductors.

$$C = \frac{\pi\epsilon}{\lg\left(\left(\frac{w}{2a}\right) + \sqrt{\left(\frac{w}{2a}\right)^2 - 1}\right)} \tag{5.24}$$

- **Conductance**

In addition a small leakage current flows between the two parallel wires. The leakage path is modeled as resistors across the two wires. This property is called conductance (G) expressed as the reciprocal of resistance. It is given in μmhos per unit length.

$$G = \frac{\pi\sigma}{\lg\left(\left(\frac{w}{2a}\right) + \sqrt{\left(\frac{w}{2a}\right)^2 - 1}\right)} \tag{5.25}$$

where σ is the conductivity of the medium.

5.3 Analysis of the Attenuation Constant in Plasma

Consider the case of a collisionless non-magnetized plasma. When the resonance is established, the time varying electric field between the pins is given by $\vec{E} = E_o e^{i\omega t}$. The resonance frequency is typically greater than electron plasma frequency $\omega >> \omega_{pe}$ is imposed using a hairpin resonator. The hairpin circuit under the resonance condition is characterized by finite resistance of the probes wire, inductance and distributed capacitance per unit length and the conductivity of the plasma.
The plasma conductivity is the one which determines the ohmic power dissipation in the plasma. It is expressed in terms of local current density $\vec{J}$ and the local electric field $\vec{E}$ through Ohm's law is given by:

$$\sigma_p = \frac{J}{E} = \sigma_r + i\sigma_i = \frac{\epsilon_o \omega_{pe}^2}{\nu_m + j\omega} = \epsilon_o \omega_{pe}^2 \frac{\nu_m - i\omega}{\nu_m^2 + \omega^2} \tag{5.26}$$

where, ν_m is the effective electron collision frequency with other heavier constituents of the plasma and ω_{pe} is the electron plasma frequency. Besides, σ_r and σ_i are the real and imaginary part of the complex conductivity, σ_p. The real part contributes of Eq. 5.26 to the ohmic heating in plasma. The imaginary part is in phase quadrature with the wave electric field. It is given by [109]:

$$I = \frac{e^2 E_o n_e}{m_e \omega} sin(\omega t) \tag{5.27}$$

In this case, there is zero net transfer of power between the wave and plasma over a wave period. The dissipated power is given by:

$$P = \int \frac{|E_o|^2}{2} \sigma_r dV \tag{5.28}$$

The real part of the plasma conductivity in low pressure plasmas ($\omega >> \nu$), is written as:

$$\sigma_r = \frac{\epsilon_o \omega_{pe}^2 \nu_m}{\omega^2} = \epsilon_o \eta \nu_{en} \tag{5.29}$$

where $\eta = \frac{\omega_{pe}^2}{\omega_r^2}$ and the electron-molecule elastic collision frequency ν_m is,

$$\nu_m =< \sigma(V_e)V_e > n_m = K(T_e)n_m = K(T_e)p/k_B T_m \tag{5.30}$$

Here, collision cross-section is σ, electron thermal speed is V_e, molecule density is n_m, molecule temperature is T_m, gas pressure is p and the Boltzmann constant is k_B. The rate constant K for electron-argon elastic collision as a function of T_e can be found in the literature [11].

Substituting the value of conductivity from Eq. 5.29 in Eq. 5.28, the total rate at which power is dissipated is given by;

$$P = \frac{|\vec{E}|^2}{2} \frac{\epsilon_o \omega_{pe}^2 \nu_m}{\omega^2} \tag{5.31}$$

The average energy stored W is given by:

$$W = \frac{1}{2} \int \epsilon |\vec{E}|^2 dv \tag{5.32}$$

The quality factor is the measure of dissipated energy in the resonator. For isotropic homogeneous dielectric, the Q-factor of the system is given by:

$$Q = \omega \frac{W}{P} = \omega \frac{\epsilon_r}{\sigma_r} \tag{5.33}$$

where, W is the average energy stored and P is the average energy lost per second. The Q-factor can also be expressed as:

$$Q = \frac{f_r}{\Delta f(FWHM)} \tag{5.34}$$

Using Eq. 5.33 and Eq. 5.34, the signal width can be obtained as:

$$\Delta f = 2\pi \frac{\epsilon_r}{\sigma_r} \tag{5.35}$$

The factors influencing the signal width are mainly ohmic losses, dielectric losses, radiation losses and coupling losses due to external circuit. In the case of hairpin resonator, the wall losses and coupling losses are not dependent on the plasma parameters since the power coupled to the resonator is constant. The radiation losses from the open end of the resonator related to the physical size of the hairpin. The radiation losses are significant in case of shorter hairpins. Therefore, the dielectric losses is the important factor responsible for determining the Q-factor of the resonance signal.

The radiation resistance (R_{rad} in Ohms) of the short-dipole antenna is given by [108]:

$$R_{rad} = \frac{1}{\pi}\omega\mu_o k(\frac{w+2a}{2})^2\frac{2}{\pi}(kl) \tag{5.36}$$

where, $l' = 2l + w$ is the total length of the antenna and λ is the wavelength. It can also be simplified in terms of frequency and dimension of hairpin ($\lambda = 4l$) as follows:

$$R_{rad} = 4(\mu_o)^2\epsilon_o f_o^2 f_r (w+2a)^2 l \tag{5.37}$$

The total resistance $R = R_{line} + R_{rad}$ of the hairpin is the sum of the radiation resistance and ohmic resistance of wires. The expressions for R_{line} and R_{rad} are given in Eq. 5.23 and Eq. 5.37 respectively. Substituting the values of L, C, and G from Eq. 5.22, Eq. 5.24 and Eq. 5.25 gives the value of α in collision-less plasma,

$$\alpha \approx \frac{\frac{13.2\times10^{-7}}{a} f_o\sqrt{\frac{\rho}{f_r}} + 23279.638\times10^{-29} f_o^3 (w+2a)^2 l}{\ln(h/a) + \sqrt{(h/a)^2 - 1}} + 188.3\frac{\sigma_p}{\sqrt{\epsilon_p}} \tag{5.38}$$

where, the 13.2×10^{-7} factor comes from the numerical value of absolute constants $\epsilon_o = 8.854 \times 10^{-12}$ F/m, $\mu_o = 4\pi \times 10^{-7} N/A^2$.
Substituting the value of σ from Eq. 5.29 in Eq. 5.38 we get:

$$\alpha \approx \frac{\frac{13.2\times10^{-7}}{a} f_o \sqrt{\frac{\rho}{f_r}} + 23279.638 \times 10^{-29} f_o^3 (w+2a)^2 l}{\ln(h/a) + \sqrt{(h/a)^2 - 1}} + \frac{\eta \nu_{en}}{\sqrt{1-\eta}} \times 1.6672 \times 10^{-9} \tag{5.39}$$

When the probe is introduced in vacuum, the value of attenuation constant can be written as;

$$\alpha \approx \frac{\frac{13.2\times10^{-7}}{a} f_o \sqrt{\frac{\rho}{f_r}} + 23279.638 \times 10^{-29} f_o^3 (w+2a)^2 l}{\ln(h/a) + \sqrt{(h/a)^2 - 1}} \tag{5.40}$$

Here all dimensional parameters are in meters and frequencies are in Hz. The signal width (Δf) and the attenuation constant (α) are related as given in Eq. 5.17. The above analysis shows that the attenuation constant and the signal width depends on the probes dimension, resistivity of the material wires, plasma frequency, collisional frequency, and resonance frequency of the hairpin. Other loss mechanisms include the induction losses which appears when the electromagnetic flux linked with the conductor cuts an adjacent conductor resulting in the induction of current in that conductor. Radiation losses are caused due to the leakage of some magnetic lines of force about a conductor during the alternating cycle. These lines of force are projected into space as radiation resulting in power losses. In the model discussed in previous section, they are quantified as radiation resistance in addition of ohmic resistance in the circuit.

5.4 Results and Discussion

5.4.1 Signal width in Non-Magnetized Plasma

Fig. 5.3 shows the plot of normalized signal width obtained from the experimental data at FWHM to the ones calculated using Eq. 5.17. The α is calculated using

Eq. 5.40. We observe the experimental values of Δf monotonically increase with vacuum resonance frequency (reducing the physical length of the hairpin).

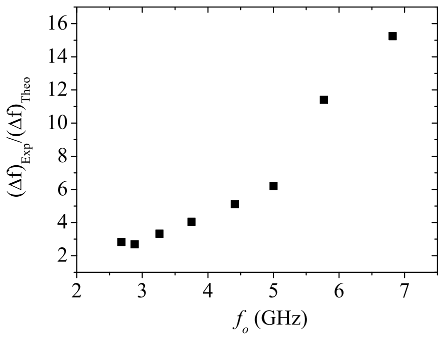

Figure 5.3: Ratio of signal width obtained in experiment (vacuum case) and theory.

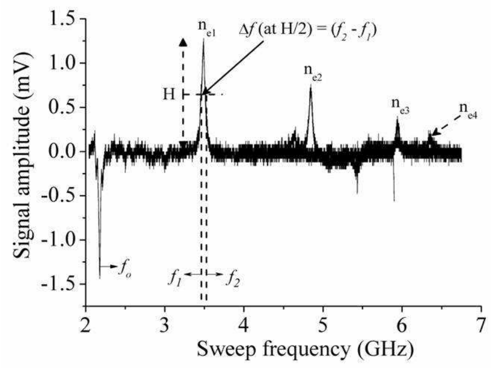

Figure 5.4: Resonance signals for different n_e, where $(n_{e1}, n_{e2}, n_{e3}, n_{e4}) = (0.92, 2.3, 3.7, 4.3) \times 10^{11} cm^{-3}$ and $f_o = 2.171$ GHz.

Dielectric Losses

The behavior of the resonance signal in plasma are presented in the Fig. 5.4. The amplitude of resonance peak monotonically reduce with increasing plasma density. Fig. 5.5 plots the normalized resonance signals of Fig. 5.4 for different rf powers in the plasma. It shows the reduction in the signal amplitude with increasing discharge power or electron density. The attenuation of the signal is greater in the case when the resonance frequency is closer to the electron plasma frequency. For example at $n_e = 4.3 \times 10^{11} cm^{-3}$, the plasma frequency $f_{pe} \approx 5.9$ GHz which is typically close to $f_r = 6.4$ GHz. The attenuation of the resonance signal is the strongest. The attenuation of the signal is quantified by the parameter $\eta = (f_{pe}^2)/(f_r^2)$. The value of η varies from 0.0 to 1.0. $\eta = 0$ is corresponding to vacuum or air and $\eta = 1.0$ corresponds to zero plasma permittivity.

Fig. 5.6 shows the variation of signal width with η. As the η approaches 1.0, the signal width values goes to infinity. At this condition, electrons resonantly gain energy from the oscillating electric field of the hairpin and dissipating the energy

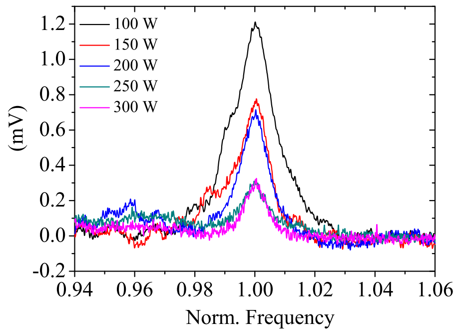

Figure 5.5: Normalized resonance signal by respective resonance frequency at 10mTorr.

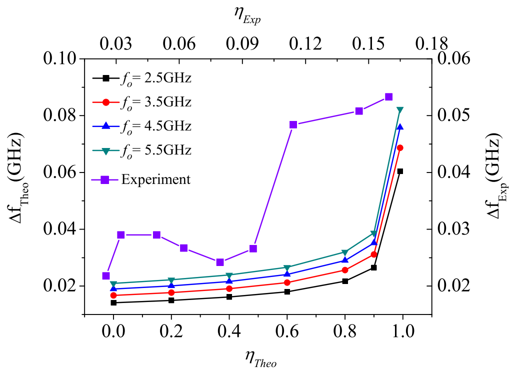

Figure 5.6: Signal width obtained from experiment and theory.

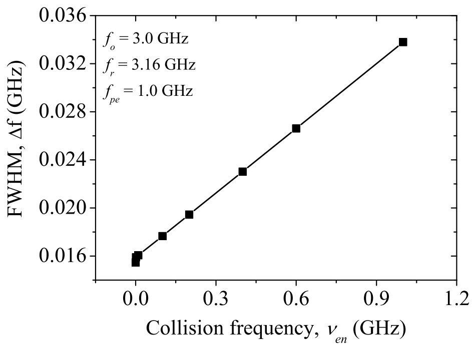

Figure 5.7: Signal width versus collision frequency.

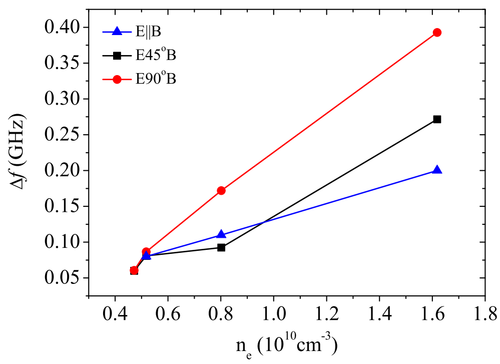

Figure 5.8: FWHM versus n_e at B = 0.012T.

via collisions with the background plasma. The frequency of the standing wave must be greater than the cutoff or plasma frequency for the real permittivity values. For frequency below the plasma frequency, the wave becomes evanescent. The signal width are plotted for η varying from 0.02 to 0.15. Beyond this range the resonance signal is hard to detect against the background noise. Therefore it is recommended that η should be kept much below unity for application of hairpin to high density plasmas typically above $10^{11} cm^{-3}$. Therefore shorter hairpins are preferred.

Collisional losses

The collisional losses are mainly caused by the collision of plasma electrons with the background neutrals. In the case of collisionless plasmas, the plasma conductivity for applied frequency $f_r(GHz) >> \nu_{en}(MHz)$ will have linear dependency on collision frequency as per Eq. 5.29. Hence, ν_{en} also affects the signal width even in the case of low pressure plasma.

Fig. 5.7 shows the effect of electron-neutral collision frequency on the signal width. The data is obtained using a Eq. 5.17 for a given probe dimension and electron density. We found that with increase in neutral gas concentration in the plasma causes increase in signal width. The electron-neutral collision frequency is large in the case of atmospheric plasmas as the ν_{en} is in the order of GHz comparable with the resonance frequency of the hairpin. The details can be found in the recent work [72, 88].

5.4.2 Signal width in Magnetized Plasma

In magnetized plasma, the dissipation of resonant energy is further enhanced due to the electron cyclotron motion about the field lines. In this case, the electrons experiencing a strong Lorentz resistive force which results in increase of impedance hairpin resonant circuit. This adversely affects the Q-factor of the resonance signal. The attenuation of signal is further dependent on the angle between the wave vector of hairpin and the direction of applied magnetic field. As per resonance signals presented in section 4.4.1, we observed that the signal attenuation is found to be greater in case of $\vec{k}||\vec{B}$ as compare to $\vec{k}\perp\vec{B}$. This is because in case of $\vec{k}||\vec{B}$, the strong electric field component between the wires of hairpin is normal to the B-field and hence electrons experiences greater Lorentz force. Therefore, in our experiments the hairpin is always situated normal to uniform B-field such that $\vec{k}\perp\vec{B}$.

In Fig. 5.8, the signal width is plotted as a function of electron density for three different rotations of the hairpin plane with respect to the magnetic field. In all three cases, $\vec{k}$ is normal to the B-field. We observed that the signal width is monotonically increasing with the electron density. However, it is greater in case of $E90^oB$, where E-field is one of the strongest component between the parallel pins of hairpin.

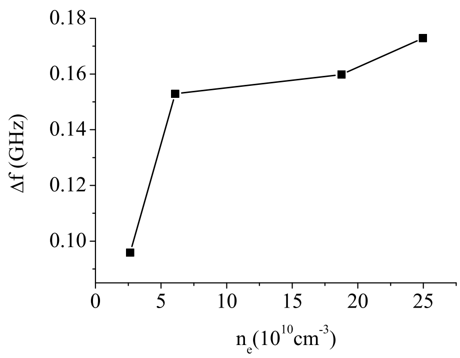

Figure 5.9: FWHM versus n_e where $f_o = 2.64GHz$ and $f_{ce} = 1.0GHz$.

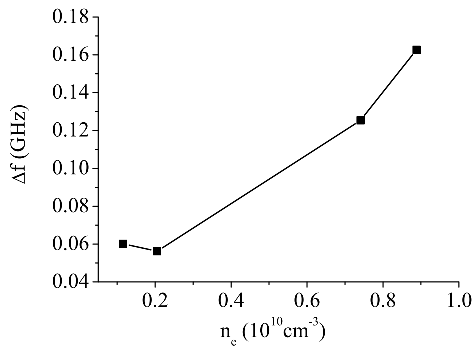

Figure 5.10: FWHM versus n_e where $f_o = 2.64GHz$ and $f_{ce} = 3.1GHz$.

In Figs. 5.9 and 5.10, we obtain the broadening Δf_r of the signal for two set of electron cyclotron frequency (or B-field strengths) of values $f_{ce} = 1.0$ GHz and $f_{ce} = 3.1$ GHz. For both cases $f_{ce} < f_r$ and $f_{ce} > f_r$, we found that signal width increases with electron density. However, the magnitude of signal width is greater in case of $f_{ce} > f_r$. The signal width for $f_{ce} < f_r$ case is corresponding to density which is one order higher in magnitude with respect to $f_{ce} > f_r$. Therefore, we found that the signal width proportionally increases with the electron density and the magnetic field strength. It also depends on which direction the probe is rotated to the B-field. The rotation effect on signal width is observed because of the three dimensional non-uniform electric field of hairpin. At strong magnetic fields, the plasma within the hairpin is itself becomes non-uniform due to curvature in the electric field. The field distribution is already presented in chapter-2 of the thesis.

5.5 Summary and Conclusion

The practical range of electron density measurement by hairpin probe strongly depends on the accurate determination of resonance signal under the background noise. The losses are found to be highest if the probe's resonance frequency is close to the electron plasma frequency. The signal is characterized by the quality factor of the probe which is inversely proportional to the signal width. This is because at lower densities around $10^8 cm^{-3}$ it is very difficult detect the small shift in the case of broad peak or low Q signal and on the other hand for high density the losses are immense, therefore the resonance signal completely muddles into the plasma. The series resonance circuit model of the hairpin is developed on the basis of transmission line theory which described the various factors and loss mechanisms affecting the signal width of hairpin probe. The model gives important information about the selection of probe material, dimension, and working range of density measurements by probe. The experimental results are qualitatively explained on the basis of a series resonant circuit model.

In the magnetized plasma, the electrons experiencing a strong $\vec{E} \times \vec{B}$ force which results in greater impedance between the pins which acts adversely on the quality, Q. The losses in the resonator can be reduced by choosing the intermediate probe resonance frequency between 2.0 to 4.0 GHz because with increase in frequency the signal gets attenuated quickly in the plasma. However, the low frequency probe has lower spatial resolution or in other words it measures an average electron density around its volume because of its longer length. It is also recommended to introduce a hairpin perpendicular to the B-field with hairpin plane along the field lines for lesser attenuation of resonance signal.

CHAPTER 6

Summary and Scope of Research Work

6.1 Highlights of PhD Work

Advantages of hairpin probe -

- It gives direct value of local electron density by measuring the plasma dielectric constant without relying on any other parameter such as electron temperature in case of classical electrical probes [36].
- The probe introduced minimal plasma perturbation because of its floating nature [2, 36].
- The hairpin probe can replace conventional electrical probes in standard Laser Photo detachment for obtaining negative ion density [28, 110].

List of shortcomings of hairpin probe -

- It measures only electron density in the plasma.

- The upper limit of electron density measurement is limited $10^{12} cm^{-3}$.
- There is no valid probe theory for its application in the strongly magnetized plasma.
- The issue of giving underestimated electron density in case of adjunct dielectric material present in the vicinity of hairpin is the major drawback for using it as a diagnostic tool. The typical examples are polymer deposition on the probe surface in the Etch industrial plasma reactors and need of probe tip holder in the form of dielectric material.
- There are only limited experimental works have been made on probe immersed in the collisional plasmas [69, 72, 88].

List of latest results presented in this PhD work -

- We have demonstrated new data processing methods based on subtracting the frequency spectrum obtained in presence of plasma with that obtained in vacuum case. This has particular advantage for detecting resonance signal over a wide range of frequency.
- We presented the dielectric shielded (semi and fully) hairpin probes and there respective analytical models for obtaining the correct electron density.
- The performance of probe is demonstrated in strongly magnetized plasma.
- We addressed factors influencing the dispersion of resonance signal in plasma.

6.2 Impact of PhD Work

The popularity of hairpin probe in the field of plasma diagnostics is limited due to several reasons. At the first place, probes are generally metallic objects that introduce perturbation in the plasmas. Therefore, they are generally avoided in plasmas used for manufacturing electronic devices. The main complexity are arises due to polymer deposition, secondary electron emission effects, high density, and presence of magnetic field. The limited range or choice of plasma parameters that the probe can measure also obstructs for developing it as a diagnostic tool.

The hairpin probe has several components such as coupling loop antenna, hairpin resonator, and coaxial feed (typically 40 cm of length); the size that is really exposed to the plasma can bring lots of impurities. Furthermore, the physical dimension of hairpin resonator (total length of about 5 cm), probe's material resistivity, and introduction of electromagnetic wave can create significant perturbation in plasma. In presence of magnetic field, the probe orientation can result in anisotropy in the electron density measurements. The dissipation of resonant energy of hairpin with increase in electron density, strong magnetic field, and collision in the plasma limits the detection of resonance signal on which the technique is actually based.

In this thesis we have touched these subjects and demonstrated useful solutions that can lead to a better design of the hairpin as a tool for practical applications. The electron density is an essential plasma parameter for quantifying the state of plasma. One of the key application is the implementation of hairpin probe as an electron density sensor in the commercial Etch plasma reactors. The probe could be used for developing relation between the various process parameters with the electron density in plasma. Furthermore, the probe could be useful for monitoring the plasma conditions for feedback control and end point detection of process. This helps in reducing the energy cost and improves the process productivity.

6.3 Summary

The motivation behind this research work is to develop a basic understanding about the characteristics of hairpin resonances under various practical situations. The practical applications are mostly limited due to (1) high plasma density, (2) strong magnetic field, and (3) polymer deposition in complex reactive plasma.

In this work, we have treated the hairpin as a series resonance circuit formed between two parallel wires having finite distributed inductance and capacitance per unit length. Based on the standard transmission line theory the hairpin circuit is investigated.

A practical application of the hairpin probe can be thought to be used in plasma chambers used for fabrication of semiconductor devices as mentioned earlier. Metallic parts exposed can introduce impurities due to sputtering of the probe surface. An idea of insulating the surface by a thick dielectric film may be promising. The systematic experiments performed with quartz dielectric shown interesting trends of electron density as presented in section 3.3.2.

Performance of hairpin in strongly magnetized plasma remained as an open issue since the invention of the probe three decades ago. This was one of the primary motivating factors addressed in this thesis. By systematically varying the magnetic field between two pole pieces of permanent bar magnet, we demonstrated for the first time that the plasma permittivity exhibits dual resonances with contrasting characteristics. They are found to be satisfy the basic dispersion relation of wave field in magnetized plasmas. However because of the large physical dimensions of the probe, the non-uniform electric field distribution, and the probe wave vector orientation in magnetic field results in a distinct contributions of plasma electrons to the resonance spectrum of hairpin.

Addressing the basic application of hairpin in magnetized plasma we have demonstrated measurement of electron density [70] over a limited parameter space of magnetic field in the filament ion source commonly known as the Kamaboko-III negative ion source [50, 111] that was operational at CEA, Caderache. Some results of that investigation was published. The probe was applied in the filter field region where the negative ions are generated and extracted. However, the major issue about the probe is that it was incapable of performing high density measurements greater than $10^{12} cm^{-3}$ due to significant loss of its resonator energy into the plasma. The issue of high density is resolved by partial shielding of hairpin tip with a dielectric material which is studied in detail in section 3.2. The analytical model is developed based on the weighted mean of dielectric medium present in the vicinity of hairpin. The model is experimentally verified. The presence of an adjacent dielectric can considerably shift the resonance band towards lower frequency. Therefore one can use this as an advantage for covering a higher density range which is limited to typically $10^{12} cm^{-3}$ with a conventional hairpin probe.

One of the major issues is the dispersion of the resonance signal in plasma due to various loss mechanism. This limits the workable measurement range of the resonance frequency signal. In order to widen the frequency range, we systematically studied the factors influencing the quality of the resonance signal which is defined by a parameter called Q-factor. In chapter-2, we presented a simulation and experimental study of hairpin resonator without the plasma. This information is particularly useful for better designing of hairpin by suitable selection of its dimension and material. In chapter-5, the series resonant circuit model of a hairpin resonator is presented. The advantage of this model is to give detailed information about the factors that can influence the quality of the resonance signal. These factors are directly related to the plasma parameters such as electron plasma frequency, electron-neutral collision frequency, and electron temperature. The calculations are based on similar approach of the circuit model described by Sugai group [72, 88] but addressed to collisional plasmas. However, the model qualitatively supports the experimental results in section 5.4 because of assumptions of lossless line ($RG \approx 0$), perfect U-shaped resonator, and ignorance of sheath around the wires. The hardware limitations such as imperfections in probe design, slight deviation from its hairpin shape, and instrumental errors; each contributes to error in the measurements.

6.4 Scope of Future Research Work on Hairpin Probe

The scope of future research work on hairpin probe is listed below on the basis of plasma under investigation:

Investigation of hairpin probe in strongly magnetized plasmas:

Strong magnetic field of about 0.1T in the plasma around the hairpin results in two resonance peaks one below and other above its vacuum resonance condition. Both signify two distinct plasma permittivity; $\kappa_p > 1$ and $\kappa_p < 1$. However, the absolute electron densities obtained using both resonance frequencies are different in magnitude. The non-uniform electromagnetic field and strong magnetic field is the expected reason behind the sampling of electron population among two resonances. However, it is still not explainable from the well known dispersion relation in case of electromagnetic wave launched in the magnetized plasma. This is mainly because of the assumption of unform electric field of resonator and equal plasma density distribution among the resonances of hairpin in the dispersion relation. The analysis of electron density using two resonances could be improved by incorporating the spatial inhomogeneity of electromagnetic field of hairpin. Furthermore, the dispersion relation needs further modification for the case of hairpin immersed in a non-uniform magnetic field region of plasma. In this case, the wave vector of hairpin makes an arbitrary angle with the magnetic lines. This is particularly important for practical application as most commercial plasma reactors such as ECR sources, Magnetron sputtering devices have non-uniform magnetic field regions.

Another situation dealing with the $\vec{E}(t) \times \vec{B}$ force acting on the plasma electrons in strong magnetic field results in stronger attenuation of the resonance signal. The signal is found to be attenuated even in low pressure plasmas where the electron-neutral collision frequency (MHz) is much less than the probe's resonance frequency (GHz). The attenuation is caused by a strong Lorentz force which increases the impedance of the hairpin circuit. The signal attenuation is found to be stronger for the case when wave-vector is parallel to the magnetic field because in this case the strongest E-field component between the hairpin wires is always normal to B-field lines and results in stronger resistive force. The series resonant model of hairpin presented in chapter-5 for studying the signal attenuation in plasma could be extended to the case of magnetized plasmas by including the conductivity tensor of magnetized plasma.

Investigation of hairpin probe in collisional plasmas:

In the recent trend of plasma technology in the field of biomedical and environmental science increases the demands of diagnostic devices for better understanding of the plasma state. They are generally operated at high pressures (10 Torr to 760 Torr). The electron density is the most important plasma parameters as the active species are mainly generated by electron-impact reactions which cause excitation, ionization, and dissociation. Determining electron density by introducing some biased probes into the plasmas can create significant plasma perturbation. The main issue with the applicability of classical electrical probes in the atmospheric plasmas is that the probe size is larger than the Debye length where the Debye length is greater than the electron mean free path. However, in the case of hairpin probe, the fundamental principle is based on measuring the plasma permittivity instead of drawing particle fluxes by biasing the probe. Therefore, by including the electron-neutral collision frequency to the dispersion formula, one can notice the modification in the resonance signal of hairpin. The parameter, signal width or Q-factor can give valuable information about the plasma state such as electron density and electron-neutral collision frequency.

Bibliography

[1] G. Neumann, U. Banziger, M. Kammeyer, and M. Lange, "Plasma-density measurements by microwave interferometry and langmuir probes in an rf discharge," *Review of Scientific Instruments*, vol. 64, pp. 19–25, 1993.

[2] R. B. Piejak, V. A. Godyak, R. Garner, B. M. Alexandrovich, and N. Sternberg, "The hairpin resonator: A plasma density measuring technique revisited," *Journal of Applied Physics*, vol. 95, no. 7, pp. 3785–3791, 2004.

[3] W. Crookes, "Lecture on british association for the advancement of science," *Sheiffield*, 1879.

[4] J. J. Thomson, "Lecture to the royal institution," *Philosophical Magazine*, 1897.

[5] I. Langmuir, "Oscillations in ionized gases," *Proc. Nat. Acad. Sci. U.S.*, vol. 14, no. 8, 1928.

[6] F. F. Chen, "Introduction to plasma physics," *Plenum Press, New York and London*, 1974.

[7] F. F. Chen, "Introduction to plasma physics and controlled fusion," *Plenum Press, New York and London*, 1984.

[8] I. H. Hutchinson, "Principles of plasma diagnostics," *Cambridge university press*, vol. second edition, 2002.

[9] M. A. Heald and C. B. Wharton, "Plasma diagnostics with microwaves," *Wiley, New York*, 1965.

[10] N. Hershkowitz and H. L. Maynard, "Plasma characterization and process control diagnostics," *Journal of Vacuum Science and Technology A*, vol. 11, no. 4, 1993.

[11] M. A. Lieberman and A. J. Lichtenberg, "Principles of plasma discharges and materials processing," *Wiley, New York*, 2005.

[12] D. B. Graves, "Plasma processing," *IEEE transactions on Plasma Science*, vol. 22, no. 1, 1994.

[13] M. Greenwald, "Fusion plasmas," *John Wiley & Sons*, 1999.

[14] Y. Okumura, Y. Fujiwara, T. Inoue, K. Miyamoto, N. Miyamoto, A. Nagase, and Y. Ohara, "High power negative ion sources for fusion at the japan atomic energy research institute (invited)," *Rev. Sci. Instrum.*, vol. 67, no. 3, 1996.

[15] U. Fantz, "Basics of plasma spectroscopy," *Plasma Sources Sci. Technol.*, vol. 15, pp. S137–S147, 2006.

[16] L. Lindberg, "Optimum design of a microwave interferometer for plasma density measurements," *J. Phys. E: Sci. Instrum.*, vol. 15, 1982.

[17] H. Meuth and E. Savillano, "Microwave plasma diagnostics," *Plasma Fusion Center, Massachusetts Institute of Technology*, 1987.

[18] Z. Shu and H. Xi-Wei, “New microwave diagnostic theory for measurement of electron density in atmospheric plasmas,” *Chinese Physics Letter*, vol. 22, no. 1, pp. 168–170, 2005.

[19] H. M. Mott-Smith and I. Langmuir, “The theory of collectors in gaseous discharges,” *Physical Review*, vol. 28, 1926.

[20] M. J. M. Parrot, L. R. O. Storey, L. W. Parker, and J. G. Laframboise, “Theory of cylindrical and spherical langmuir probes in the limit of vanishing debye number,” *Physics of Plasmas*, vol. 25, no. 2388, 1982.

[21] T. E. Sheridan, “How big is a small langmuir probe?,” *Physics of Plasmas*, vol. 7, no. 3084, 2000.

[22] J. D. Norgard and R. M. Sega, “B-dot probe measurements,” *Final Technical Report by Rome Air Development Center, NY 13441-5700*, 1990.

[23] E. T. Everson, P. Pribyl, C. G. Constantin, A. Zylstra, D. Schaeffer, N. L. Kugland, and C. Niemann, “Design, construction, and calibration of a three-axis, high-frequency magnetic probe (b-dot probe) as a diagnostic for exploding plasmas,” *Rev. Sci. Instrum.*, vol. 80, p. 113505, 2009.

[24] A. Kono and K. Kato, “Measurement of negation-ion density in high density c_4f_8 plasma using a laser photodetachment technique combined with a millimeter-wave open resonator,” *Applied Physics Letter*, vol. 77, no. 4, 2000.

[25] A. G. Nikitin, F. E. Balghuti, and M. Bacal, “Comparison of negative ion density measurements by probes and by photodetachment,” *Plasma Sources Science and Technology*, vol. 5, pp. 37–42, 1996.

[26] G. A. Hebner and I. C. Abraham, “Characterization of electron and negative ion densities in fluorocarbon containing inductively driven plasmas,” *Journal of Applied Physics*, vol. 90, no. 10, pp. 4929–4937, 2001.

[27] J. Bradley, R. Dodd, S. D. You, N. Sirse, and S. K. Karkari, “Resonance hairpin and langmuir probe-assisted laser photodetachment measurements of the negative ion density in a pulsed dc magnetron discharge,” *Journal of Vacuum Science and Technology A*, vol. 28, no. 3, 2011.

[28] J. Conway, N. Sirse, S. K. Karkari, and M. M. Turner, “Using the resonance hairpin probe and pulsed photodetachment technique as a diagnostic for negative ions in oxygen plasma,” *Plasma Sources Sci. Technol.*, vol. 19, no. 6, 2010.

[29] J. A. Tagle, P. C. Stangeby, and S. K. Erents, “Errors in measuring electron temperature using a single langmuir probe in a magnetic field,” *Plasma Physics and Controlled Fusion*, vol. 29, no. 3, pp. 297–301, 1987.

[30] R. A. Pitts and P. C. Stangeby, “Experimental tests of langmuir probe theory for strong magnetic fields,” *Plasma Physics and Controlled Fusion*, vol. 32, no. 13, pp. 1237–1248, 1990.

[31] R. Jones, “Electrostatic probe characteristics in a magnetic field,” *Transactions of the Kansas Academy of Science*, vol. 94(3-4), pp. 153–159, 1991.

[32] E. Stamate and K. Ohe, “On the surface condition of langmuir probes in reactive plasmas,” *Applied Physics Letters*, vol. 78, no. 2, 2001.

[33] H. Amemiya and S. Bhattacharjee, “Comment on ”on the surface condition of langmuir probes in reactive plasmas” [appl. phys. lett. 78, 153, 2001],” *Applied Physics Letters*, vol. 79, no. 16, 2001.

[34] J. Y. Bang, Y. Kyoung, D. H. Kim, and C. W. Chung, “A plasma diagnostic technique using a floating probe for the dielectric deposition process,” *Plasma Sources Science and Technology*, vol. 20, no. 065005, p. 7, 2011.

[35] R. L. Stenzel and R. W. Gould, "Upper-hybrid resonance absorption, emission and heating of an afterglow plasma column," *Journal of Applied Physics*, vol. 42, no. 11, pp. 4225–4234, 1971.

[36] R. L. Stenzel, "Microwave resonator probe for localized density measurements in weakly magnetized plasma," *Review of Scientific Instruments*, vol. 47, no. 5, pp. 603–607, 1976.

[37] J. A. Bittencourt, "Fundamentals of plasma physics," *Springer-Verlag, New York*, 2004.

[38] L. Tonks, "Plasma-electron resonance, plasma resonance and plasma shape," *Physical Review*, vol. 38, 1931.

[39] S. A. Schelkunoff, "Electromagnetic waves," *Van Nostrand, New York*, 1943.

[40] E. C. Jordan and K. G. Balmain, "Electromagnetic waves and radiating systems," *Prentice-Hall, Inc.*, 1968.

[41] S. J. Orfanidis, "Electromagnetic waves and antennas," *ECE Department, Rutgers University, NJ*, 2008.

[42] M. Lapke, T. Mussenbrock, R. P. Brinkmann, C. Scharwitz, M. Boke, and J. Winter, "Modeling and simulation of the plasma absorption probe," *Applied Physics Letter*, vol. 90, no. 121502, 2007.

[43] T. Shirakawa and H. Sugai, "Plasma oscillation method for measurements of absolute electron density in plasma," *Japanese Journal of Applied Physics*, vol. 32, pp. 5129–5135, 1993.

[44] J. Kim, S. Choi, Y. Shin, and K. Chung, "Wave cutoff method to measure absolute electron density in cold plasma," *Review of Scientific Instruments*, vol. 75, no. 8, p. 2706, 2004.

[45] D. R. Boris, R. F. Fernsler, and S. G. Walton, "The lc resonance probe for determining local plasma density," *Plasma Sources Science and Technology*, vol. 20, no. 2, 2011.

[46] M. Lapke, T. Mussenbrock, and B. R. . P., "The multipole resonance probe: A concept for simultaneous determination of plasma density, electron temperature, and collision rate in low-pressure plasmas," *Applied Physics Letter*, vol. 93, no. 051502, 2008.

[47] R. W. Dreyfus, J. M. Jasinski, R. E. Walkup, and G. S. Selwyn, "Optical diagnostics of low pressure plasmas," *Pure and Applied Chemistry*, vol. 57, no. 9, pp. 1265–1276, 1985.

[48] C. H. Chang, C. H. Hsieh, H. TWang, J. Y. Jeng, K. C. Leoul, and C. Lin, "A transmission-line microwave interferometer for plasma electron density measurement," *Plasma Sources Science and Technology*, vol. 16, pp. 67–71, 2007.

[49] J. Hopwood, C. R. Guarnieri, S. J. Whitehair, and J. J. Cuomo, "Langmuir probe measurements of a radio frequency induction plasma," *Journal of Vacuum Science and Technology A*, vol. 11, no. 1, 1993.

[50] B. Crowley, D. Homfray, S. J. Cox, D. Boilson, H. P. L. de Esch, and R. S. Hemsworth, "Measurement of the electron energy distribution function by a langmuir probe in an iter-like hydrogen negative ion source," *Nuclear Fusion*, vol. 46, pp. S307–S312, 2006.

[51] N. S. J. Braithwaite and R. N. Franklin, "Reflections on electrical probes," *Plasma Sources Sci. Technol.*, vol. 18, no. 014008, 2009.

[52] M. B. Hopkins, "Langmuir probe measurements in the gaseous electronics conference rf reference cell," *Journal of Research of the National Institute of Standards and Technology*, vol. 100, no. 4, 1995.

[53] K. Takayama and H. Ikegami, "Plasma resonance in a radio-frequency probe," *Phys. Rev. Lett.*, vol. 5, no. 6, pp. 238–240, 1960.

[54] R. S. Harp, "The behavior of the resonance probe in a plasma," *Applied Physics Letters*, vol. 4, no. 11, 1964.

[55] I. N. Moskalev and A. M. Stefanovskii, "Plasma diagnostics by means of open cylindrical resonators," *Moscow, Energoatomizdat*, 1985.

[56] S. G. Bilen, J. M. Haas, F. S. Gulczinski, and A. D. Gallimore, "Resonance-probe measurements of plasma densities in electric-propulsion plumes," *35th AIAA/ASME/SAE/ASEE Joint Propulsion Conference and Exhibit*, 1999.

[57] S. Dine, J. P. Booth, G. A. Curley, C. S. Corr, J. Jolly, and J. Guillon, "A novel technique for plasma density measurement using surface wave transmission spectra," *Plasma Sources Science and Technology*, vol. 14, pp. 777–786, 2005.

[58] J. Kim and K. C. Jungling, "Measurement of plasma density generated by a semiconductor bridge: related input energy and electrode material," *ETRI Journal*, vol. 17, no. 2, 1995.

[59] F. A. Haas, J. Al-Kuzee, and N. S. J. Braithwaite, "Hairpin resonator probe measurements in rf plasmas," *Applied Physics Letter*, vol. 87, 2005.

[60] R. B. Piejak, J. Al-Kuzee, and N. S. J. Braithwaite, "Hairpin resonator probe measurements in rf plasmas," *Plasma Sources Science and Technology*, vol. 14, pp. 734–743, 2005.

[61] N. S. Siefert, B. L. Sands, and B. N. Ganguly, "Electron and metastable state interactions in two-step ionization waves," *Applied Physics Letter*, vol. 89, 2006.

[62] N. S. Siefert, B. N. Ganguly, B. L. Sands, and G. A. Hebner, "Decay of the electron number density in the nitrogen afterglow using a hairpin resonator probe," *Journal of Applied Physics*, vol. 100, 2006.

[63] S. K. Karkari and A. R. Ellingboe, "Effect of radio-frequency power levels on electron density in a confined two-frequency capacitively-coupled plasma processing tool," *Applied Physics Letter*, vol. 88, no. 101501, 2006.

[64] V. Milosavljevic, S. K. Karkari, and A. R. Ellingboe, "Characterization of the pulse plasma source," *Plasma Sources Science and Technology*, vol. 16, pp. 304–309, 2007.

[65] S. K. Karkari, C. Gaman, A. R. Ellingboe, I. Swindells, and J. W. Bradley, "A floating hairpin resonance probe technique for measuring time-resolved electron density in pulse discharge," *Measurement Science and Technology*, vol. 18, pp. 2649–2656, 2007.

[66] S. K. Karkari, A. R. Ellingboe, C. Gaman, I. Swindells, and J. W. Bradley, "Electron density modulation in an asymmetric bipolar pulsed dc magnetron discharge," *Journal of Applied Physics*, vol. 102, 2007.

[67] G. A. Curley, "The dynamics of the charged particles in a dual frequency capacitively coupled dielectric etch reactor," *PhD Thesis*, pp. 67–87, 2008.

[68] S. K. Karkari, A. R. Ellingboe, and C. Gaman, "Direct measurement of spatial electron density oscillations in a dual frequency capacitice plasma," *Applied Physics Letter*, vol. 93, no. 071501, 2008.

[69] B. L. Sands, N. S. Siefert, and B. N. Ganguly, "Design and measurement considerations of hairpin resonator probes for determining electron number density in collisional plasmas," *Plasma Sources Science and Technology*, vol. 16, pp. 716–725, 2007.

[70] S. K. Karkari, G. S. Gogna, D. Boilson, M. M. Turner, and A. Simonin, "Performance of a floating hairpin probe in strongly magnetized plasma," *Contribution to Plasma Physics*, vol. 50, no. 9, pp. 903–908, 2010.

[71] G. A. Curley, L. Gatilova, S. Guilet, S. Bouchoule, G. S. Gogna, N. Sirse, S. K. Karkari, and J. P. Booth, "Surface loss rates of h and cl radicals in an inductively coupled plasma etcher derived from time-resolved electron density and optical emission measurements," *Journal of Vacuum Science and Technology A*, vol. 28, no. 2, 2010.

[72] J. Xu, J. Shi, J. Zhang, Q. Zhang, K. Nakamura, and H. Sugai, "Advanced high-pressure plasma diagnostics with hairpin resonator probe surrounded by film and sheath," *Chinese Physics B*, vol. 19, no. 7, 2010.

[73] G. S. Gogna and S. K. Karkari, "Microwave resonances of a hairpin probe in a magnetized plasma," *Applied Physics Letter*, vol. 96, no. 151503, 2010.

[74] J. W. Coburn and M. Chen, "Optical emission spectroscopy of reactive plasmas: A method for correlating emission intensities to reactive particle density," *Journal of Applied Physics*, vol. 51, no. 3134, 1980.

[75] X. Zhu and Y. Pu, "Optical emission spectroscopy in low-temperature plasmas containing argon and nitrogen: determination of the electron temperature and density by line-ratio method," *J. Phys. D: Appl. Phys.*, vol. 403001, p. 24, 2010.

[76] X. Zhu and Y. Pu, "A simple collisionalradiative model for low-pressure argon discharges," *J. Phys. D: Appl. Phys.*, vol. 40, pp. 2533–2538, 2007.

[77] K. Kano, M. Suzuki, and H. Akatsuka, "Spectroscopic measurement of electron temperature and density in argon plasmas based on collisional-radiative model," *Plasma Sources Science and Technology*, vol. 9, pp. 314–322, 2000.

[78] D. L. Crintea, U. Czarnetzki, S. Iordanova, I. Koleva, and D. Luggenholscher, "Plasma diagnostics by optical emission spectroscopy on argon and comparison with thomson scattering," *J. Phys. D: Appl. Phys.*, vol. 42, no. 045208, 2009.

[79] X. Zhu, Y. Pu, N. Balcon, and R. Boswell, "Measurement of the electron density in atmospheric-pressure low-temperature argon discharges by line-ratio method of optical emission spectroscopy," *J. Phys. D: Appl. Phys.*, vol. 42, no. 142003, p. 5, 2009.

[80] M. Laroussi, "Relationship between the number density and the phase shift in microwave interferometry for atmospheric pressure plasmas," *International Journal of Infrared and Millimeter Waves*, vol. 20, no. 8, 1999.

[81] V. G. Denisov, V. A. Isaev, and A. I. Smirnov, "Effect of ponderomotive nonlinearity on the propagation of intense microwaves along long lines in transparent plasma," *Soviet Journal of Plasma Physics*, vol. 13, 1987.

[82] J. Kim, E. Schamiloglu, B. Martinez-Tovar, and K. C. Jungling, "Measurement of plasma density generated by a semiconductor bridge," *Electronics Letters*, vol. 7, no. 7, 1994.

[83] J. Kim, E. Schamiloglu, B. Martinez-Tovar, and K. C. Jungling, "Temporal measurement of plasma density variations above a semiconductor bridge (scb)," *IEEE Transactions on Instrumentation and Measurement*, vol. 44, no. 4, 1995.

[84] I. G. Kondrat'ev, A. V. Kostrov, A. I. Smirnov, A. V. Strikovskii, and A. V. Shashurin, "Two-wire microwave resonator probe," *Plasma Physics Report*, vol. 28, no. 11, pp. 977–983, 2002.

[85] A. V. Kostrov, A. I. Smirnov, and D. V. Yanin, "Microwave resonator probe diagnostics of plasma density fluctuations," *Plasma Physics Report*, vol. 13, no. 1, pp. 209–211, 2007.

[86] D. V. Yamin, A. V. Kostrov, A. I. Smirnov, and A. V. Strikovsky, "Diagnostics of plasma density nonstationary perturbations," *Technical Physics*, vol. 53, no. 1, pp. 129–133, 2008.

[87] F. A. Haas, J. Al-Kuzee, and N. S. J. Braithwaite, “Electron and ion sheath effects on a microwave hairpin probe,” *Applied Physics Letter*, vol. 87, no. 201503, 2005.

[88] J. Xu, K. Nakamura, Q. Zhang, and H. Sugai, “Simulation of resistive microwave resonator probe for high-pressure plasma diagnostics,” *Plasma Sources Science and Technology*, vol. 18, p. 9pp, 2009.

[89] I. Liang, K. Nakamura, and H. Sugai, “Modeling microwave resonance of curling probe for density measurements in reactive plasmas,” *Applied Physics Express*, vol. 066101, 2011.

[90] “Cst microwave studio,” *http://www.cst.com.*

[91] U. S. Inan and A. S. Inan, “Engineering electromagnetics,” *California: Addison Wesley Longman*, 1999.

[92] P. Iordanov, B. Keville, J. Ringwood, S. Doherty, and R. Faulker, “On the closed-loop control of an argon plasma process,” *Irish Signals and Systems Conference*, 2006.

[93] G. Cunge, B. Crowley, D. Vender, and M. M. Turner, “Characterization of the e to h transition in a pulsed inductively coupled plasma discharge with internal coil geometry: bi-stability and hysteresis,” *Plasma Sources Sci. Technol.*, vol. 8, pp. 576–586, 1999.

[94] G. Cunge, B. Crowley, D. Vender, and M. M. Turner, “Anomalous skin effect and collisionless power dissipation in inductively coupled discharges,” *Journal of Applied Physics*, vol. 89, no. 7, 2001.

[95] A. Rashidian, K. Forooraghi, and M. T. Aligodarz, “Investigations on two-segment dielectric resonator antennas,” *Microwave and optical technology letters*, vol. 45, no. 6, 2005.

[96] J. C. Rautio, "Measurement of planar substrate uniaxial anisotropy," *IEEE TRANSACTIONS ON MICROWAVE THEORY AND TECHNIQUES*, vol. 57, no. 10, 2009.

[97] J. C. Rautio and B. J. Rautio, "Shielded dual-mode microstrip resonator measurement of uniaxial anisotropy," *IEEE TRANSACTIONS ON MICROWAVE THEORY AND TECHNIQUES*, vol. 59, no. 3, 2011.

[98] W. Yu, X. Yang, Y. Liu, and R. Mittra, "Electromagnetic simulation techniques based on the fdtd method," *Wiley series in microwave and optical engineering*, p. 24, 2009.

[99] I. Dey and S. Bhattacharjee, "Experimental investigation of standing wave interactions with a magnetized plasma in a minimum-b field," *Physics of Plasmas*, vol. 15, no. 123502, 2008.

[100] J. Bergman, "The magnetized plasma permittivity tensor," *Physics of Plasmas*, vol. 7, no. 8, 2000.

[101] T. H. Stix, "Waves in plasmas: Highlights from the past and present," *Physics of Fluids B*, vol. 2, no. 8, 1990.

[102] D. Gahan and M. B. Hopkins, "Collisionless electron power absorption in capacitive radio-frequency plasma sheaths," *Journal of Applied Physics*, vol. 100, no. 043304, 2006.

[103] C. Hayden, "Investigation of ion mass diagnostics for plasma processing," *PhD Thesis*, p. 38, 2009.

[104] "Honeywell s-c-ss94a2-ic, hall effect transducer," *http://ie.farnell.com/honeywell-s-c/ss94a2/ic-hall-effect-transducer/dp/1208001*.

[105] P. J. Petersan and S. M. Anlage, "Measurement of resonant frequency and quality factor of microwave resonators: Comparison of methods," *Journal of Applied Physics*, vol. 84, no. 6, 1998.

[106] A. Kumar and S. Sharma, "Measurement of dielectric constant and loss factor of the dielectric material at microwave frequencies," *Progress in Electromagnetics Research PIER*, vol. 69, pp. 47–54, 2007.

[107] E. Vasekova, "Spectroscopic studies of etching gases and microwave diagnostics of plasmas related to the semiconductor industry," *PhD Thesis*, pp. 141–163, 2006.

[108] L. K. Warne, W. A. Johnson, R. S. Coats, R. E. Jorgenson, and G. A. Hebner, "Model for resonant plasma probe," *Sandia report*, vol. SAND2007-2513, pp. 42–44, 2007.

[109] H. Margenau, "Conduction and dispersion of ionized gases," *Physical Review*, vol. 69, no. 9 and 10, 1946.

[110] G. A. Hebner, "Characterization of electron and negative ion densities in fluorocarbon containing inductively driven plasmas," *Journal of Applied Physics*, vol. 90, no. 10, 2001.

[111] D. Boilson, P. L. de EscH, R. S. Hemsworth, M. Kashiwagi, P. Massmann, and L. Svenssonand, "Long pulse operation of the kamaboko iii negative ion source," *Rev. Sci. Instrum.*, vol. 73(2), 2002.